Influence of Foundation Rigidity on the Out-Of-Plane Flexural Response of Slender Masonry Walls

by

Alan Alonso Rivers

In partial fulfillment of the requirements for the degree of

Doctor of Philosophy

in

STRUCTURAL ENGINEERING

Department of Civil and Environment Engineering
University of Alberta

ABSTRACT

Masonry walls with effective height-to-thickness (kh/t) ratios over 30 are commonly found in single-storey buildings such as school gymnasiums, warehouses, and industrial facilities. Stringent design requirements apply for walls with $kh/t > 30$ in North American Standards (CSA S304-14, TMS 402-16) due to the perceived vulnerability of these elements to second-order effects. One of these requirements from CSA S304-14 consists of neglecting the stiffness provided by the foundation, regardless of the connection between the wall and the foundation, the type of foundation, or the soil type. Although not explicitly stated in the standard, this concern is believed to be based on the potential material degradation at the wall base due to the expected rotational demand under repeated loads and the need for simplified design expressions before the availability of specialized software. In contrast, the American masonry design standard (TMS 402-16) allows using any base condition for any height-to-thickness ratio. This consideration leads to underestimating the wall capacity compared to the case in which the foundation rigidity is considered.

As a result of previous studies, accounting for foundation rigidity is an untapped source of stiffness that could be used to reduce the impact of assuming a pinned base in the design of masonry walls with a height-to-thickness ratio greater than 30. In this study, the influence of the wall-foundation interaction on the out-of-plane flexural response of tall-slender masonry walls subjected to combined axial and lateral loads is examined, aiming to propose effective height factors to be used in the design of slender masonry walls on strip footings on common soils and develop construction recommendations to improve the wall-foundation connection.

To achieve this objective, experimental and numerical studies were conducted. The experimental program consisted of two full-scale partially grouted masonry walls with a h/t of 46 that were tested under combined eccentric axial and cyclic lateral loads. The fixity at the base varied from pinned, partially fixed, and fixed conditions, while the top was roller support during all the tests. Data obtained from the experimental program was used to assess the influence of the rotational base stiffness on the out-of-plane response in terms of strength, stiffness, base damage, and expected failure modes. The numerical study consisted of developing a finite element analysis model of the typical loadbearing slender masonry walls, including the static soil-foundation-structure interaction. The model was validated using the results from the experimental phase and similar studies to predict the global and local behaviour of the walls. The validated model was used in a parametric study to create a database of the wall-foundation interaction effect on the wall response. The database is then used to obtain the equivalent rotational base stiffness from different sizes of strip footings, foundation depths, and soil types. The values of rotational base stiffness were used to perform stability analyses on walls with different h/t ratios to obtain elastic height factors to be used in the design of slender masonry walls. Finally, construction recommendations were proposed to improve the behaviour of the wall-foundation connection.

PREFACE

This thesis includes original research conducted by Alan Alonso Rivers. Two journals and one conference paper have been published/under review/in preparation for publication and were used as the basis of this thesis. The details of the corresponding chapters are summarized below:

A version of Chapter 3 has been published as **Alonso, A.; Gonzalez, R.; Cruz, C.; and Tomlinson, D., *"Pre-test analysis of the effect of rotational base stiffness on loadbearing slender masonry walls"*, in the proceedings of the 14th Canadian Masonry Symposium in Montreal, Canada, 2021.** For the consistency and coherence of this thesis, contents have been modified, removed, or added from the published paper. Alan Alonso was responsible for conceptualization, methodology development, model development, analysis implementation, and paper composition. Rafael Gonzalez and Douglas Tomlinson were involved in the paper composition and revision. Carlos Cruz was in charge of conceptualization, supervision, funding acquisition, and paper revision.

A version of Chapter 4 is under review as **Alonso, A.; Gonzalez, R.; Elsayed, M.; Banting, B.; Guzman, M.; Pettit, C.; Li, Y.; Tomlinson, D.; and Cruz-Noguez, C. *"Experimental testing of tall-slender masonry walls with different base stiffnesses"*, in a journal paper.** For the consistency and coherence of this thesis, contents have been modified, removed, or added from the published paper. Alan Alonso was responsible for conceptualization, methodology development, setup design/construction, experimental testing, data analysis, and paper composition. Rafael Gonzalez and Mahmoud Elsayed were involved in setup–design/construction, experimental test, data analysis, and paper revision. Bennet Banting, Monica Guzman, Clayton Pettit, and Yong Li were involved in the technical paper revision. Douglas Tomlinson was involved in the conceptualization, supervision of experimental tests, paper composition, and paper revision. Carlos Cruz was in charge of conceptualization, supervision of experimental tests, funding acquisition, and paper revision.

A version of Chapter 5 is in preparation as **Alonso, A.; Gonzalez, R.; Elsayed, M.; Billota, M.; Deng, L.; Tomlinson, D.; and Cruz-Noguez, C. *"The effect of the wall-foundation interaction on the out-of-plane flexural response of slender masonry walls"*, in a journal paper.** For the consistency and coherence of this thesis, contents have been modified, removed, or added from the published paper. Alan Alonso was responsible for conceptualization, methodology development, model development, analysis implementation, and paper composition. Rafael Gonzalez, Mahmoud Elsayed, and Miguelangel Bilotta were involved in the paper composition, model development, and revision. Lijun Deng and Douglas Tomlinson were involved in the paper composition and revision. Carlos Cruz was in charge of conceptualization, supervision, funding acquisition, and paper revision.

DEDICATION

To my wife, Leivy, and my daughter, Avril.
Both of you are the reason I keep going and never surrender.
Leivy, thank you for your unconditional support during all these years.
¡Gracias por confiar en mi!

To my mother, Lulú, I would never be who I am without all your sacrifices.
¡Gracias por enseñarme a ser un hombre de verdad!

And especially to my grandmother, Eva†, thanks for all your support and guidance.
You were the faithful personification of a true leader.
¡Gracias por enseñarme que en mi vocabulario no debe exister la frase “No puedo”!

This work would have never been done without all your support and life lessons.
This is for all of you!

ACKNOWLEDGEMENTS

I would like to thank my supervisor, Dr. Carlos "Lobo" Cruz-Noguez, for his patience, support and guidance during my research and when I needed a word of encouragement. I believe that the word "thanks" is too short to express my gratitude. I would like to extend my gratitude to the committee members, Dr. Douglas Tomlinson and Dr. Ali Imanpour, for their guidance, teaching, and invaluable input/feedback to enrich this research. I have learned much from both of you during this journey.

To the wolfpack, but especially to my colleagues and friends, Rafael Gonzalez, Mahmoud Elsayed, Miguelangel Bilotta, and Odin Guzman. Thanks for all the time, knowledge, advice, and hard work you put available when I needed it the most. I am very grateful that I can call you friends – this is priceless!

I would also like to thank the technicians, Greg Miller and Cameron West, for their help in the experimental stage of this work. The full-scale testing outside of the structural lab would not have been possible without your help and full support.

To all the people at Scorpio Masonry in Edmonton, especially Chris Ambrozic, Rob Munro, Louis St. Laurent, Kery Donaghey, and Justin German, for their patience, making everything easier for us to test our tall masonry walls. And, of course, to their experienced masons, Rey, Memo, and Alfredo, who built the full-scale specimens.

Funding for this research has been provided by the Masonry Contractor Association of Alberta (MCAA), the Canada Masonry Design Centre (CMDC), the Canadian Masonry Producers Association (CCMPA), the Natural Sciences and Engineering Research Council (NSERC) Collaborative Research and Development Grant Program, and the Mexican National Council of Science and Technology (CONACYT).

I would never be here without my first opportunity in engineering. Thanks, Ing. Juan Capallera, for your constant encouragement to be a better engineer and person. <u>The beginning</u>!

TABLE OF CONTENTS

LIST OF TABLES

LIST OF FIGURES

1 INTRODUCTION

1.1. Background

Masonry as a construction technique has evolved, mostly empirically, over thousands of years. The first masonry structures were built under the premise that "the more massive the cross-section, the safer the structure will be". This can be noticed through the historical evidence in the most iconic worldwide masonry structures, like the Great Wall of China or the Mesoamerican Pyramids. As the human need for complex structures grew along with structural design knowledge, engineers began to develop allowable stress design considerations for designing masonry structures. However, the same old practice of "massive cross-sections" continued due to the need for a gravity-based design behaviour in unreinforced masonry.

With the advent of reinforced masonry and motivated by the need for design procedures for taller and more slender wall construction, forty-one years ago, the American Concrete Institute (ACI) and the Structural Engineers Association of Southern California (SEASC) published a Test Report on Slender Walls (1982). This report was used as a reference to inform the development of the masonry standards in North America at the time (CSA S304.1-M94 1994, TMS 602-95 1995). Since there have been no significant changes in experimental programs on slender walls conducted after the SEASC (1982) report, the design principles gleaned from that study still influence modern North American masonry design standards (TMS 402-16 2016, CSA S304-14 2019). With new construction technologies that can build taller walls with smaller cross-sections and specialized structural software, the old design principles used in loadbearing masonry walls under out-of-plane loads are losing their competitive edge in tall wall applications.

The current Canadian masonry design standard (CSA S304-14) sets requirements that apply when the effective height-to-thickness ratio $\left({}^{kh}/_{t}\right)$ in flexural loadbearing walls exceeds 30:

- Minimum wall thickness of 140 mm, avoiding raked joints
- Eccentric pin end conditions must be assumed
- Factored axial load is limited to 10% of the effective cross-section capacity
- The steel reinforcement provided must be less or equal to the balanced condition

The problem of designing a loadbearing, masonry tall wall under out-of-plane loads is relatively simple. Due to their slenderness, the design is governed by flexure and, in general, out-of-plane shear is usually not a concern due to the large wall spans. The factored design moments that must be resisted may be significant due to second-order effects leading to a large amount of steel reinforcement being required. However, both masonry design standards (TMS 402-16 2016, CSA S304-14 2019) limit the allowed steel reinforcement. An alternative to providing the required flexural strength consists of using wider blocks, increasing the moment arm in the wall, and reducing the steel reinforcement ratio to be standard-compliant. However, wider blocks are more expensive and make the wall thicker, leading to an economically impractical masonry wall design compared to other systems. The problem could be mitigated by either strengthening or stiffening the wall. Strengthening the wall involves using high-strength material to increase the flexural strength with less steel (Babatunde 2017, Fortes et al. 2018, De Santis et al. 2019), while stiffening techniques reduce second-order moments via the inclusion of pilasters or in-line concealed columns (Entz 2019), and accounting for untapped sources of stiffness (Pettit and Cruz-Noguez 2021, Pettit et al. 2022), such as foundations. Alternative steel configurations, such as near-surface-mounted reinforcement (Sparling et al. 2020, Sparling and Palermo 2023), may be used to increase both strength and stiffness of a wall.

A relatively inexpensive way to stiffen a tall wall is to account for the base stiffness provided by the wall-foundation interaction. However, under the CSA S304-14 (2019), this is not permitted for walls with ${kh}/_{t} \leq 30$ while the TMS 402-16 (2016) does not have such a restriction. The reluctance in the Canadian standard to account for the base stiffness could be due to: (1) the need for simplified and conservative design equations before computers and specialized structural analysis software were more readily available; and (2) the lack of experimental data regarding the degradation at the wall-foundation interface under cyclic loadings. This research project aims to clarify the influence of foundation rigidity on the out-of-plane flexural response of slender masonry walls, proposing effective height factors for design and construction recommendations for tall walls on typical strip footings and common soils.

1.2. Problem statement

Loadbearing concrete masonry walls are an effective structural system for low- to mid-rise structures such as warehouses, industrial buildings, theatres, community centres and school gymnasiums. These walls are usually subjected to combined gravity and out-of-plane loads founded on strip footings. In these applications, it is common to have walls with an effective height-to-thickness $\left({kh}/{t}\right)$ ratio greater than 30, which are susceptible to second-order effects. Therefore, special requirements for these walls exist in North American masonry design standards (TMS 402-16 2016, CSA S304-14 2019).

Many studies (Liu and Dawe 2001, 2003, Liu and Hu 2007, Pettit et al. 2022) have proven how the Canadian standard (CSA S304-14 2019) is conservative when calculating the effective flexural stiffness to account for the slenderness effects on slender walls. Due to this conservatism, engineers use larger moments to design slender masonry walls, translating into more steel required in their cross-sections. To satisfy CSA S304-14 (2019), wider masonry block units are required to ensure a balanced cross-section, which makes the wall uneconomical. A cost-effective solution is to increase the stiffness of the wall and thus reduce the amount of steel required to account for the foundation rigidity. It is evident from the available literature that just a few researchers after the ACI-SEASC (1982) report have accounted for the effect of base stiffness on the out-of-plane performance of masonry walls (Isfeld et al. 2019, Pettit and Cruz-Noguez 2021, Pettit et al. 2022). These studies have shown how implementing base stiffness increases the out-of-plane capacity, decreases the lateral deflections, and consequently reduces the second-order moments.

As a result of these previous studies, there is a need to investigate the influence of foundation rigidity in walls with height-to-thickness ratios greater than 30 with realistic loads and realistic support conditions, aspects that are not entirely covered in previous studies.

1.3. Objectives

This research project aims to clarify the influence of foundation rigidity on the out-of-plane flexural response of slender masonry walls, proposing effective height factors and construction recommendations for tall walls on typical strip footings and common soils.

Three phases were planned to achieve the main goal of this study: experimental, analytical, and assessment. The specific objectives for each phase and the tasks required to complete them are presented.

1. *Experimental investigation of the influence of base stiffness on the out-of-plane response of slender masonry walls to find any material degradation due to cyclic loading.*

Task 1.1.- Design the full-scale specimens representing the standard construction procedures from Alberta and the current Canadian design provision.

Task 1.2.- Pre-test analysis simulation to obtain the eccentric axial load to be applied, the expected lateral pressure resistance, and the expected failure.

Task 1.3.- Design the offsite setup needed to test the full-scale specimens.

Task 1.4.- Test two tall-slender masonry walls under combined eccentric axial load and cyclic uniform lateral pressure using an airbag to simulate a realistic wind load. Variating the base condition for each specimen.

Task 1.5.- Collecting the data obtained from the experimental program to evaluate how the base stiffness affects the out-of-plane performance of the wall.

2. *Developing an analysis model to predict the out-of-plane response of slender masonry walls, including of the static soil-structure interaction.*

Task 2.1.- Developing a finite element model using a macro-modelling approach to capture the overall response of slender masonry walls with different base stiffnesses.

Task 2.2.- Validating the developed model with experimental results from the literature available and using the results from objective (1).

Task 2.3.- Implementing the static soil-structure interaction (SSI) to the model to obtain equivalent rotational base stiffness values from different strip footing geometries, soils, and embedment depths.

Task 2.4.- Parametric analysis using the model developed – including the static SSI interaction and changing key parameters to simulate different wall conditions to create a database.

3. *Assessment of the collected data from the experimental phase and parametric analysis to develop recommendations to include base stiffness in the design of slender masonry walls.*

Task 3.1.- Assessing the collected data from the experimental phase and the parametric analysis.

Task 3.2.- Doing stability analysis to obtain effective height factor "*k*" values according to the foundation conditions.

Task 3.3.- Proposing construction recommendations to improve the behaviour of the wall-foundation connection on typical strip footings and common soil types.

1.4. Scope

This study is focused on evaluating the out-of-plane performance of slender masonry walls to obtain effective height factors for design and construction recommendations. The methods used in this study explore the probable material and instability failures due to the combined eccentric axial load and out-of-plane uniform pressure. This research does not account for the out-of-plane shear failure mechanism. Although uncommon in masonry walls with a height > 2.5 m under out-of-plane loads, which are flexure-dominated, the out-of-plane shear failure should be accounted for on short walls with no axial load subjected to significant out-of-plane loads (e.g., parapets).

The loads considered in this study are the same as those used when designing single-storey buildings in non-seismic areas. The axial loads come from the self-weight of the wall and tributary loads from the roof, and the lateral loads are assumed to be a uniform pressure from the wind.

The so-called "large P-delta" effects are assumed to be small on flexible roof systems subjected to wind loads compared to the large deflections expected on flexible slender walls. Therefore, the experimental setup fully restrains the horizontal displacement at the top of the wall. Neglecting the large P-delta effects for the studied loading case could be considered the worse case scenario. The large P-delta effects coming from the sway of the structure subjected to seismic events are not considered in this study. However, small P-delta effects are considered in this study, which come from the deflected shape of the wall due to external loads (wind loads and roof system) and deflections.

Only partially grouted walls with conventional (low) vertical reinforcement ratios are considered in this study, as these are typical in single-storey masonry buildings. The walls are assumed to be supported by a strip footing under different soil types, footing widths, and foundation depths.

1.5. Organization of thesis

This thesis is organized into six chapters as follows:

Chapter 1: Presents a background to establish a problem statement, and the objectives and scope are discussed.

Chapter 2: Provides a literature review, including masonry wall testing and numerical studies on loadbearing masonry walls.

Chapter 3: Presents the pre-test analysis where a numerical model of the specimen was developed. Results from this analysis were used to design the experimental setup and obtain the adequate loads to be used in the experimental stage. *Taks 1.1 and 1.2 from objective 1 were conducted.*

Chapter 4: Presents the experimental methodology used in the research. Aspects such as specimens and setup details, simulation of base stiffness, loading protocol, and experimental results are discussed. *Tasks 1.3 to 1.5 were conducted to complete objective 1.*

Chapter 5: Presents the development of an analysis model for determining the effect of base stiffness on the out-of-plane performance of slender masonry walls. Static soil-structure interaction, lap-splice zone, and material and geometric nonlinearities are included in the model. Results from this analysis model were used to obtain effective height factors for slender walls on strip footings and common soils. Finally, construction recommendations were proposed to enhance the wall-foundation interaction. *Tasks 2.1 to 2.4 and Tasks 3.1 to 3.3 were conducted to complete objectives 2 and 3.*

Chapter 6: Presents the results and conclusions of the study in addition to recommendations for future research work.

2 LITERATURE REVIEW

2.1. Introduction

Loadbearing masonry walls are an effective structural system in single-storey buildings and are usually subjected to combined gravity and out-of-plane loads. In these applications, it is common to have masonry walls with an effective height-to-thickness ratio greater than 30. The mechanics of these types of walls follow the same principle proposed by MacGregor et al. (1970) for slender concrete columns.

As the slenderness ratio $\left({kh}/{t}\right)$ increases, the axial load capacity of very slender walls decreases due to elastic buckling. However, for more practical wall heights, this decrease is a combination of material failure and stability (inelastic buckling), as illustrated in Figure 2.1. Therefore, accounting for slenderness effects is critical when designing slender masonry walls.

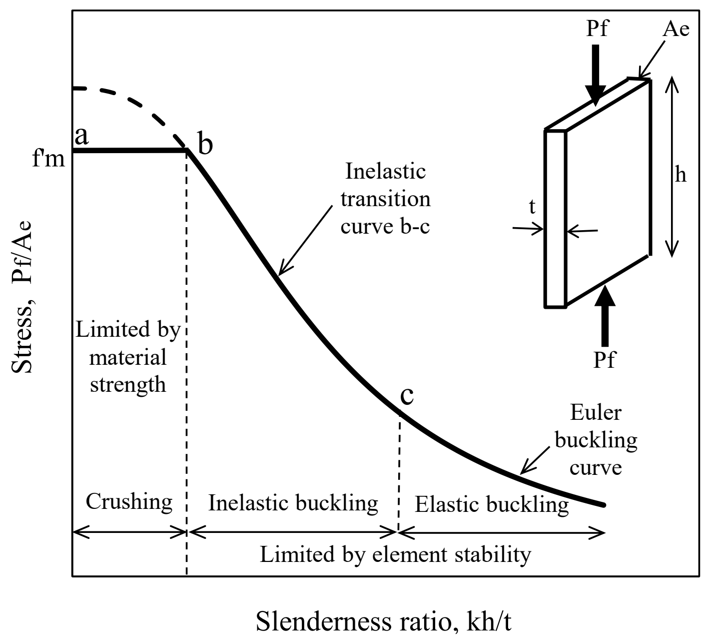

Figure 2.1 – Effect of slenderness on compression capacity of masonry walls (Drysdale and Hamid 2005)

This chapter presents an overview of the design Canadian standard (CSA S304-14 2019) to analyze and design masonry walls with a height-to-thickness ratio equal to or greater than 30, as well as the experimental, analytical, and numerical research efforts to improve the current design methods during the last 53 years.

2.2. Summary of CSA S304-14 masonry provisions

CSA S304-14 (2019) defines thresholds for consideration of slenderness effects on masonry walls and classifies them into three categories:

1) Masonry walls that meet Eq. (2.1) are denominated non-slender walls, and slenderness effects can be neglected since the failure is limited by material strength (Figure 2.1). No special restrictions need to be applied, and values of k can be different than 1 for different cases of boundary conditions (Table 2.1).

$$\frac{kh}{t} < \left(10 - 3.5\left({}^{e_1}/_{e_2}\right)\right) \tag{2.1}$$

Where k is the effective height factor, h is the height of the wall, t is the thickness of the wall, e_1 and e_2 are the small and large virtual eccentricities, respectively, acting at the top or bottom of the wall.

Table 2.1 – Effective Height Factors (*k*) from CSA S304-14 (2019)

		k			
Top	Hinged	0.81	0.91	0.95	1.00
	Elastic	0.80	0.86	0.90	0.95
	Elastic	0.80	0.83	0.86	0.91
	Stiff	0.80	0.80	0.80	0.81
		Stiff	Elastic	Elastic	Hinged
		Bottom			

Note: *For walls with a free restriction at the top but fixed base, k shall be taken equal to 2.*

2) Walls meeting Eq. (2.2) are termed moderately slender walls, and values of k can be different than 1 for different cases of boundary conditions (Table 2.1). Slenderness effects must be accounted for since the failure is limited by a combination of material strength and stability of the element (Figure 2.1).

$$\left(10 - 3.5\left({}^{e_1}/_{e_2}\right)\right) < \frac{kh}{t} \leq 30 \tag{2.2}$$

3) Walls with ${}^{kh}/_{t} \leq 30$ are known as slender walls, and k must be taken equal to 1. Slenderness effects and special provisions must be accounted for in their design.
   - Minimum wall thickness of 140 mm
   - Pinned end conditions must be assumed, inducing symmetrical single curvature
   - Limiting the factored axial load to 10% of the cross-section capacity
   - The maximum steel reinforcement provided shall be less than or equal to the balanced condition given by Eq. (2.3).

$$\frac{c}{d} = \frac{600}{600 + f_y} \tag{2.3}$$

CSA S304-14 (2019) recommends calculating the design moment for very slender walls in the middle of the section. Figure 2.2 illustrates the case of a wall with a pin-pin end condition under out-of-plane uniformly distributed pressure and an eccentric axial load. There are two types of flexural moments acting on that wall: primary moments (M_p), and secondary moments (M_s). The primary moments originate from the external load acting on the wall, such as eccentric axial loads, wind, earthquakes, soil pressure, or applied moments. The secondary moments arise from the deflections due to the first-order moments. Therefore, the total factored moment (M_T) is the sum of the primary and secondary moments shown in Eq. (2.4).

$$M_T = M_p + M_s \tag{2.4}$$

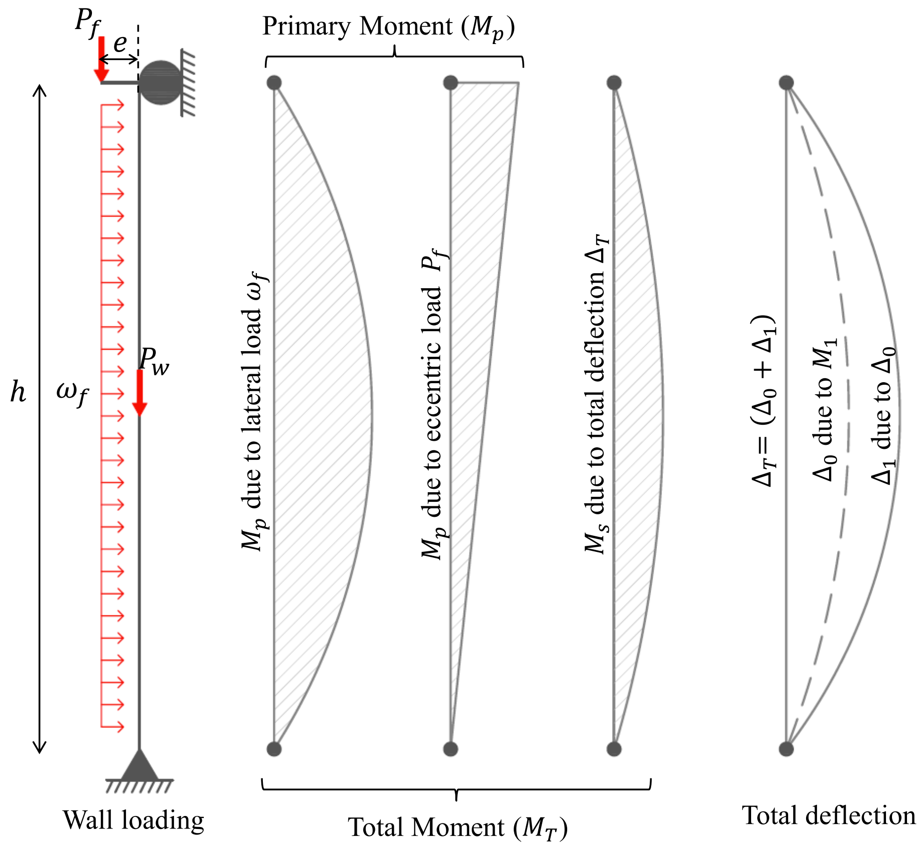

Figure 2.2 – Slender wall loading and moment-deflection correlation

CSA S304-14 (2019) proposed two methods to account for secondary moments: $P\delta$ method and the moment magnifier (MM) method. The $P\delta$ method calculates the secondary moments (M_s) by iteration until convergence is reached, while the MM method is able to obtain the total factored moment (M_T) in a single calculation by Eq.(2.5), making it a more popular choice among designers.

$$M_T = M_p\left(\frac{C_m}{1-\left(\frac{P_f+P_w}{P_{cr}}\right)}\right) \tag{2.5}$$

Where C_m is the equivalent moment diagram factor used to account for different moment distributions for single or double curvature by Eq. (2.6)

$$C_m = 0.6 + 0.4\frac{M_1}{M_2} \geq 0.4 \tag{2.6}$$

M_1 is the smaller factored end moment taken as a negative for double curvature, and M_2 is the larger end moment always taken as positive. The ratio ${M_1}/{M_2}$ maybe taken as 1.0 if the eccentricities e_1 and e_2 are less than or equal to $0.1t$ or when lateral loads contribute more than 50% of the factored primary moment.

P_f is the eccentric axial load, P_w is the wall self-weight above the mid-height, and P_{cr} is a modified version of the Euler buckling load by the CSA S034-14 (2019) using Eq. (2.7).

$$P_{cr} = \frac{\pi^2 \phi_{er} (EI)_{eff}}{(1 + 0.5\beta_d)(kh)^2} \tag{2.7}$$

Where ϕ_{er} is a reduction factor (0.75 for reinforced masonry and 0.65 for unreinforced masonry), which intends to account for the effects of material variability on buckling and deflection calculations and β_d is the creep factor and is the ratio of factored dead load moment to total factored moment, which accounts for the long-term deflections by dividing the effective stiffness by $1 + 0.5\beta_d$, kh is the effective height of the wall, and $(EI)_{eff}$ is the effective flexural rigidity.

$$(EI)_{eff} = E_m \left[0.25I_o - (0.25I_o - I_{cr}) \left(\frac{e - e_k}{2e_k} \right) \right] \tag{2.8}$$

$(EI)_{eff}$ has an upper and lower limit as $E_m I_{cr} \leq (EI)_{eff} \leq 0.25 E_m I_o$.

The modulus of elasticity shall be taken as $E_m = 850 f'_m$, f'_m is the compressive strength of masonry, I_o is the moment of inertia of the uncracked effective cross-section, I_{cr} is the moment of inertia of the cracked cross-section, e is the virtual eccentricity, and e_k is the kern eccentricity.

The problems faced by engineers when designing masonry walls with a slenderness ratio of over 30 are the accurate prediction of the effective flexural rigidity $(EI)_{eff}$ and the effective height of the wall (kh). The estimation of the effective flexural rigidity is complex due to the tensile cracking and the plastic strains present at a nonlinear rate during the loading history of the wall. Although the effective height factor (k) accounts indirectly the effects of boundary conditions in

Eq.(2.7), a realistic prediction of k is challenging since the real boundary conditions at the base of the wall are neither fixed ($k_{fixed} = 0.7$) nor pinned ($k_{pinned} = 1.0$), but some value in between these theoretical values ($k_{fixed} < k_{realistc} < k_{pinned}$). Compensating for these challenges, CSA S304-14 (2019) is relatively conservative, setting special design requirements. For instance, the imposed pinned base condition reflects a more flexible wall in the out-of-plane direction than a wall with a real base condition, increasing the value of M_p. Moreover, due to the conservative, effective flexural rigidity calculation by Eq.(2.8), a larger value of M_T is obtained by amplifying M_p using the Eq. (2.5).

Therefore, when designers calculate the steel needed using the large value of M_T, often the steel obtained does not meet the special requirement imposed by Eq. (2.3). As an alternative to meeting the requirement, thicker concrete masonry units (CMUs) are needed to reduce the reinforcement ratio, ensure ductility in the out-of-plane performance of slender walls and avoid brittle failures. Consequently, the design of masonry walls with a slenderness ratio over 30 is economically impractical compared with other systems.

2.3. Experimental Programs of Masonry Walls

In the 1970s, engineers used stress correction factors or empirical equations to account for slenderness effects in designing slender walls. Yokel et al. (1970) investigated the slenderness effect and axial load eccentricity on slender masonry walls to aim for a rational design method. Sixty reinforced/unreinforced concrete masonry walls of different height-to-thickness ratios ($^{h}/_{t}$) were tested (20, 32, and 40). All walls were tested under axial loads at various eccentricities using fixed-pinned (bottom-top) boundary conditions. As the slenderness ratio increased, the wall presented large displacements under relatively small increases in axial loads. Also, a significant loss of stiffness was observed when the load eccentricity was increased during the test. Even though the flat end condition used in the test resembles a fixed base, a small rotation occurred during the 10 ft (3.05 m) wall test. The deflected shape of these walls was similar to pin-pin end conditions. It was concluded that a relatively minor rotation is associated with a significant loss of end fixity. Results from the test showed that the slenderness and load eccentricity affect the out-of-plane performance of masonry walls, setting the basis for the development of rational design methods for masonry walls under eccentric axial loads.

A year later, Yokel et al. (1971) tested ninety masonry walls of bricks and concrete block units under a combination of axial and out-of-plane loads using an MTS machine and an airbag, respectively, under fixed-pinned (bottom-top) boundary conditions. The specimens were 8 ft (2.40 m) high with a $h/_t$ ratio of 12, and the axial load was concentric. Results from prism testing indicated that the flexural-compressive strength of masonry exceeds the axial compressive strength under large eccentricities. During the assessment of current methods to account for slenderness effects using moment magnification, it was concluded that the tensile cracking of the cross-section should be accounted for to get a reasonable agreement with those observed during testing. The authors proposed an equation for evaluating the flexural rigidity (EI) of masonry walls at failure:

$$EI = E_i I_n \left[0.2 + \frac{P}{P_o}\right] \leq 0.7 E_i I_n \tag{2.9}$$

Where, E_i is the tangent modulus of elasticity and I_n is the gross moment of inertia of the uncracked section. The factor $\left[0.2 + \frac{P}{P_o}\right]$ intends to include the cracking effects in the cross-section. In which P_o is the axial load capacity of the wall, and P is the applied compressive load. Factors such as slenderness ratio and load eccentricity were not considered in Eq. (2.9).

To examine the current theories used to evaluate the strength and factors affecting the performance of concrete masonry walls under combinations of axial loads and bending moments, Hatzinikolas et al. (1978a, 1978b) conducted an experimental study on 68 walls bending in double curvature under pinned-pinned boundary conditions. The wall height varied between 2.40 m and 4.40 m, with $h/_t$ ratios of 12 to 22, and no out-of-plane load was used. The walls were subjected to concentrated moments at each end through an eccentric axial load at the top and by adjusting the pin at the wall base to create an eccentricity. This study proposed adapting the MM method from reinforced concrete methods, introducing the concept of effective stiffness, which attempts to predict the flexural rigidity (EI) of masonry walls based on the cracked cross-section of the specimens. Results concluded that walls tested in double curvature increased their capacity significantly, but their mode of failure was more brittle than single curvature walls. The author proposed Eq. (2.10) to capture the flexural rigidity (EI) of concrete masonry walls, incorporating similar factors to those recommended for concrete design.

$$E_m I = E_m I_o \left[\frac{1}{2} - \frac{e}{t}\right] \geq 0.1 E_m I_o \tag{2.10}$$

Where, E_m is the modulus of elasticity, I_o is the uncracked moment of inertia, e is the load eccentricity, and t is the wall thickness. Additionally, it was proved that the moment of inertia of a cracked wall section could be approximated by Eq.(2.11).

$$I = 8\left[\frac{1}{2} - \frac{e}{t}\right]^3 I_o \tag{2.11}$$

Due to the market demand for taller walls, concerns about the stability and failure modes of slender masonry walls have increased. The American Concrete Institute (ACI) and the Structural Engineers Association of Southern California (SEASC) tested 30 full-scale wall panels to address these concerns (1982). Nine of the thirty wall panels were built using Concrete Masonry Units (CMUs) with h/t ratios of 29, 36, and 48 (Figure 2.3). The wall panels were tested under combined eccentric axial and lateral loads with pinned-pinned boundary conditions. Findings from this study led to the determination of allowable deflection limits for masonry walls, confirmed the adequate ductile response of under-reinforced masonry walls, and established safe limits on axial loads. This report was used as a reference to inform the development of the following masonry standards in North America (CSA S304.1-M94 1994, TMS 602-95 1995).

Figure 2.3 – Experimental setup and specimens ready to be tested (1982)

In 1994, CSA S304.1-M94 (1994) introduced Eq. (2.8) to obtain the effective flexural rigidity $(EI)_{eff}$ to include the slenderness effects when applying the $P\delta$ method or Moment Magnifier (MM) method in the design of masonry walls. The same equation is still used in the current Canadian design standard (CSA S304-14 2019).

A few years later, Liu et al. (1998) conducted an experimental program testing 72 full-scale concrete masonry walls subjected to eccentrical axial loads to accurately obtain flexural rigidity. The specimens were 800 mm wide, 1200 mm high, and 150 mm and 190 mm thick. The flexural rigidity was obtained based on the moment-curvature relationship using the strain reading during the experiment. Results showed no reduction in the modulus of elasticity while the stress-strain relationship of masonry remained linear. When the stress-strain relationship of masonry became nonlinear under high axial loads, a reduction in flexural rigidity was observed due to cracking. Two equations were proposed from the database generated by the experimental results.

$$EI_{eff} = 0.7E_m I_o \quad for \quad 0 \leq \frac{e}{t} \leq 0.18 \tag{2.12}$$

$$EI_{eff} = 2.7E_m I_o e^{-7.5\left(\frac{e}{t}\right)} \geq E_m I_{cr} \quad for \quad \frac{e}{t} > 0.18 \tag{2.13}$$

Where, E_m is the modulus of elasticity, I_{cr} is the cracked moment of inertia, I_o is the gross moment of inertia, and e is the axial load eccentricity.

After neglecting the presence of lateral loads, Liu and Dawe (2001) tested another set of thirty-six reinforced concrete masonry walls under combined axial and lateral loads in pin-pin boundary conditions. The specimens had the same geometry as the previous experimental program but included vertical reinforcement in a single or double layer. The purpose of this new set of walls tested is the same as the previous one, obtain flexural rigidity, but this time include steel reinforcement and the combined action of vertical and lateral loads. The effective flexural rigidity was obtained by Eq.(2.14). using the strain values recorded during the test at the tension and compression faces of the wall,

$$EI = \frac{M}{\phi} \tag{2.14}$$

Where M is the applied moment, ϕ is the curvature $\phi = \frac{\varepsilon_1 - \varepsilon_2}{t}$ (ε_1, ε_2 are the strains at the tension and compression faces of the wall, and t is the thickness of the wall).

This study showed that the lateral load capacity increased when the vertical load was increased to 60% of the pure axial load capacity. However, when the vertical load was increased beyond that point, it caused a decrease in the lateral load capacity. The experimental values of flexural rigidity obtained were larger than those estimated by the CSA S304.1-M94 (1994), concluding that the code procedure is conservative when walls fail primarily by compression.

To achieve superior structural performance on SMWs under out-of-plane and gravity loads, Amrhein (1998) proposed altering any of the following factors: Higher-strength units, placing the rebar closer to the face-shell, and implementing the inherent base fixity from the proper connection between the wall and foundation. The implementation of any of these could increase the strength or stiffness of the wall, decreasing the lateral deflection and consequently reducing the second-order effects, resulting in steel reinforcement or wall thickness reductions.

Sparling et al. (2020, 2023) explored reinforcement arrangement through near-surface mounted (NSM) reinforcement to strengthen the wall. This technique is commonly used to retrofit unreinforced masonry walls and consists of making some notches in the external faces of the wall to place the rebars using mortar. The experimental program consisted of four reinforced masonry walls with different cross-sections: 1) Fully grouted (FG) with conventional reinforcement, 2) FG with NSM reinforcement, 3) Partially grouted (PG) with conventional reinforcement, and 4) Hollow section with NSM reinforcement. The specimens were 3,200 mm tall, 1,200 mm wide, and 190 mm thick, with a $h/_t$ ratio of 16.8. The walls were tested under combined vertical and cyclic lateral loads on a pin-pin condition (Figure 2.4). Results of this study showed that the stiffness of the walls with NSM reinforcement was equivalent to the walls conventionally reinforced under low applied loads. When loads reach the yielding point, the walls with NSM reinforcement exhibited twice the stiffness of the walls with conventional reinforcement.

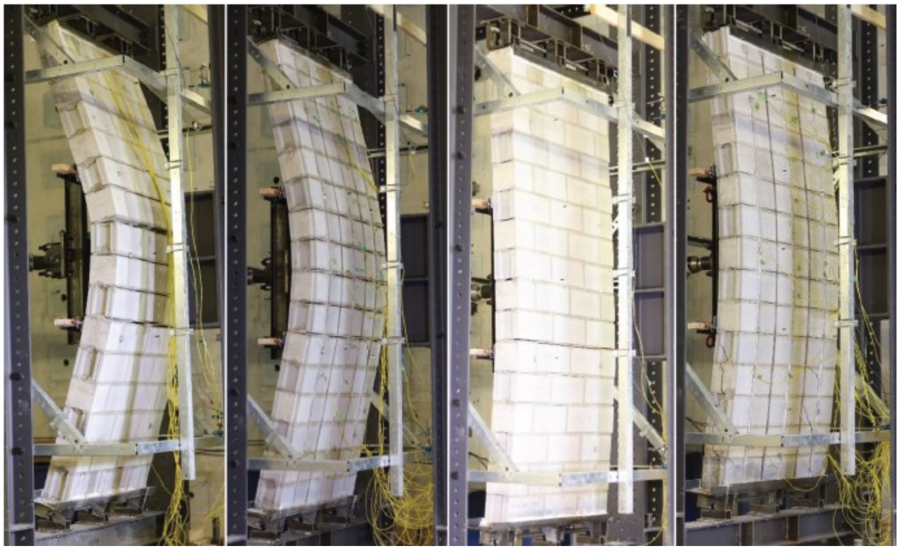

Figure 2.4 – Deflected shape of specimens tested (Sparling et al. 2020)

A few years later, Sparling and Palermo (2023) brought NSM reinforcement to tall masonry walls. The experimental program consisted of four reinforced masonry walls, two of them were PG walls with conventional reinforcement, and the other two were hollow walls with NSM reinforcement. The specimens were 7,800 mm tall, 1,200 mm wide, and 190 mm thick, with a $h/_t$ ratio of 41. The walls were tested under combined vertical and cyclic lateral loads under a pin-pin condition. The results were similar to the previous experimental study of the authors, finding that the NSM reinforcement increases the moment capacity of the cross-section as well as increases the stiffness of the wall, resulting in lower out-of-plane displacements, which reduce the second-order effects and increase the out-of-plane resistance and ductility compared with the walls with conventional reinforcement. Although this alternative is great for retrofitting damaged walls, this technique has disadvantages when constructing new walls. For instance, rebars are exposed to weather conditions or fire, modification on blocks could increase the cost, and consideration of mechanical connectors and possible rebar buckling when walls are too high.

A few studies of walls with non-zero rotational base stiffness have shown how base stiffness significantly affects out-of-plane wall behaviour. Mohsin (2005) was a pioneer in investigating the role of base stiffness on slender loadbearing masonry walls. The experimental program consisted of eight slender masonry walls with different base stiffnesses (0, 1,000, 5,000, and 10,000 kN-m/rad) under eccentric axial load. The specimens were divided into 2 groups of 4 walls, 5 m tall and 6 m tall ($h/_t$ ratios of 28.6 and 33.9, respectively). This study showed how the presence of base stiffness significantly reduced the second-order effects by limiting the deflection, thus increasing the loadbearing capacity of the wall. Pettit et al. (2022) noted that as the level of rotational base stiffness was increased, the increase in load-carrying capacity began to diminish since the base stiffness was approaching the fixed condition, which acts as an upper limit. This means that even with a small base fixity value, the out-of-plane behaviour of walls tends to emulate the fixed base condition. The effective flexural rigidity calculated during the tests was compared to the values obtained from the North American Standards (TMS 402-16 2016, CSA S304-14 2019), concluding that the standard is overly conservative. The values obtained from the experimental program were up to 12-times larger than the Canadian standard, much more conservative than the US standard. It is noted that the study did not investigate the effect of the combined eccentric axial and out-of-plane loads, which is a typical load combination on these types of walls.

To understand the degree of fixity at the base of the wall, which is not usually designed to ensure a moment connection, Isfeld et al. (2019) tested three PG walls with pinned and fixed base conditions under vertical load and combined vertical-lateral loading. The specimens were 2,400 mm tall, 1,200 mm wide, and 190 mm thick with conventional reinforcement (2-15 @600 mm). The study indicated that walls tested under a pinned base condition exhibit significantly more deflections than those with a fixed base. When the wall was subjected to pure axial load, the maximum deflection ratio $\left[\frac{\Delta max_{pin}}{\Delta max_{fix}}\right]$ was 4.3, while the maximum deflection ratio increased to 8.2 when the loading protocol changed to combined axial-lateral loads. The latter indicates how base fixity has a more pronounced effect on decreasing the lateral displacements on walls subjected to lateral loads than on walls subjected to purely axial loads. This study demonstrated that although no additional measures were used to ensure a moment connection at the wall base compared to typical construction practices, a double curvature deflected profile was obtained when the support was not forced to be a pin. Since the $h/_t$ ratio of the specimens was 12.6, the slenderness effects were not a significant factor in this study. Additionally, the degradation at the base of the wall due to cyclic loading was not explored.

Pettit and Cruz-Noguez (2021) tested four masonry walls under gravity and cyclic lateral loading with different rotational base stiffnesses (2,300, 5,000, and 9,500 kN-m/rad) to capture any possible degradation at the wall base (Figure 2.5). The specimens were PG walls with conventional reinforcement (2-15M @600 mm), 2,400 mm tall, 1,200 mm wide, and 190 mm thick, with a slenderness ratio of 12.6. The effect of rotational base stiffness on loadbearing walls was significant when comparing loadbearing capacity and midspan deflection with pinned base walls. The increase in loadbearing capacity seems to be due to the change of moment distribution, which occurs in walls with rotational base stiffness. Degradation of the base fixity under cyclic loading was not significant because no visible damage was observed at the base of the wall prior to failure. The findings presented in this study are limited to moderately slender walls. Thus, there is a need to investigate the influence of base stiffness on walls with a slenderness ratio of over 30.

Figure 2.5 – Experimental setup and wall specimen to be tested (Pettit and Cruz-Noguez 2021)

2.4. Numerical Modelling of Masonry Behaviour

The experimental programs have laid the groundwork for the present knowledge of masonry. However, executing a comprehensive experimental program frequently faces economic, time, and practical constraints. Numerical modelling has emerged as an excellent solution to overcome the constraints presented in the experimental programs by providing reliable and cost-effective predictions of complex global and local behaviours.

Numerical modelling of masonry walls using the finite element (FE) method can be generally divided into micro- and macro-modelling. The micro-modelling approach explicitly models the interaction among the masonry units, mortar, and grout. This alternative effectively captures the local behaviour of masonry walls, but it is more computationally expensive. The macro-modelling approach treats the masonry assemblage as a homogeneous material, with no distinction between the masonry units, mortar, or grout. This alternative effectively captures the global behaviour of masonry walls with a lower computational cost, but it is limited when trying to capture detailed modes of failure.

2.4.1. Micro-modelling

Page (1978) was a pioneer in using a micro-modelling approach on brick masonry walls subjected to in-plane loads. The author used 8-node plane stress continuous elements assuming isotropic elastic properties to simulate the masonry units, while nonlinear linkage elements were used to simulate the mortar joints. The stiffness matrix was derived from relative displacement vectors in the normal and shear directions. Unfortunately, the failure criteria were not defined, and the model could not capture the ultimate loads.

Later, Ali et al. (1986) implemented a local failure criterion for the joint and brick masonry elements. The model was developed using 2D plane stress elements, and three failure criteria were defined: (1) fracture of mortar under tension-compression or tension-tension states of stress, (2) crushing of the brick under compressive stresses, and (3) bond failure at the interface of the joint and brick elements. The model was validated with experimental results available at the moment showing good agreement.

Sayed-Ahmed and Shrive (1995) developed a more rigorous finite element model for 7-course height masonry wallets. The model used 8-node shell elements, the interaction between the masonry unit and the mortar joint was simulated by 3D continuous elements, and geometric and material nonlinearity was considered (elasto-plastic behaviour was assumed for the mortar and masonry). The numerical results had a good agreement compared with the experimental results of the 7-course height wallets. A difference from previous numerical models, this model was able to capture the failure of the specimens based on the appearance of cracks and instability effects.

Lotfi and Shing (1994) developed a finite element model of unreinforced masonry walls using interface elements in the mortar joints, while the smeared crack approach was used in the masonry assemblage. This model was able to accurately predict the shear behaviour of the mortar joints. Using interface elements was reported to be an efficient approach to predicting the loadbearing capacity of masonry walls and identifying local failure modes.

Yi and Shrive (2001) developed a 3-D finite element model for unreinforced masonry walls, separately modelling the masonry units, mortar joints, and grouted cores. The mortar joints and masonry units were modelled using shell elements, while the grouted courses were modelled using solid elements. Also, the cracking propagation was modelled with a smeared crack approach. The model was able to capture failure modes related to progressive cracking propagation, web-splitting, and crushing of mortar joints, showing moderate agreement with previous experimental results.

2.4.2. Macro-modelling

Wang et al. (1997) developed a macro model for tall cavity masonry walls using beam-column elements available in the commercial software ABAQUS. The masonry was treated as homogenous using a predefined concrete material model available in the software, with the ability to capture tensile cracking with a linear tension softening branch. The Newton-Raphson algorithm was used with a load control protocol until the peak load was reached. After the post-peak load, the analysis changed to a modified risk algorithm to capture the softening of the wall. The model predicted the masonry behaviour when the numerical results were compared.

Lopez et al. (1999) proposed a homogeneous masonry element to account for the anisotropic nature of the material. The main feature of this model was the precise prediction of cracking propagation in all directions with greater computational efficiency compared with other micro-models. To reduce the computational cost considerably, the authors used the theory of mapped spaces to transform the anisotropic behaviour of the masonry into an isotropic space based on a modified Mohr-Coulomb criterion. The model showed a good correlation with the experimental results during the validation process. Although the model was unable to predict the fracture mechanism of the masonry, this model was the basis for practical modelling approaches for large-scale masonry structures.

Another homogenization technique to model masonry elements was proposed by Ma et al. (2001). The authors introduced a representative volume element (RVE) to capture the equivalent elastic properties, strength, and failure modes of masonry assembly. An equivalent stress-strain relationship for the RVE was proposed based on the constitutive relationships of masonry units and mortar. Three modes of failures were defined in the numerical model: (1) tensile failure of the mortar, (2) combined shear failure of brick and mortar, and (3) crushing failure of the brick.

The model reported an excellent alternative to model walls subjected to in-plane loads; however, it is not recommended for walls under out-of-plane loads.

Using a macro-modelling approach, Liu and Dawe (2003) developed an analytical model to perform a parametric analysis on the effective flexural rigidity of loadbearing masonry walls. The masonry wall was idealized using beam-column elements and accounting for material and geometrical nonlinearities. The analytical and experimental results from Liu and Dawe (2001) showed an excellent correlation. This model demonstrated the effectiveness of developing simplified numerical models based on moment-curvature relationships for flexural masonry walls.

Dona et al. (2018) modelled two cantilever reinforced masonry walls using the open-source software framework (OpenSees). The fibre-based model was used to account for a distributed material nonlinearity, while the corotational transformation was used to account for the geometrical nonlinearity. The material model *Concrete02* was used to simulate the homogenized masonry assemblage with a failure criterion based on the maximum masonry strain. The validation of the model and the parametric study showed the effectiveness of fibre-based section models to evaluate the performance of reinforced masonry walls.

Pettit (2019) developed a mechanic-based model to predict the out-of-plane behaviour of loadbearing walls, accounting for the presence of rotational base stiffness ($0 < RBS < \infty$). The model is based on the differential equation governing the displacement of elastic beam-column elements under combined axial and distributed lateral load, including the material and geometrical nonlinearities through a fibre-section approach. The model was able to capture a good agreement on the load-displacement response of previous experimental studies and predict the material or stability failure in masonry walls.

Metwally et al. (2022) developed a finite element model using OpenSees to investigate the probabilistic behaviour of reinforced masonry walls under out-of-plane loads. The model used displacement-based fibre beam-column elements. The behaviour of the masonry assembly was simulated using the material model *Concrete02* while the reinforcement steel was simulated using the material model *Steel01* (Figure 2.6). To validate the numerical model, the experimental results from the ACI-SEAC (1982) report showed reasonable accuracy in predicting the overall load-displacement behaviour. The probabilistic analysis showed that the randomness in bar location, related to construction quality, significantly contributes to the scatter of load capacity in slender walls.

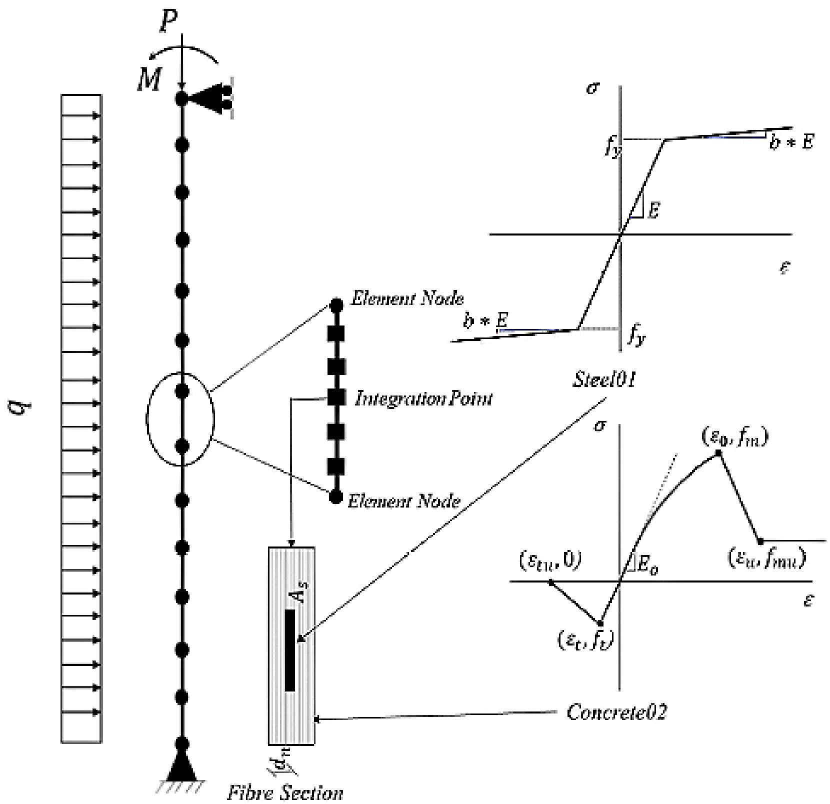

Figure 2.6 – Schematic drawing of the numerical model (Metwally et al. 2022)

2.5. Soil-Structure Interaction (SSI) in Masonry Structures

Fixed or pinned bases are boundary conditions commonly used in numerical/analytical models for simplicity. However, the structural response under static/dynamic loads can be influenced (beneficially or detrimentally) by the interaction among the superstructure, substructure, and underlying soil. This interaction is known as the soil-structure interaction (SSI). In practical designs, it is not common to account for the SSI effects due to the lack of unified guidelines and the belief that SSI is always beneficial (Bapir et al. 2023). Therefore, this simplification could lead to under- or over-designs.

There are two main approaches to evaluating the SSI (2012): (1) the direct analysis and (2) the substructure approach. The (1) direct analysis represents the soil as a continuum using a micro-modelling approach and interface elements to connect the soil mesh and the foundation (Figure 2.7). This method is more detailed for complicated geometries and soils, giving a wide range for solving SSI problems. However, it is rarely used in practice due to its high computational cost and complexity. The (2) substructure approach consider the soil and structure responses separately, and using superposition principles, the final structural response, including the SSI, is obtained. The procedure of this method is divided into three main steps: (i) obtaining the foundation input motion (FIM), (ii) obtaining the impedance functions that define the stiffness and damping of the soil domain to be used in a macro-modelling approach (Figure 2.7), and (iii) calculating the response of the structure using the impedance functions and the FIM.

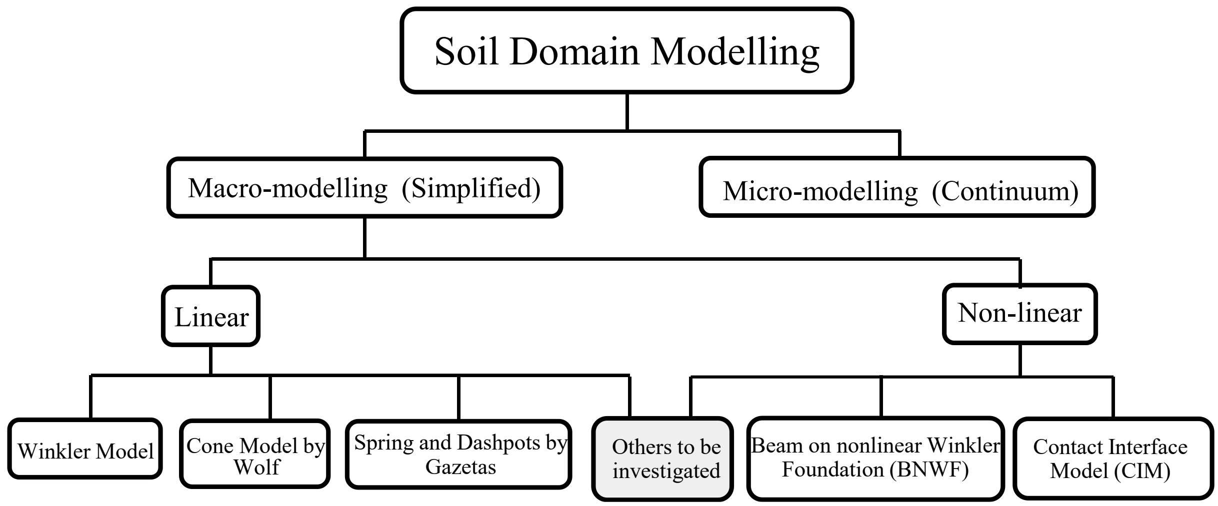

Figure 2.7 – Soil domain modelling techniques (Bapir et al. 2023)

Due to the detail of the required structural response, researchers opt to model the soil domain as a continuum (Masia Mark J. et al. 2004, Güllü and Jaf 2016, Piro et al. 2020, de Silva 2020, Fathi et al. 2020). On the other hand, the macro-modelling approach is used more often to model the soil domain if the simplified model is enough for the required structural response. For instance, Petti et al. (2021, 2022) developed a linear-elastic Winkler model of a strip footing to obtain the out-of-plane rotational stiffness for different sizes of strip footings and soil types (Figure 2.8). The soil-foundation interaction was captured by defining elastic springs along the bottom edge of the foundation with a tributary vertical stiffness to each spring. Analyzing the possible combinations, the rotational stiffness values from the analysis provided range from 1,500 to 12,000 kN-m/rad from where 2,300, 5,000, and 9,500 kN-m/rad were selected to be used in their experimental program.

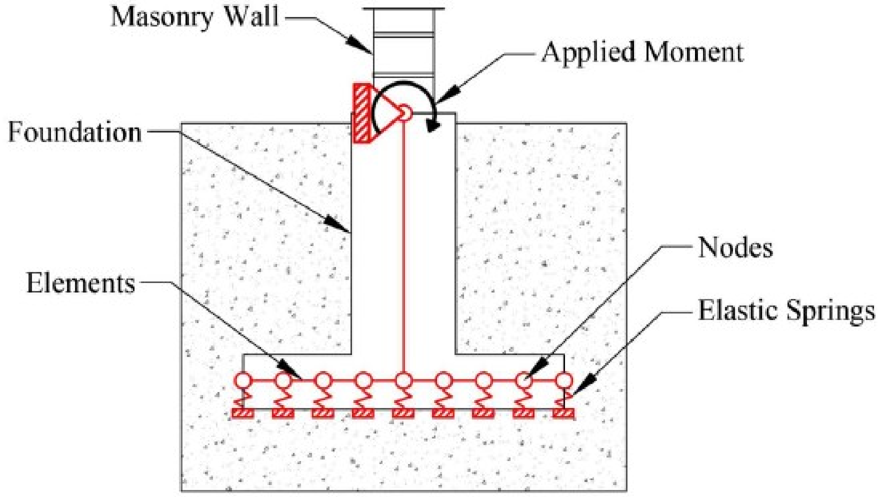

Figure 2.8 – Finite element foundation model (Pettit et al. 2022)

2.6. Gaps in research

Based on the survey and analysis of the literature review presented in this chapter, there is a need to investigate the accuracy of the flexural stiffness and influence of foundation rigidity in walls with height-to-thickness ratios greater than 30 and re-evaluate the conservative special design requirements by CSA S304-14 (2019).

Even though the previous studies on base stiffness demonstrated the benefits of accounting for it, some important factors for the out-of-plane behaviour of slender walls have not been considered. For instance, Mohsin (2005) did not investigate the effect of combined axial and out-of-plane loads, a typical load condition on loadbearing walls. Walls tested by Isfeld et al. (2019) were limited to *h/t*= 12.6, making slenderness effects insignificant, and the base degradation under cyclic loading was not explored. Pettit and Cruz-Noguez (2021) used a three-point bending configuration at midspan to apply the lateral load, which may not accurately represent a lateral pressure due to wind loads, and the slenderness effects were not significant because of the low value of *h/t* (12.6). While the parametric analysis of the soil-foundation interaction for different types of soils and strip footing sizes did not account appropriately for the embedment, and the soils were modelled in the linear-elastic range.

This study aims to provide experimental data on the effect of the rotational base stiffness on the out-of-plane response of slender masonry walls and any possible degradation at the wall-foundation connection under repeated loads. Two full-scale specimens were tested under a combination of gravity and lateral loads using different base stiffnesses, including the high slenderness ratio, realistic load combinations, and realistic support conditions – aspects not entirely covered in previous studies. Results were analyzed to study the wall capacity, deflected shapes, moment profiles, flexural capacity, and material degradation at the wall base. Additionally, a parametric analysis was developed to provide data on the effect of the soil-structure interaction on masonry walls with different height-to-thickness ratios, soil types, foundation widths, and foundation depths. Results from the parametric analysis were analyzed to obtain the equivalent rotational base stiffness for all possible combinations. The equivalent rotational base stiffness was used in stability analysis for different height-to-thickness ratios to obtain effective height factors k. Finally, providing construction recommendations for slender masonry walls on strip footings and common soil types.

3 PRE-TEST ANALYSIS OF THE EFFECT OF ROTATIONAL BASE STIFFNESS ON LOADBEARING SLENDER MASONRY WALLS [1]

Slender masonry walls with a slenderness ratio over 30 are widely used in Canada in single-storey buildings. However, the design of these walls tends to have stringent limits and requirements under the Canadian masonry standard (CSA S304-14). One of those requirements is neglecting the base stiffness provided by the foundation despite its inherent rotational base stiffness. This concern is based on the potential for plastic hinge formation near the base due to the concentrated rotational demand. Due to the limited information on this topic, there is a need to investigate the structural performance of slender masonry walls by accounting for base stiffness. A numerical simulation was used to obtain the expected out-of-plane performance of slender masonry walls with pinned base and different rotational base stiffness conditions. The same height-to-thickness ratio, loads, and reinforcement ratio were used to compare their performance. This pre-test analysis was used to design the experimental setup and obtain an adequate load for the specimens to be tested in the experimental stage. Moreover, the experimental results from the next stage and the parametric analyses will generate design recommendations regarding permissible slenderness ratios, axial load levels, and ductility requirements.

3.1. Introduction

The design of masonry walls with an effective height-to-thickness ($^{kh}/_{t}$) ratio over 30 tends to have stringent limits by the Canadian masonry standard code (CSA S304-14 2019). Design provisions require ductile behaviour with significant deformation before the masonry crushing, not buckling failure. To meet this performance, slender masonry walls often require thicker blocks and more steel reinforcement, making them economically impractical. Moreover, the wall must be designed assuming a pinned condition at the base, neglecting the base stiffness provided by the foundation. This assumption is based on the expected degradation of the masonry near the wall base due to the concentrated rotational demand under cyclic loads. This simplification could lead to underestimating the real capacity of slender masonry walls.

[1] A version of Chapter 3 has been published as Alonso, A.; Gonzalez, R.; Cruz, C.; and Tomlinson, D., "Pre-test analysis of the effect of rotational base stiffness on loadbearing slender masonry walls", in the proceedings of the 14th Canadian Masonry Symposium in Montreal, Canada, 2021.

Since 1980, there has been no innovation in slender masonry walls when the American Concrete Institute (ACI) and the Structural Engineers Association of Southern California (SEASC) created a Test Report on Slender Walls (1982). Thirty full-scale, reinforced concrete and masonry walls with pinned-pinned conditions were tested under combined axial and lateral loads. Nine of the 30 panels were built using concrete masonry units (CMU) with 29, 36, and 48 slenderness ratios. This report was used as a reference to develop the following Canadian masonry design standard (CSA S304.1-M94 1994) until the current one (CSA S304-14 2019). Therefore, the stringent limits placed on slender masonry wall design codes seem to come from the ACI-SEASC report (1982).

To achieve superior structural performance on tall masonry walls under out-of-plane and gravity loads, Amrhein (1998) proposed altering any of the following factors: using higher-strength units, placing the rebar closer to the face-shell, and accounting for the inherent base stiffness from the proper connection between the wall and foundation. When accounting for the base stiffness, the slender masonry walls would increase their flexural stiffness, decreasing the lateral deflection and reducing the second-order effects. This could lead to reductions in steel reinforcement or a reduction in the wall thickness. In many cases, slender masonry walls with a slenderness ratio over 30 require a wall thickness of up to 300 mm to comply with code requirements. Reducing the wall thickness to 200 mm or even 250 mm will lead to more economical wall designs while maintaining satisfactory strength and reliable structural performance.

Mohsin (2005) was a pioneer in testing loadbearing tall walls simulating the rotational base stiffness provided by the foundations since most of the studies were tested using a pin condition at the base. Eight full-scale slender masonry walls were tested under an eccentric axial load, significantly reducing the second-order effects and incrementing the loadbearing wall capacity. Also, the effective flexural rigidity was obtained and compared with the calculated using the CSA S304.1-M94 (1994), showing that the Canadian standard obtained conservative values. However, Mohsin's (2005) study was limited to eccentric axial loads neglecting the out-of-plane loads. Therefore, Pettit (2019) investigated the effect of the rotational base stiffness on masonry walls combining gravity and out-of-plane loads. Four moderately slender masonry walls were tested, and it was concluded that the effect of the rotational base stiffness on loadbearing masonry walls increases the wall capacity. Nevertheless, these walls were not susceptible to the second-order effect, the presence of which will decreases the wall capacity.

As a result of these previous studies, there is a need to compile, review, and process the data of slender masonry walls generated in the last 40 years to take advantage of modern construction/design practices and better understand their structural performance using a real base condition. The first stage is this numerical study, obtaining the loads used in the experimental stage. Moreover, a small parametric analysis was conducted to compare the performance of slender masonry walls between the pinned base condition and the non-zero rotational base stiffness, using the same slenderness ratio, loads, and reinforcement ratio.

3.2. Numerical Model

The numerical model was developed using the Open System for Earthquake Engineering Simulation (OpenSees) open-source software (McKenna et al. 2000). A nonlinear finite-element (FE) 2D model was created using a macro-modelling approach (Figure 3.1). This model consists of a masonry wall subdivided into 30 nonlinear beam-column type elements using a fibre section with distributed plasticity. The top of the wall is restrained along the X direction in the global axis and free in the Y direction and rotation. The base of the wall is restrained in the X and Y global axes and free rotation or non-zero rotational stiffness.

The material nonlinearity was reproduced using the uniaxial stress-strain models from the OpenSees library. The longitudinal steel reinforcement was simulated using the material model *Steel02* with isotropic strain hardening based on the Guiffre-Menegotto-Pinto (1973) model. The homogenous behaviour of the masonry assembly was simulated using the material model *Concrete02* based on the Kent-Scott-Park (1971) model. The proposed model by Priestley and Elder (1983) was adopted in this study to calculate the ultimate stress of the masonry fibres; the maximum compressive strength was assumed to happen at a strain of 0.002. Moreover, the maximum tensile strength of the masonry was assumed to be 0.65 MPa, linear elastic until cracking and linear tension softening.

The macro-model of the slender masonry wall was analyzed using a push-over analysis where an eccentric axial load is applied at the top of the wall. After the load is fully applied and sustained, the lateral load is applied along the height of the wall until the target displacement at midspan is achieved. The second-order effects are considered by using the geometric transformation law available in the OpenSEES library (*corotational transformation*). A zero-length element is used to recreate the rotational base stiffness when a non-zero base stiffness is required.

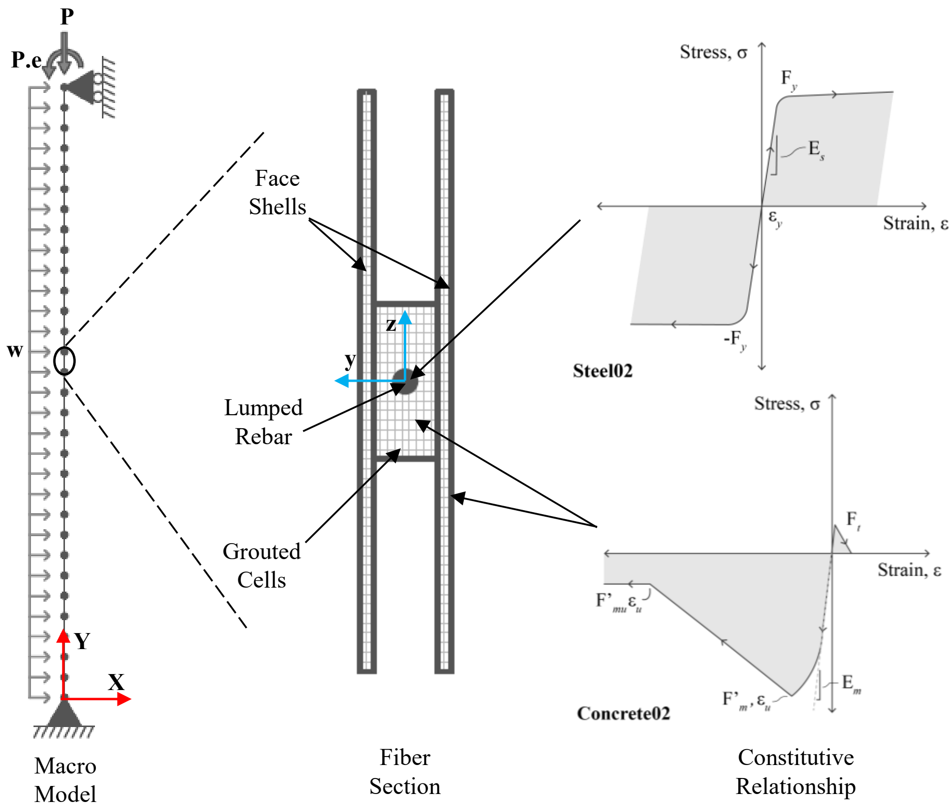

Figure 3.1 – Masonry wall macro-model (global axes: red; local axes: blue)

3.2.1. Model validation

Two experimental tests with different loading protocols were used to validate the model predictions. The first study used was the Test Report on Slender Walls (1982) by the ACI-SEASC. Although this report was developed more than 40 years ago, it is still one of the most commonly used as a reference on tall wall studies. Nine fully grouted (FG) reinforced-masonry tall walls were tested under combined eccentric axial load and uniform out-of-plane lateral pressure applied using an airbag. Only four of the nine panels were compared in Figure 3.2. The second study used to validate the model was conducted by Mohsin (2005) at the University of Alberta. Two groups of four partially grouted (PG) reinforced-masonry walls with slenderness ratios of 28.6 and 33.9 were tested under an eccentric axial load on the top of the specimen. Only two of the eight panels were compared in Figure 3.3. In both cases, a reasonable correlation is observed when comparing the experimental results against the model prediction.

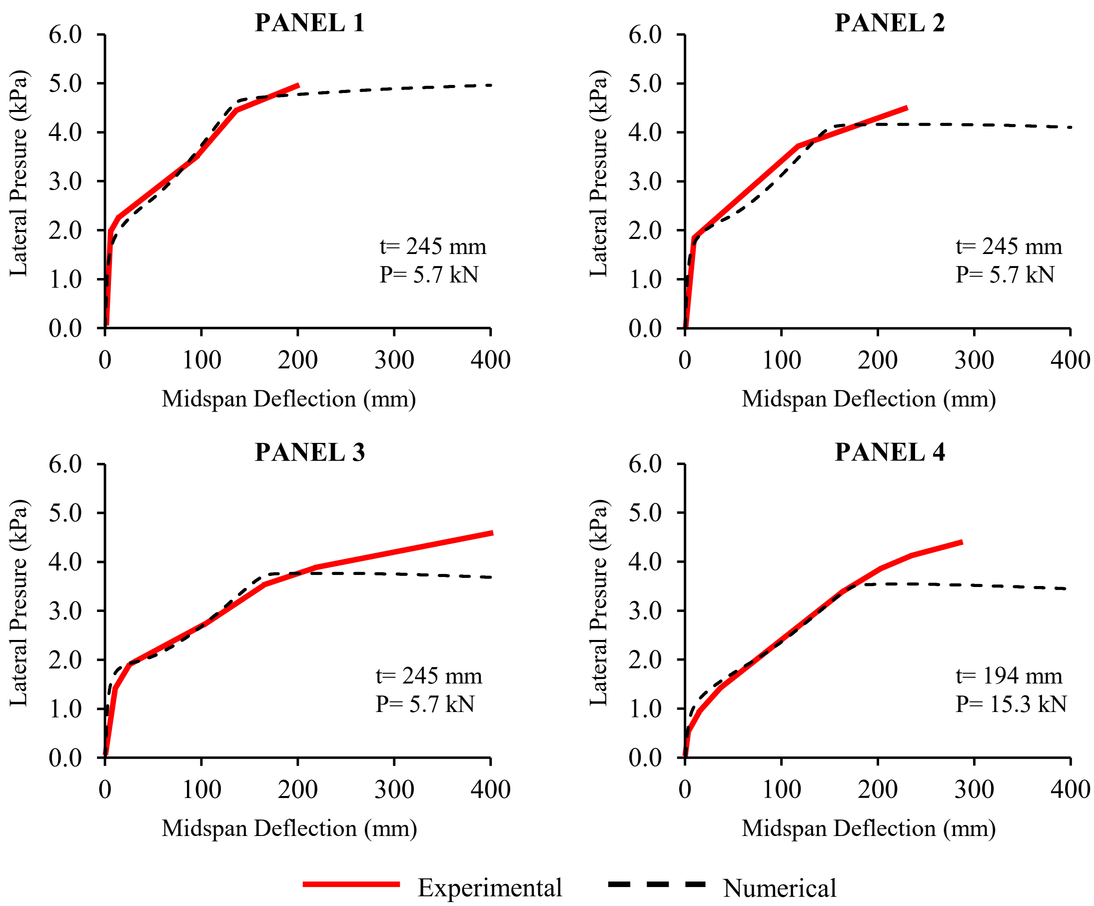

Figure 3.2 – Model validation using the Test Report on Slender Walls (1982)

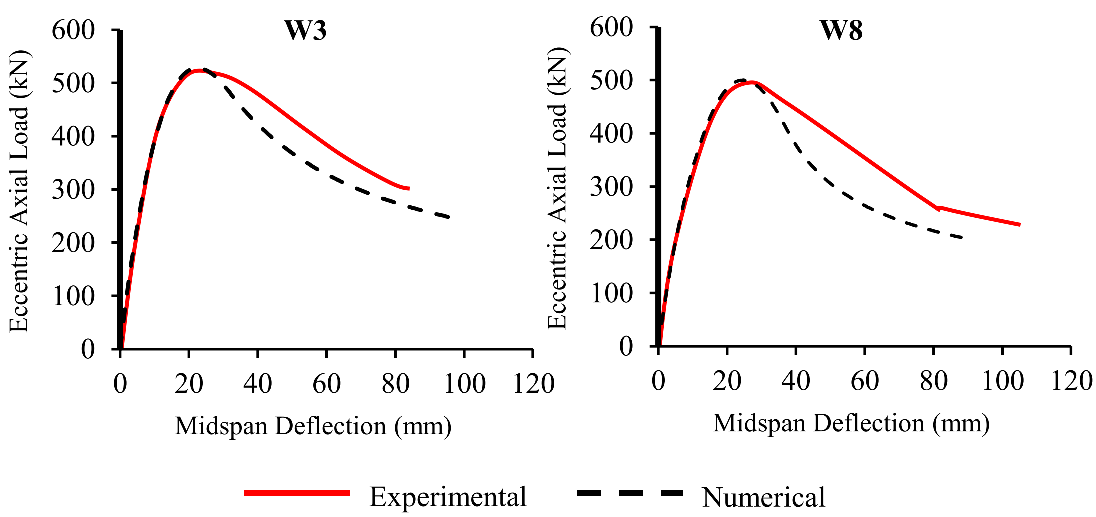

Figure 3.3 – Model validation using Mohsin's (2005) experimental results

3.3. Specimen analysis

A parametric analysis of the control specimen proposed for the experimental stage was conducted in this study. The objective was to obtain the optimal eccentric axial load to be applied because slender walls are susceptible to second-order effects and can fail due to instability. Also, it is crucial to establish a limit to stop the test because it could be dangerous if the specimen is tested until material failure.

Information provided by experienced masons and masonry designers was used to define typical reinforcement schemes for tall walls. The specimens to be tested are partially grouted walls built using standard 20 cm concrete masonry units (CMUs) laid in a running bond pattern. The wall will be 8.75 m high, 1.19 m wide, and 0.19 m thick, obtaining a slenderness ratio of 46. The reinforcement details are representative of typical masonry wall designs for non-seismic areas. The vertical reinforcement consists of 2-15M bars @ 600 mm apart. Code-compliant bond beams with a single 10M bar (every 12 courses) and 9-gauge ladder-type joint reinforcement (every 2-courses) were provided along the height of the wall. The horizontal reinforcement provides structural integrity to the wall in the out-of-plane direction. When in-plane lateral forces are applied to the wall (not in the scope of this study), this reinforcement resists the in-plane shear. Geometry and reinforcement details can be found in Figure 3.4. The material properties were based on Petti's (2019) study. The material test was done in the Morrison Structural Laboratory at the University of Alberta and conducted following the Canadian code. The masonry construction materials used are representative of the province of Alberta. For the masonry, the compressive strength obtained was $f'm= 16.8\ MPa$, the tensile strength was $fr=0.65\ MPa$, and the maximum stress-strain was 0.002. For the steel reinforcement, the yield stress obtained was $fy=533\ MPa$ and Young's Modulus of $E_s= 199\ GPa$. A value of $23.6\ kN/m^3$ as volumetric weight was used for the wall self-weight calculation, according to the information provided by Drysdale and Hamid (2005).

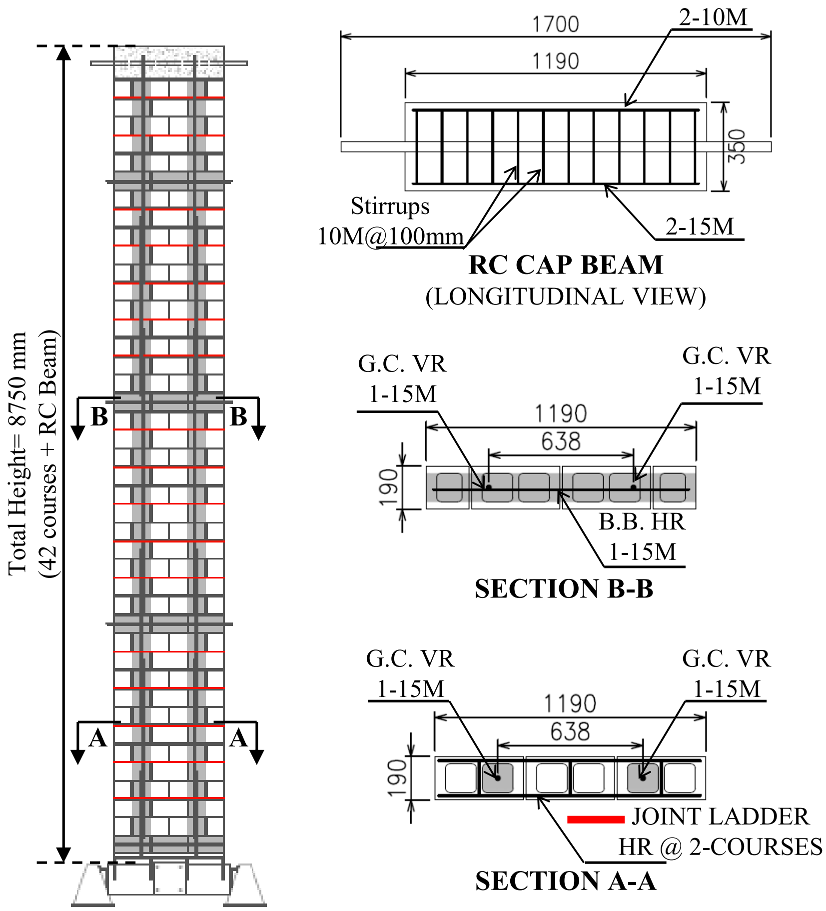

Figure 3.4 – Specimens geometry and reinforcement (units in mm)

3.3.1. Eccentric axial load

A push-over analysis was applied to the proposed specimen with different eccentric axial loads. A value of 170 mm as eccentricity was used, and 20 mm of out-of-straightness at the middle of the wall was assumed due to possible imperfection during the construction. The pinned-pinned condition was used to analyze the specimen since this would be the more critical condition.

Figure 3.5 shows the overall out-of-plane wall capacity under different eccentric axial loads. It is evident that while the eccentric axial load increases, the maximum lateral pressure in the wall decreases. When the eccentric axial load increases from 5 kN to 15 kN, the maximum lateral pressure decreases by 25%. Meanwhile, with the increment of the eccentric axial load from 15 kN to 25 kN, the lateral pressure decreases by 33%. Although the increment of the eccentric axial load of 10 kN was the same for the first and second scenarios, the decrease percentage differed. Finally, when the eccentric axial load of 50 kN was applied, the wall reached 0.22 kPa of maximum lateral pressure before failing due to instability. This is because slender walls are susceptible to second-order effects and buckle before material failure.

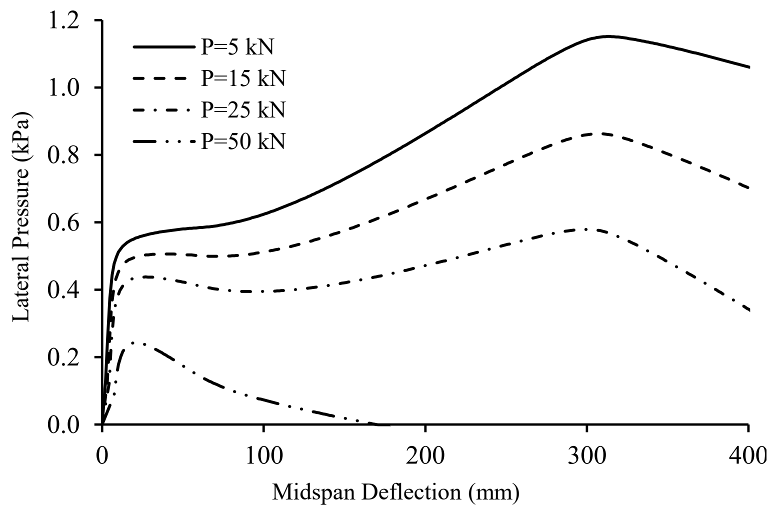

Figure 3.5 – Capacity curve under different eccentric axial loads

3.3.2. Primary and secondary moment interaction

To get a better understanding of second-order effects in the tall masonry walls to be tested, Figure 3.6 shows the interaction between the primary moment (M_p) and the secondary moment (M_s) to form the total moment (M_T) versus the deflection at midspan. The first characteristic that can be noticed is that when the eccentric axial load increases, the slop of M_s also increases while M_p tends to decrease. In the first scenario, when P= 5 kN, M_T is composed mostly by M_p while M_s contributes with a lower percentage, but M_s constantly increases as the wall also deforms without exceeding M_p. In the second scenario, when P=15 kN, MT is still mainly composed of M_p. However, after M_p reaches the maximum peak at 311 mm of midspan deflection, as well as M_s still increasing up to 378 mm of deflection, M_s becomes greater than M_p. The third scenario, when P=25 kN, shows a similar behaviour as the second scenario but with the difference that M_s becomes grater than M_p at 239 mm of midspan deflection before M_p reaches its maximum peak. Finally, in the fourth scenario, when P= 50kN, it is evident how the wall fails due to early instability when M_p reaches its maximum peak at 30 mm of midspan deflection. Therefore, second-order effects are not significant in the first scenario. In the second scenario, second-order effects were present, but the wall was stable before reaching its maximum lateral pressure. The third scenario also presented second-order effects that became more significant, reaching values of M_s greater than

M_p making the wall unstable before reach its maximum lateral pressure. The last scenario shows a typical instability failure, when M_p reaches its maximum peak and shows no resistance to lateral pressure after the maximum peak.

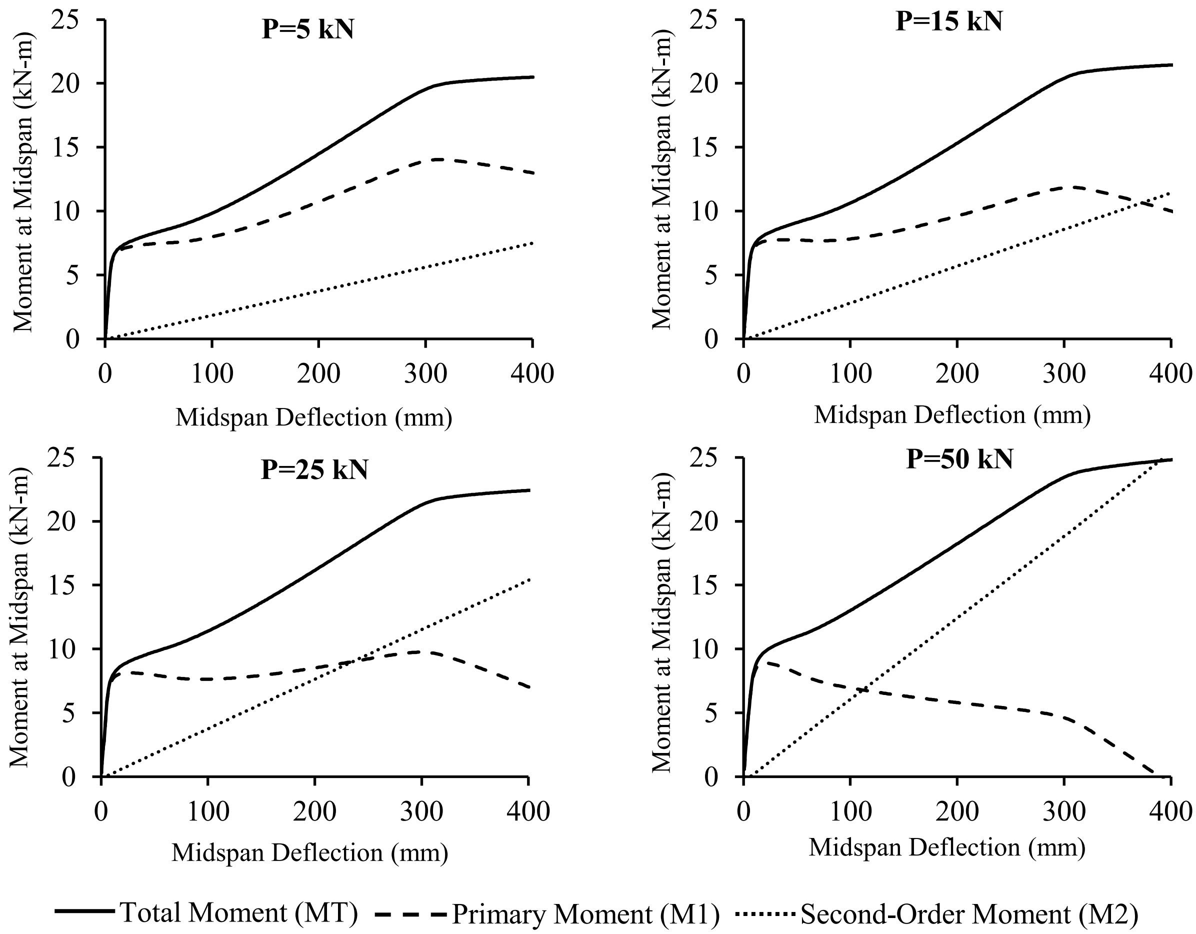

Figure 3.6 – Moment interaction at midspan under different eccentric axial loads

3.4. Expected results

As a result of the previous analysis, the value of 15 kN was selected to be applied eccentrically at the top of the specimen in the experimental stage. Moreover, it is recommended to stop the test close to 311 mm of midspan deflection to avoid a sudden failure Figure 3.7.

Figure 3.8 shows the deflected shape profile predicted at cracking, yielding, and the proposed limit deflection before instability failure. Also, it is important to mention that crushing of masonry is not achieved under these boundary conditions and loads.

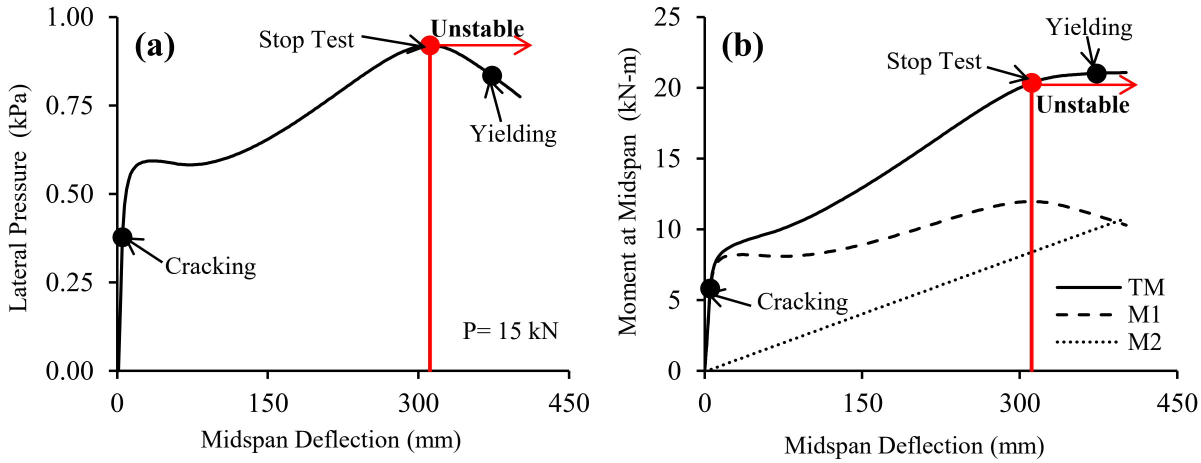

Figure 3.7 – Expected experimental results at midspan: (a) Capacity curve; (b) M_p and M_s interaction

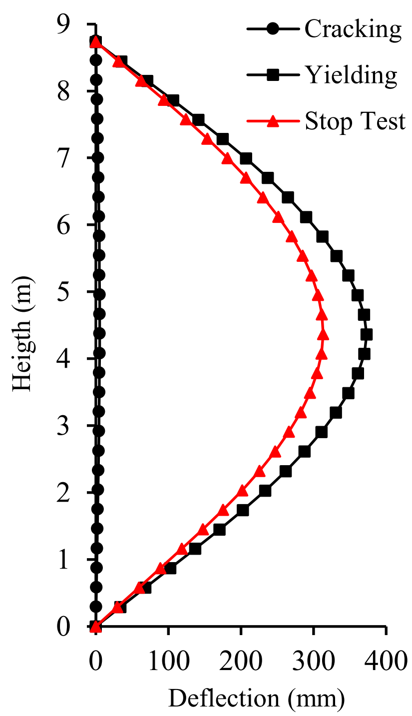

Figure 3.8 – Expected deflected profile

3.5. Rotational base stiffness effect

To investigate the effect of the rotational base stiffness (RBS) in the specimens to be tested, three different RBS (250, 500, and 1,000 kN-m/rad) were used to compare the pinned-pinned and fixed-pinned conditions (RBS= 0 kN-m/rad and RBS= ∞ kN-m/rad, respectively).

Figure 3.9a shows the increment of the wall capacity while the RBS increases. When the RBS=250, 500, and 1,000 were applied, an increment of 88, 120, and 131% was observed in the maximum peak of lateral pressure. Moreover, it can be seen that the yield displacement is shifted among the five curves. That means that yield displacement decreases while RBS increases. After achieving the yield displacement, the capacity curves show a decrement, resulting in a flexural stiffness drop due to initial stability.

The deflected profiles with different RBS shown in Figure 3.9b were plotted at the maximum peak of lateral pressure according to Figure 3.9(a). When the RBS=250, 500, and 1,000 are applied, decreases of 8, 9, and 18% of the maximum displacement can be observed. Although the differences in the maximum deflection were not significant with RBS= 250 and 500 kN-m/rad values, a higher lateral pressure was required to achieve this maximum displacement compared to the pinned base condition. Moreover, the maximum displacement position is no longer the midspan when the RBS is different than zero.

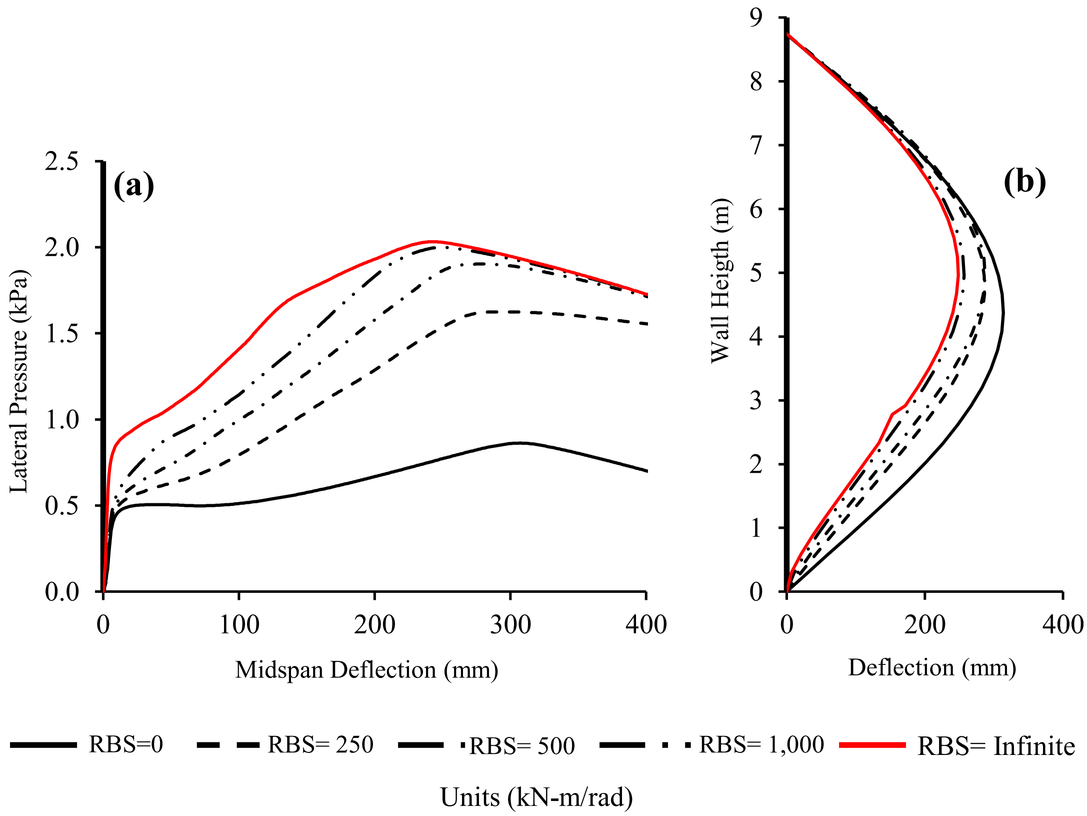

Figure 3.9 – RBS comparison: (a) Capacity curve; (b) Deflected profile

3.6. Summary

The macro model developed was able to predict the out-of-plane performance of slender masonry walls subjected to combined lateral and eccentric axial loads according to the experimental results used in the validation phase. A value of 15 kN as the eccentric axial load was determined to be applied to the specimens during the experimental stage. Moreover, a value of midspan displacement close to 300 mm will be set as the target displacement during the control specimen test to maintain the safety of the test.

The out-of-plane performance of slender masonry walls under eccentric axial loads and uniform lateral pressure appears to be significantly influenced by base stiffness. Even with the smallest value of rotational base stiffness, the capacity increased by 88% and the deflection decreased by 8%. However, the material degradation near the base should be investigated to avoid sudden failures due to masonry crushing.

The result of this analysis was used to design specimens, the loads expected in the experimental setup, and the predicted behaviour during the experimental stage. Finally, the experimental results from the next stage and the parametric analyses will generate design recommendations for the presence of base stiffness.

Note: *Tasks 1.1 and 1.2 from objective 1 were addressed in this chapter.*

4 EXPERIMENTAL TESTING OF TALL-SLENDER MASONRY WALLS WITH DIFFERENT BASE STIFFNESSES [2]

Loadbearing concrete masonry walls are an effective structural system to resist combined out-of-plane and gravity loads. A large portion of the market for these walls is comprised by single-storey warehouse and industry buildings, and public-use structures such as theatres, community centres, and school gymnasiums. In these applications, it is common to have tall walls with an effective height-to-thickness ratio greater than 30. North American masonry design standards (CSA S304-14 and TMS 402-16) have special design requirements for these types of masonry walls due to their perceived vulnerability to second-order effects. In particular, one of CSA S304-14 requirements consists of assuming a pinned base condition to calculate design moments and deflections, which severely impacts the available strength and stiffness of tall masonry walls. The objective of this study is to assess the influence of the rotational base stiffness on the out-of-plane response of slender masonry walls subjected to cyclic loading in terms of strength, stiffness, base damage, and failure modes. Two full-scale, partially grouted, slender masonry walls were tested under combined eccentric axial load and cyclic lateral out-of-plane pressure. The tests showed increased flexural capacity and decreased deflections in the out-of-plane direction when rotational stiffness at the base is accounted for, with limited degradation at the wall base observed during cyclic loading. Results suggest that accounting for the presence of the base stiffness provides additional strength to the wall, which may lead to more economical masonry wall designs while maintaining satisfactory strength and reliable structural performance.

4.1. Introduction

The Canadian masonry standard, CSA S304-14 (2019), sets special requirements for designing tall loadbearing masonry walls when the effective height-to-thickness ratio ($^{kh}/_{t}$) exceeds 30 – a minimum thickness, a maximum reinforcement ratio for ductility, pin-pin boundary conditions, and a maximum compressive axial load of 10% of the cross-section capacity. Typical slender masonry wall design under combined gravity and out-of-plane loads involves selecting appropriate

[2] A version of Chapter 4 is under review as Alonso, A.; Gonzalez, R.; Elsayed, M.; Banting, B.; Guzman, M.; Pettit, C.; Li, Y.; Tomlinson, D.; and Cruz-Noguez, C. "Experimental testing of tall-slender masonry walls with different base stiffnesses", by a journal paper.

block sizes, amounts of flexural steel reinforcement, and grouting schemes to resist bending moments amplified by second-order effects. Out-of-plane shear forces for walls with ${kh}/{t} > 30$ is not usually of concern due to the large wall spans. The factored design moments that must be resisted may be significant due to second-order effects leading to large amounts of flexural steel reinforcement being required. However, the amount of reinforcement that can be placed in a wall is limited by masonry design standards (TMS 402-16 2016, CSA S304-14 2019) to ensure ductile behavior. To keep the reinforcement ratio low, while using the same block thicknesses (wider blocks lead to uneconomical wall solutions), options are twofold: (1) strengthening the wall by using high-strength materials (Babatunde 2017, Fortes et al. 2018, De Santis et al. 2019), and (2) stiffening techniques that aim to reduce second-order moments via the inclusion of pilasters or in-line concealed columns (Entz 2019), and accounting for untapped sources of stiffness (Pettit and Cruz-Noguez 2021, Pettit et al. 2022), such as foundations. Alternative detailing arrangements, such as near-surface-mounted reinforcement techniques (Sparling et al. 2020, Sparling and Palermo 2023), may be used to increase both the strength and stiffness of a wall.

As part of the "stiffening" techniques, a relatively inexpensive way to mitigate the problem is to account for the rotational base stiffness provided by the wall-foundation interaction in slender walls. Under CSA S304-14 (2019), this is not permitted as a pin end condition must be assumed at the base for walls with ${kh}/{t} > 30$. Interestingly, TMS 402-16 (2016) does not have such a restriction. The reluctance in the Canadian standard to account for the base stiffness could be due to: i) the need for simplified and conservative design expressions before computers and specialized structural analysis software were more readily available, and ii) the lack of experimental data about the degradation at the wall-foundation interface. Current code provisions for designing slender masonry walls are based on a small set of experimental programs that have resulted in conservative design provisions. These can be traced to Yokel et al. (1970, 1971), who investigated slenderness effects and axial load eccentricities on slender masonry walls. Two sets of concrete masonry walls of different h/t ratios (12, 20, 32, and 40) were tested under fix-pin boundary conditions. Results showed that large values of slenderness (h/t) ratios and load eccentricity affect the out-of-plane performance of the wall, leading to large deflections and stiffness loss. Hatzinikolas et al. (1978a, 1978b) conducted tests on 68 walls (h/t ratios ranged from 12 to 22) bending in double curvature under pin-pin boundary conditions, with concentrated moments at each end. They concluded that walls tested in double curvature increased their capacity by up to four times compared with walls bending in single curvature, but their mode of failure was more brittle.

The American Concrete Institute (ACI) and the Structural Engineers Association of Southern California (SEASC) tested 30 full-scale wall panels to address concerns regarding the stability and failure modes of slender walls. Nine of the thirty wall panels were fully grouted concrete masonry walls with h/t ratios of 30, 38, and 51. These walls had relatively low reinforcement ratios (A_s/bt= 0.21%, 0.27%, and 0.36%) and subjected to light axial loads (P/P_n= 0.30%, 0.38%, and 0.19%, respectively). Wall panels were tested under combined eccentric axial and lateral loads with pin-pin boundary conditions, demonstrating a stable ductile response. The test conditions and results from this study (ACI-SEASC 1982) would become one of the milestones to inform the development of the North American masonry standards at the time (CSA S304.1-M94 1994, TMS 602-95 1995).

Later studies on masonry walls also had pin-pin boundary conditions, neglecting the effect of the base stiffness provided by the wall-foundation connection. For example, Liu and Dawe (2001, 2003) investigated the accuracy of the CSA S304.1-M94 (1994) to calculate the effective flexural rigidity and proposed a new equation in which Liu and Hu (2007) investigated its accuracy. Bean Popehn et al. (2008) studied the potential for buckling failure on slender, unreinforced masonry walls. Sparling et al. (2020, 2023) investigated the near-surface mounted (NSM) reinforcement technique to increase the strength and resiliency in new masonry construction – usually used for retrofitting damaged masonry structures.

After the ACI-SEASC (1982) report, few studies have addressed the effect of base stiffness on the out-of-plane behaviour of masonry walls. Mohsin (2005) pioneered the investigation of the role of base stiffness on slender, loadbearing masonry walls. Eight full-scale masonry walls were tested under eccentric axial loads. The experimental program was divided into two groups; the first consisted of four walls with a $h/t = 28.6$ and the second was compromised by four walls with a $h/t = 33.9$. Four support stiffnesses (0, 1,000, 5,000, and 10,000 kN-m/rad) were used for both wall groups to compare their behavior. Results showed that base stiffness reduced 30% of the second-order effects by limiting deflection while increasing the loadbearing capacity by 55%. Isfeld et al. (2019) investigated the fixity level at the base of walls without a connection between the wall and the fixed support. Three reinforced masonry walls with a h/t of 12.6 were tested under axial and combined axial and out-of-plane loads. Results showed that the base fixity reduced deflections (in the uncracked elastic range) by 90% on walls subjected to combined axial and lateral loads compared to the 80% reduction obtained when walls were under axial loads only. Simple support conditions, consisting of blocks mortared to a steel channel secured to the strong floor of the laboratory, led to deflected profiles in double curvature during the tests. Pettit and Cruz-Noguez (2021) investigated the effect of rotational base stiffness on loadbearing walls under combined gravity and cyclic lateral loads. Four masonry walls with $h/t = 12.6$ were tested with different rotational base stiffnesses (2,300, 5,000, and 9,500 kN-m/rad) to capture any possible degradation at the wall base. Findings showed an increase in lateral load capacity from 67.4% to 93.5% when comparing walls with base stiffness to walls with a pinned base. This increment was attributed to the change in moment distribution due to the presence of base stiffness. No material degradation at the base of the wall was observed during the cyclic loading before failure.

Even though the previous studies related to base stiffness demonstrated the benefits of accounting for base stiffness, some important factors for the out-of-plane behaviour of slender walls have not been considered. For instance, Mohsin (2005) did not investigate the effect of combined axial and out-of-plane loads, a typical load condition on loadbearing walls. Walls tested by Isfeld et al. (2019) were limited to $h/t = 12.6$ making slenderness effects not significant, and the base degradation under cyclic loading was not explored. Pettit and Cruz-Noguez (2021) used a three-point bending configuration at midspan to apply the lateral load, which may not accurately represent a lateral pressure due to wind loads, and the slenderness effects were not significant because the low value of $h/t = 12.6$.

This study aims to provide experimental data on the effect of the rotational base stiffness on the out-of-plane response of slender masonry walls and any possible degradation at the wall-foundation connection under repeated loads. Two full-scale specimens were tested under a combination of gravity and lateral loads using different base stiffnesses, including a high slenderness ratio, realistic load combinations, and realistic support conditions – aspects not entirely covered in previous studies. Results were analyzed to study the wall capacity, deflected shapes, moment profiles, flexural capacity, and material degradation at the wall base.

4.2. Experimental program

4.2.1. Test walls

Two full-scale, partially grouted (PG) walls were built using standard 20-cm hollow concrete masonry units (CMUs) with a specified compressive strength of 15 MPa. The blocks were laid in a running bond pattern. The walls were 8.75 m tall, 1.19 m wide, and 0.19 m thick, resulting in $h/t = 46$. The vertical reinforcement consists of 2-15M (area of 200 mm^2 each) bars at 600 mm. Bond beams with a single 10M bar (area of 100 mm^2) at 2400 mm. Ladder-type, 9-gauge joint reinforcement (area of 21.5 mm^2 – two rods) at 400 mm was provided along the height of the wall. The reinforcement details are representative of typical masonry wall designs for non-seismic areas. The walls were built over a base plate, on which two 15M bars were welded to simulate a satisfactory wall-foundation connection. These bars were spliced to the reinforcement in the wall as per CSA S304-14 (2019), with a 700 mm lap splice. The base plate was attached to a rotating fixture that had the ability to simulate different base conditions (fixed, pinned, and rotational stiffness values in between). Wall-1 was tested under pinned and fixed base conditions, while Wall-2 was tested under pinned, partially fixed, and fixed base conditions. Reinforcing details and the general geometry of the full-scale specimen can be found in Figure 4.1.

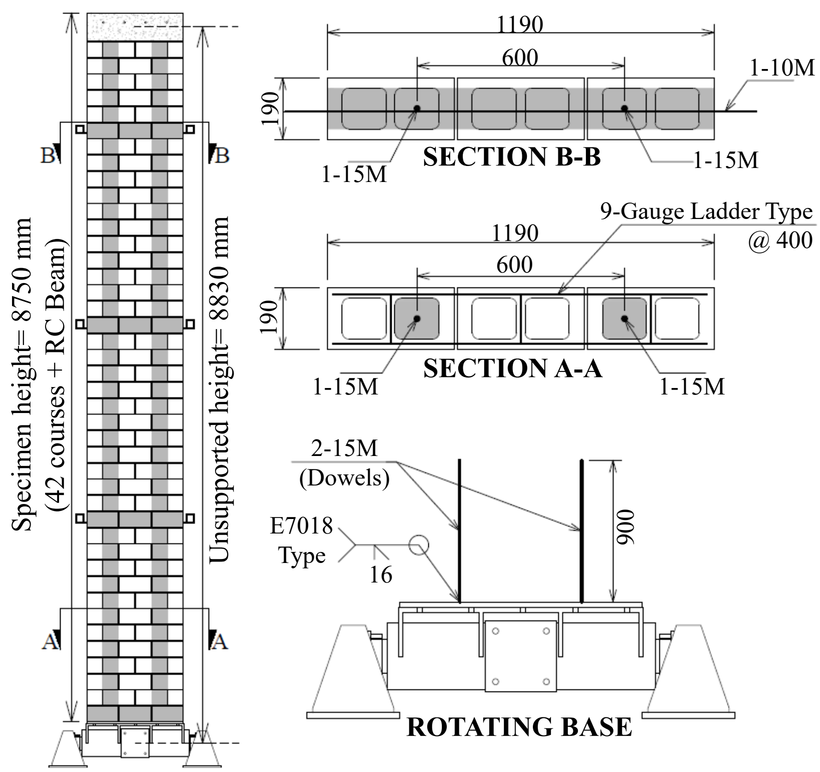

Figure 4.1 – Specimens' geometry and reinforcement (units in mm)

Table 4.1 shows the cracking moment (M_{cr}), the nominal moment capacity (M_n), the maximum nominal axial load allowed (P_{n_max}), and the Euler buckling load (P_{cr}) of the specimens, according to the CSA S304-14 (2019) and TMS 402-16 (2016), using the actual material properties described in the next section.

Table 4.1 – Specimen nominal design values

Standard	M_{cr} (kN-m)	M_n (kN-m)	P_{n_max} (kN)	P_{cr} (kN)
CSA S304-14	5.6	18.0	243.7	61.8
TMS 402-16	5.9	17.9	121.8	79.2

Notes: All reduction factors used equal to 1.
Tensile strength was based on CSA S304/TMS 402 tabular values

4.2.2. Material properties

Mortar and grout

Type S mortar and coarse grout from premixed bags with a specified minimum compressive strength of 12.5 MPa and 20.6 MPa, respectively, were used during the walls and prism construction. The compressive strength of the mortar was determined by crushing six 50 mm × 50 mm × 50 mm mortar cubes per wall under concentric axial loads as specified by CSA A179 (2014). The compressive strength of the grout was determined by crushing four 100 mm × 200 mm cylindrical grout samples per wall under a concentric axial load as specified by CSA A179 (2014). The compressive strength of mortar cubes and grout cylinders from both walls is presented in Table 4.2, as specified by Annex C of CSA S304-14 (2019).

Table 4.2 – Material properties of mortar and grout

Specimen	Wall-1			Wall-2		
	Compressive strength (MPa)					
	Average	COV (%)	Specified	Average	COV (%)	Specified
Mortar	16.8	2.8	16.1	23.0	4.1	21.5
Grout	24.9	4.7	22.7	25.5	2.5	24.4

Masonry assemblage

Standard 20-cm concrete masonry units (CMUs), with a specified compressive strength of 15 MPa, were used to build ten 5-course prisms (five grouted and five ungrouted). The CMUs and the prisms were tested under a concentric axial load as specified by Annex D of CSA S304-14 (2019). The compressive strength of CMUs and prisms is presented in Table 4.3, as specified by Annex D of CSA S304-14 (2019).

Table 4.3 – Material properties of the masonry assemblage

Specimen	Compressive strength (MPa)			Modulus of Elasticity (MPa)		
	Average	COV (%)	Specified	Average	COV (%)	Specified
20-cm CMU	25.3	9	21.7	--------	-------	--------
5-courses grouted prisms	24.3	10	19.8	17,260	6	15,630
5-courses ungrouted prisms	21.7	9	18.6	22,500	9	19,220

Reinforcing steel

The vertical and horizontal steel reinforcement used to build the two full-scale walls are Gr. 400 15M and 10M bars, respectively. Three steel rebar coupons per bar size were tested in tension to determine their averaged properties according to ASTM A615 (2004), as shown in Table 4.4.

Table 4.4 – Average material properties of the steel reinforcing

Property	10M	COV (%)	15M	COV (%)
Nominal diameter (mm)	11.3	--------	16.0	--------
Nominal area (mm^2)	100	--------	200	--------
Yield strength (MPa)	453	0.3	429	0.6
Ultimate strength (MPa)	720	0.5	650	0.3
Modulus of elasticity (MPa)	192,935	1.9	193,222	2.1

4.2.3. Experimental Setup

The experimental setup was based on the ACI-SEASC (1982) protocol. Figure 4.2 shows the main components of the experimental setup described in this section. The setup consists of three main parts: the out-of-plane load-resisting system (steel frame), a lateral bracing system for the top and bottom supports of the wall, and the load application systems (gravity and out-of-plane loads). The out-of-plane load-resisting system is a self-reacting steel truss frame. At the top, a steel fixture was designed to allow vertical displacement and out-of-plane rotation while preventing horizontal displacements. At the bottom, a fixture was designed to simulate pinned, partially fixed, or fixed base conditions. This device is a steel cylinder with roller bearings at each end, allowing rotation to simulate the pinned condition. If a specific rotational base stiffness is desired, a steel beam is attached through a rigid connection while the other end is simply supported on a screw pile; the cross-section properties of the steel beam and its length are dimensioned such that they provide the required rotational stiffness at the wall base. Full fixity is achieved by locking the steel cylinder with bolts that prevent rotation.

The eccentric gravity load (e= 170 mm) at the top of the wall is provided by a water tank hung from a lever arm resting on a structural steel angle attached to the top of the wall, which simulates a steel-joist roof system connection to the side of a masonry wall. The out-of-plane lateral pressure is applied with a pressurized airbag located between the reacting steel frame and the back of the masonry wall.

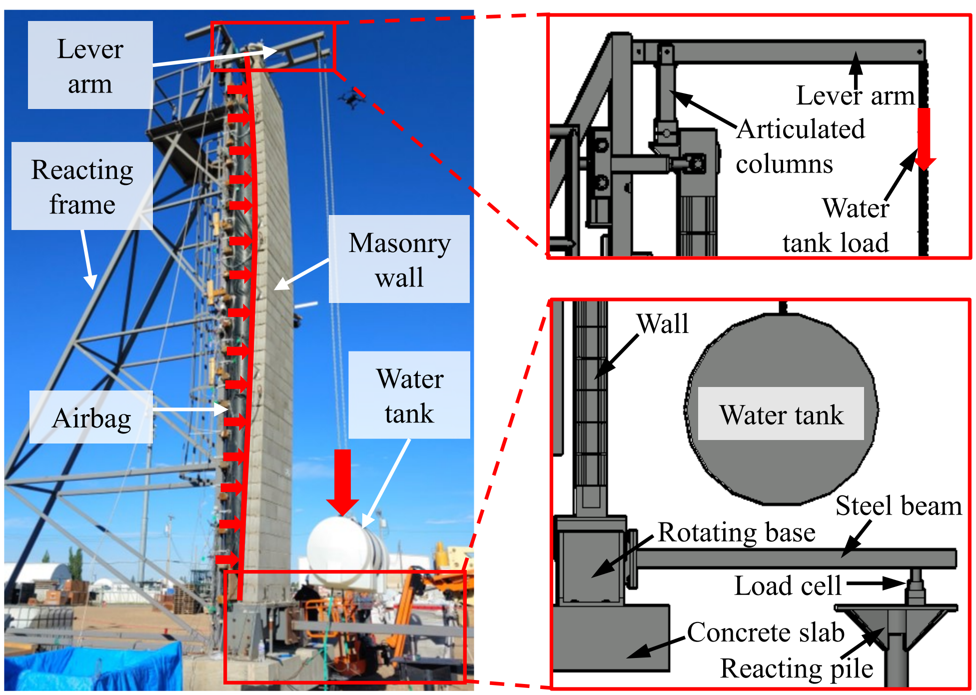

Figure 4.2 – Experimental setup

4.2.4. Instrumentation

The instrumentation consisted of strain gauges, load cells, inclinometers, potentiometers (POTs), pressure gauges, a weather station, and six cameras strategically placed to monitor the wall during the test. Sixteen strain gauges distributed on the vertical reinforcement captured the strains at critical locations where maximum values of the flexural moment were expected to occur on the wall: at wall base, midspan, and approximately 0.65 of the wall height (0.65h). Sixteen strain gauges were placed on the CMUs at the same location as the rebar strain gauges on the compression side of the wall. Two load cells were placed at the top of the wall to monitor the vertical load applied to the wall during the test. Two inclinometers were placed at each wall end to measure rotation at the supports. Ten POTs were distributed along the wall height to capture the deflected shape of the wall during testing. Pressure gauges were used to monitor the pressure applied to the wall. Additionally, a weather station was installed at the top of the steel frame to take temperature and wind measurements since the test was carried out outdoors.

4.2.5. Rotational base stiffness

The rotational stiffness value for the partially fixed condition was based on the soil-foundation interaction study by Pettit (2019) and Pettit and Cruz-Noguez (2021). Pettit and Cruz-Noguez used a finite-element analysis using 2D linear-elastic spring elements to capture the rotational base stiffness (RBS) of different sizes of strip footings in soils that vary their modulus of subgrade reaction (Table 4.5).

Table 4.5 – RBS range for typical strip footings of tall masonry walls (Pettit 2019)

Strip footing sizes (mm)	Soil Type	Modulus of Subgrade (kN/m^3)	Range of RBS (kN-m/rad)
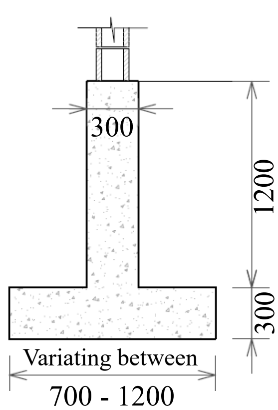	Loose sand	5, 600	250 – 500
	Clay	30, 000	1,300 – 2,300
	Medium/Dense Sand	35, 200	
	Silty Dense Sand	36, 000	
	Clay medium	56, 000	2,450 – 3,500
	Dense Sand	96, 000	

The main objective of this study consists of the investigation of the response of a slender masonry wall under 3 different RBS values: pinned (RBS= 0), fixed (RBS= ∞) and a partially fixed condition (0< RBS< ∞). The partial fixity value selected for the test intended to represent an average value of RBS consistent with Table 4.5, accounting for the experimental constraints in the setup: (1) the location of the support screw pile and (2) the dimensions of the beam that could be attached to the rotating fixture. A steel HSS 102×102×6.4 (HSS 4×4×1/4) element with an unsupported length of 1.75 m was selected as the stiffening element in the steel cylinder, providing an RBS value of 1,150 kN-m/rad (Figure 4.3).

Figure 4.3 – Rotational base stiffness simulation

4.2.6. Loading protocol

Combined eccentric vertical and cyclic out-of-plane loads were applied to test the wall specimens. First, a sustained eccentric vertical load of 15 kN (24% and 19% of P_{cr} from Table 4.1) was applied at the top of the wall. A compressor inflated the airbag until a specified midspan displacement was achieved. Then, the airbag was deflated to remove the imposed displacement, which finalized a load cycle.

Wall-1 was tested in six cycles (Figure 4.4a) to record the cracked, service, and yielding stages under a pinned base condition (with one fully fixed cycle interspersed to test the rotating base fixture), and these results served as a reference for the rest of the test. Wall-2 was tested in six rounds of cycles up to different midspan target displacements. The first three rounds of cycles consisted of two cycles per base stiffness – fixed, partially fixed, and pinned (∞, 1,150, and 0 kN-m/rad, respectively). The rest of the cycles were done under a fixed base condition, pushing the wall beyond the service limit to the yielding stage (Figure 4.4b). The loading protocol was intended to compare different base conditions through the uncracked, cracked, service, and yielding stages and capture any possible degradation at the wall-foundation connection.

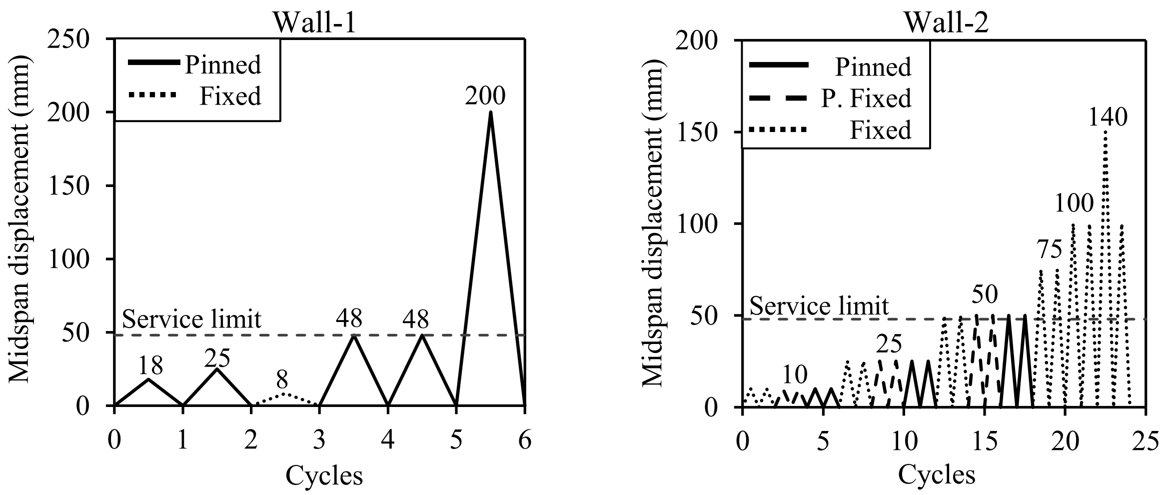

(a) **(b)**

Figure 4.4 – Loading protocol: (a) Wall-1; (b) Wall-2

4.2.7. Calculation of moments and moment-curvature analysis

The moments in the wall with pinned, partially fixed, or fixed base can be calculated using Eqs. (4.1 – 4.3) at any height (x), respectively. The moment profiles are accounting for first-order moments (airbag pressure + eccentric load at the top), second-order moments ($P\cdot\Delta$), and the presence of the rotational base stiffness (RBS), if any, as shown in Figure 4.5.

$$M_{pinned} = \frac{\omega x}{2}(h-x) + Pe\left(\frac{x}{h}\right) + (P+P_w)\Delta_x \tag{4.1}$$

$$M_{p\_fixed} = \frac{\omega x}{2}(h-x) + Pe\left(\frac{x}{h}\right) + (P+P_w)\Delta_x + RBS\cdot\theta\left(1-\frac{x}{h}\right) \tag{4.2}$$

$$M_{fixed} = \frac{3\omega h}{8}(h-x) - \frac{\omega(h-x)^2}{2} - \frac{Pe}{2}\left(1-\frac{3x}{h}\right) + (P+P_w)\Delta_x \tag{4.3}$$

Where ω is the uniform distributed load magnitude, h is the unsupported height, e is the vertical load eccentricity, P is the external vertical load, P_w is the self-weight of the upper half of the wall, Δ_x is the displacement at x, RBS is the rotational base stiffness, and θ is the rotation at the base.

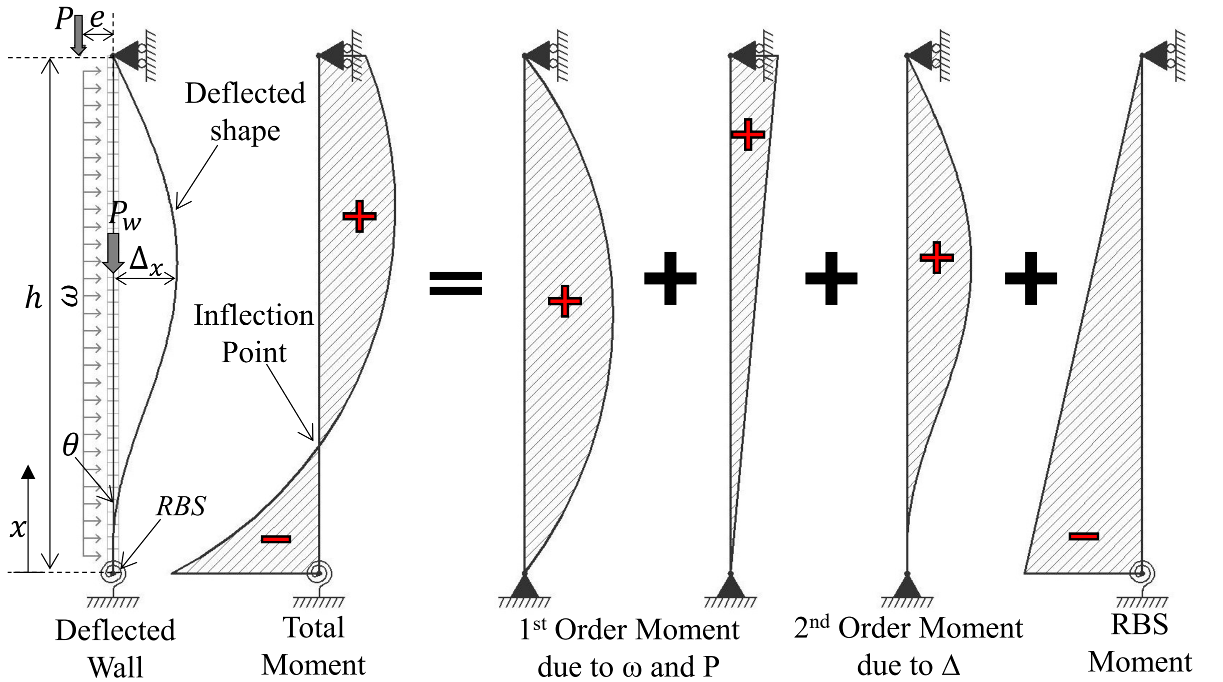

Figure 4.5 – Moment profile distribution (Pettit and Cruz-Noguez 2021)

A moment-curvature analysis for the wall cross-section, for flexure in the out-of-plane direction, was conducted with a fibre-section approach. The model by Priestley and Elder (1983) for masonry was used, with a f_m'= 19.3 MPa (calculated using the weighted average of the 5-course grouted and ungrouted f_m' values in Table 4.3). The tensile strength of masonry was conservatively taken as 0.55 MPa, a lower bound as per CSA S304-14 (2019). A Menegotto and Pinto (1973) steel model with strain hardening was used for the steel reinforcement, using the average yield stress and modulus of elasticity in Table 4.4. For the axial load, in addition to the water tank weight (15 kN), three cases were analyzed: (1) 100% of the wall self-weight (SW), equal to 29.7 kN, (2) 50% of SW, and (3) no SW.

Figure 4.6 shows that there is little sensitivity to the axial load, as it is very low compared to the section capacity (1.3% of $A_e f_m'$). Average values for the cracking (M_{cr}), yielding (M_y), and ultimate (M_u) moment were determined to be 5.7 kN-m, 16.5 kN-m, and 18.5 kN-m, respectively. There is a reasonable correspondence with the nominal standard values reported in Table 4.1. The values from the moment-curvature analysis will be used to aid in determining the condition of the walls during each loading cycle.

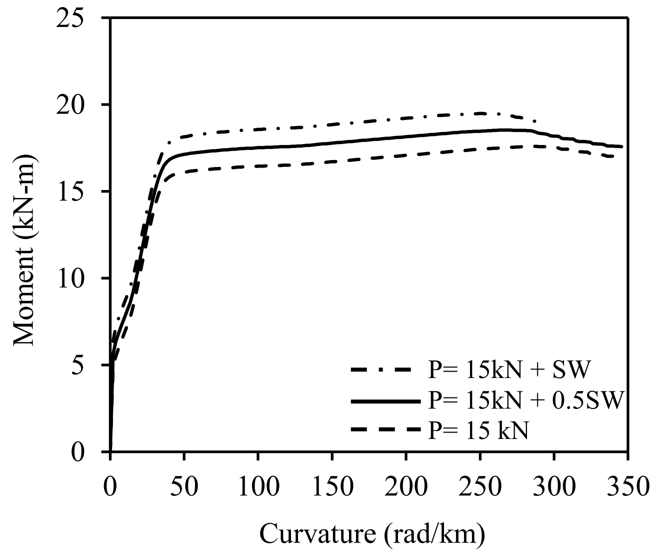

Figure 4.6 – Moment-curvature analysis

4.3. Experimental results

The following sections describe the wall tests in terms of load (pressure/moment) and displacement, and the damage observed on the walls. The weather conditions (temperature and wind speed) during testing did not appear to affect the presented results. The weather station captured average wind gust speeds of NW 14 km/hr and SE 24 km/hr, and average temperatures of 17°C and 7°C, during the tests of Wall-1 and 2, respectively.

4.3.1. Load-displacement response

Wall-1

Figure 4.7a and Table 4.6 show the load-displacement history of Wall-1. The first two cycles took the wall to the cracked stage. After the eccentric axial load was applied, the airbag was inflated until Wall-1 with a pinned base reached a midspan displacement of 18 mm at 0.38 kPa (6.1 kN-m or $1.1M_{cr}$). Wall-1 with pinned base was loaded again up to a target midspan displacement of 25 mm, at 0.41 kPa (6.7 kN-m or $1.2M_{cr}$).

The base of the wall was changed to a fixed base condition, and the airbag was inflated up to 8.4 mm of midspan displacement (0.35 kPa). A 165% increase in stiffness was observed in the third cycle compared with the second cycle. Figure 4.7b shows a comparison of the load-displacement response for the 25 mm cycle (pinned base) and the 8.4 mm cycle (fixed base). At the same pressure (0.35 kPa), the midspan displacement for Wall-1 with a pinned base was 1.82 times greater than that measured in the wall with a fixed base. At the same displacement (8.4 mm), the required out-of-plane pressure to deform Wall-1 with a fixed base condition was 1.75 times greater when compared to the pinned base condition. This could reveal a significant reserve of strength and stiffness at the early, uncracked-elastic stages if the rotational base stiffness (0< RBS< ∞) of the foundation is accounted for.

The test of Wall-1 under pinned base continued with two cycles at the serviceability limit (48 mm) set by CSA S304-14 (2019) for an 8.75 m wall. The average out-of-plane pressure was 0.54 kPa. The last cycle of Wall-1 with pinned base had the objective of reaching the yield strain of the reinforcing bars. The pressure was applied to Wall-1 up to a target displacement of 200 mm. Yielding was observed in the bars at the midspan of the wall at 185 mm (1.12 kPa) of midspan displacement, and an associated moment of 19.6 kN-m ($1.2M_y$). The pressure remained essentially constant at 1.12 kPa from 185 mm to 200 mm, after which the test was terminated because of safety considerations. A residual displacement of 55 mm was captured at the end of the last cycle, indicating a large plastic displacement in the wall. Wall-1 showed a stable response during the test without any noticeable material deterioration or wall instability, even when a 72% stiffness loss was measured after the last cycle compared to the initial stiffness in the first cycle.

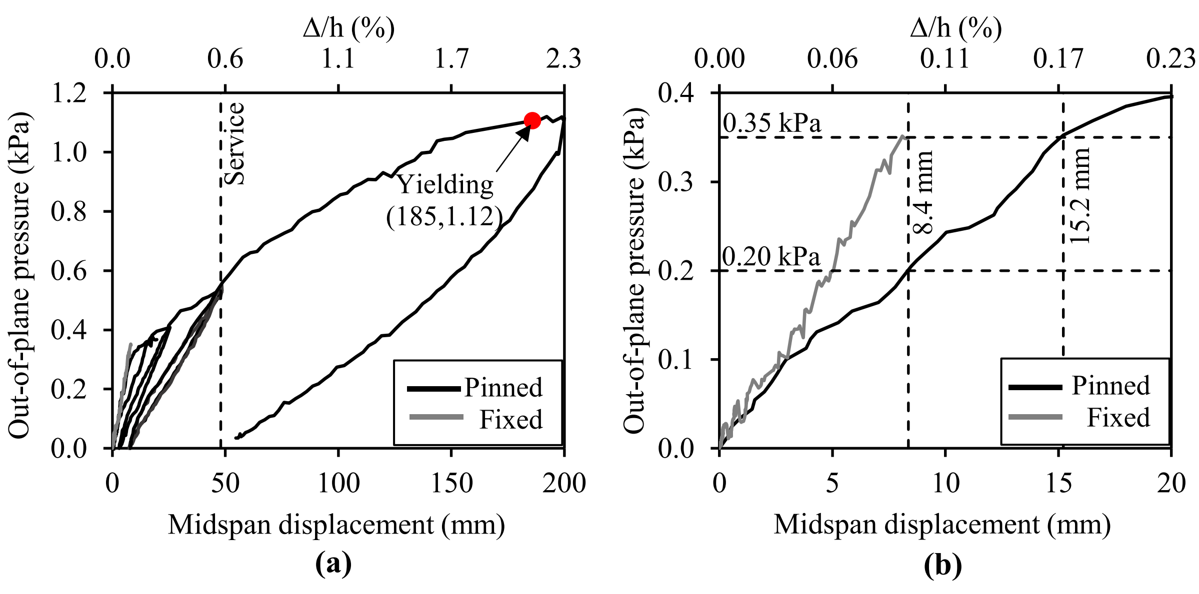

Figure 4.7 – Load - displacement history of Wall-1: (a) all loading cycles; (b) base comparison

Table 4.6 – Summary of test results of Wall-1

Cycle	Base Support	Δ (mm)	Δ/h (%)	OOPP (kPa)	M_{base} (kN-m)	$M_{midspan}$ (kN-m)	$\Delta_{Residual}$ (mm)
1[a]	Pinned	18	0.20	0.38	0.6	6.1	--------
2	Pinned	25	0.29	0.41	0.6	6.7	3
3	Fixed	8	0.09	0.35	-3.8	3.3	--------
4	Pinned	48	0.54	0.53	1.0	8.7	8
5	Pinned	48	0.54	0.55	1.0	8.9	8
6	Pinned	200	2.26	1.12	2.8	20.0	55

Note: [a]Instrument malfunction. OOPP= out-of-plane pressure.

Wall-2

Figure 4.8a and Table 4.7 show the load-displacement history of Wall-2. In the first round of six cycles (two cycles per base condition), Wall-2 was loaded up to 10 mm of midspan displacement. The average pressures at this stage under fixed, partially fixed, and pinned base conditions were 0.60 kPa, 0.41 kPa, and 0.26 kPa, respectively. Although the intention was to keep the wall uncracked, the wall exceeded the cracked moment during the first two cycles (fixed base), when the moment at the base of the wall reached $1.4M_{cr}$ and $1.3M_{cr}$.

In the second round of six cycles, Wall-2 was loaded up to 25 mm of midspan displacement, half of the serviceability limit. Results showed 141% and 74% increments in out-of-plane pressure when the wall was under a partially fixed and fixed base condition, respectively, compared to the wall with pinned base. Wall-2 with fixed base resisted twice the out-of-plane pressure compared to Wall-1 with pinned base at 25 mm of midspan displacement (Figure 4.8b).

Wall-2 was loaded up to a midspan displacement of 50 mm during the third round of six cycles to reach the service deflection limit. An increment of 180% and 121% for required out-of-plane pressure was observed when the wall was tested under fixed and partially fixed base conditions, respectively, compared to the wall with pinned base. Wall-2 with fixed base resisted 2.13 times more out-of-plane pressure compared to Wall-1 with pinned base at 48 mm of midspan displacement (Figure 4.8b). The residual displacements reached 18.5%, 20.7%, and 26.4% of the service deflection limit at midspan for the fixed, partially fixed, and pinned base conditions, respectively. The maximum moment at serviceability conditions was recorded in the first two cycles, when Wall-2 had a fixed base, with M_{base} = $0.83M_y$.

The remaining cycles had the objective of reaching the yielding strain in the reinforcement of Wall-2 with a fixed base and comparing the performance of Wall-2 to Wall-1 with pinned base at the same stage. Six cycles on Wall-2 with fixed base targeted 75, 100, and 140 mm (two cycles each) to capture material degradation at the base. The final cycle, intended to be 140 mm, was stopped at 100 mm due to safety concerns. While Wall-1 reached yielding at 185 mm, Wall-2 reached the yielding stage at the locations of the maximum moment (at the base and $0.65h$) when the midspan displacement was 120 mm. The moment at the base was 21.1 kN-m ($1.3M_y$) and the moment at $0.65h$ was 16.0 kN-m ($0.97M_y$). The relatively early onset of yielding in Wall-2 was attributed to the cumulative damage caused by the additional cycles to different target displacements and base conditions on this wall compared to Wall-1. Even with this added damage, Wall-2 with fixed base resisted 62% more pressure and had 148% greater secant stiffness than Wall-1 with pinned base at the yielding stage. Wall-2 showed a stable response during the test without any noticeable material deterioration or wall instability.

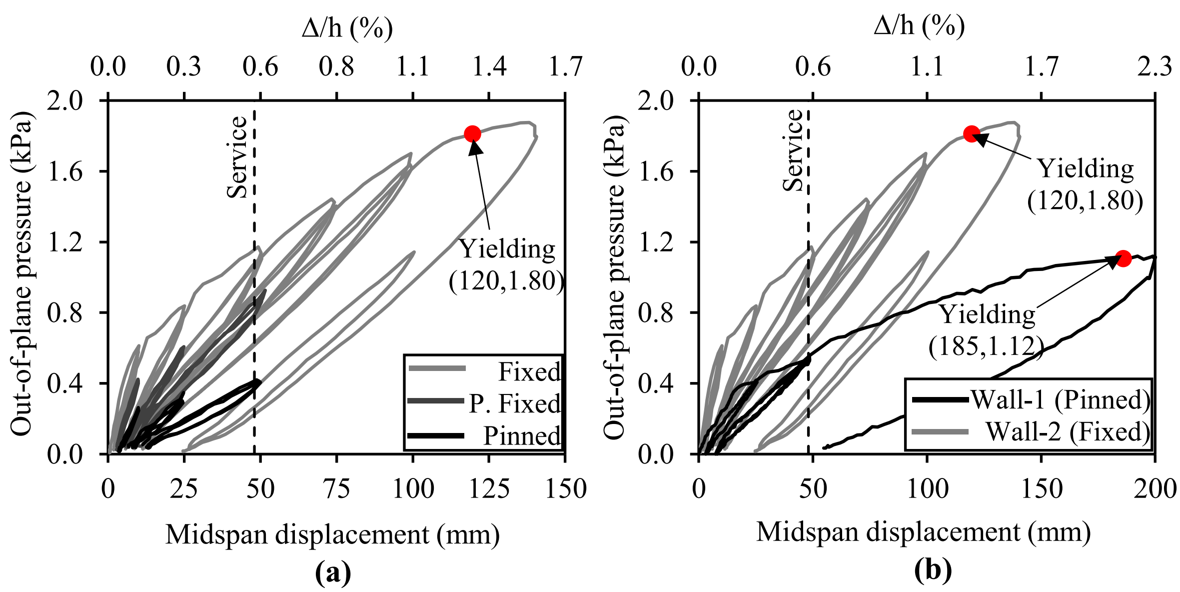

Figure 4.8 – Load - displacement history of Wall-2: (a) base comparison; (b) compared with Wall-1

Table 4.7 – Summary of test results of Wall-2

Round	Cycle	Base Support	RBS (kN-m/rad)	Δ (mm)	Δ/h (%)	OOPP (kPa)	M_{base} (kN-m)	$M_{midspan}$ (kN-m)	$\Delta_{Residual}$ (mm)
1st	1	Fixed	∞	10.2	0.12	0.61	-8.0	4.0	1.8
	2	Fixed	∞	10.0	0.11	0.58	-7.6	3.9	2.3
	3	P. Fixed	1,150	10.0	0.11	0.40	-1.9	4.9	2.9
	4	P. Fixed	1,150	9.8	0.11	0.42	-1.8	4.8	2.9
	5	Pinned	0	10.0	0.11	0.26	0.6	4.6	3.5
	6	Pinned	0	10.0	0.12	0.26	0.5	4.4	3.6
2nd	7	Fixed	∞	25.1	0.28	0.84	-10.5	5.7	5.8
	8	Fixed	∞	25.1	0.28	0.80	-10.0	5.5	5.6
	9	P. Fixed	1,150	25.0	0.28	0.61	-6.9	4.9	6.0
	10	P. Fixed	1,150	24.5	0.28	0.60	-6.9	4.8	6.0
	11	Pinned	0	25.0	0.28	0.35	1.0	6.0	8.9
	12	Pinned	0	24.5	0.28	0.30	0.9	5.3	8.4
3rd	13	Fixed	∞	50.2	0.57	1.14	-13.7	7.9	8.6
	14	Fixed	∞	50.4	0.57	1.11	-13.4	7.8	9.2
	15	P. Fixed	1,150	51.5	0.58	0.93	-8.8	7.7	9.4
	16	P. Fixed	1,150	50.4	0.57	0.87	-8.8	7.5	10.5
	17	Pinned	0	49.7	0.56	0.41	1.6	7.4	12.7
	18	Pinned	0	50.0	0.57	0.41	1.6	7.4	12.7
4th	19	Fixed	∞	74.3	0.84	1.42	-16.8	10.2	8.7
	20	Fixed	∞	74.9	0.85	1.40	-16.6	10.1	8.9
5th	21	Fixed	∞	99.5	1.13	1.70	-19.9	12.4	11.4
	22	Fixed	∞	99.7	1.13	1.62	-19.0	11.9	12.1
6th	23	Fixed	∞	140.6	1.59	1.80	-21.6	14.4	26.6
	24	Fixed	∞	100.5	1.14	1.15	-13.8	9.5	24.6

Note: RBS= rotational base stiffness; OOPP= out-of-plane pressure.

4.3.2. Deflection profiles and base stiffness relationship

The presence of partial or full fixity at the base led to increments in the capacity to resist out-of-plane pressure for the same displacements compared to the case in which a pinned base condition is used (Figure 4.8). Rotational stiffness at the base reduces out-of-plane displacements and leads to double curvature that becomes noticeable in slender elements such as the ones tested, even at uncracked and serviceability stages. Figure 4.9 shows how the deflections of Wall-2 with fixed base and partially fixed were reduced in a range of 67% to 73% and 29% to 53%, respectively, compared with the wall with pinned base.

4.3.3. Moment response and second-order effects

The total moment (M_T) profile of Wall-2 with a partially fixed base was compared to the M_T profiles under pinned and fixed base conditions. The comparison was made at three different out-of-plane pressure levels, before the yielding of the bars. The rotational base stiffness (RBS) redistributes the moment along the height of the wall (when the wall cracks) and leads to large moments at the base. For low pressures (Figure 4.10a), the midspan moments of the partially fixed wall and the pinned wall are similar, but as the pressure increases (Figure 4.10b-c) – after cracking, the moment at the partially-fixed case starts resembling that from the fixed base condition.

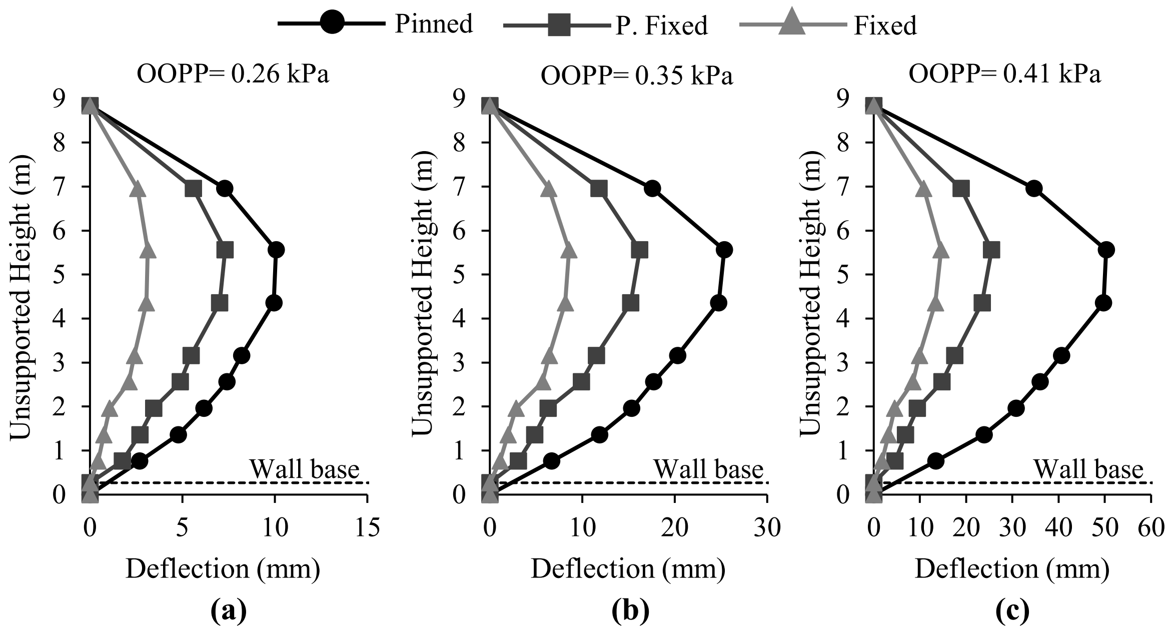

Figure 4.9 – Wall-2 deflected profile comparison (a) at 0.26 kPa; (b) at 0.35 kPa; (c) at 0.41 kPa

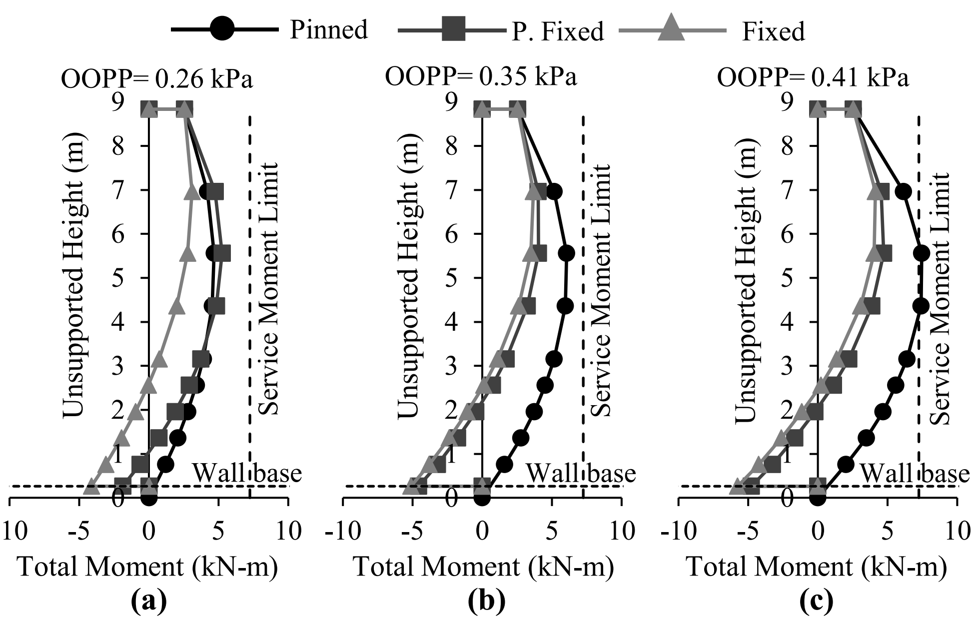

Figure 4.10 – Wall-2 moment profile comparison: (a) at 0.26 kPa; (b) at 0.35 kPa; (c) at 0.41 kPa

Figure 4.11a compares M_T and second-order moment (M_2) profiles of Wall-2 (fixed base) at the maximum out-of-plane pressure (1.12 kPa) applied to Wall-1 (pinned base) during the test. The maximum moment observed in Wall-1 (pinned base) was $1.1M_u$ at midspan, while in Wall-2 (fixed base) M_T was $0.4M_u$ at midspan and $0.7M_u$ at the base. The decrease of M_T at midspan of Wall-2 (fixed base) is attributed to the 77% reduction of M_2 compared with Wall-1 (pinned base), which is directly proportional to the reduction of deflections (from 200 mm to 46.3 mm) at midspan due to the presence of base stiffness.

Figure 4.11b compares the M_T and the M_2 profiles of Wall-1 (pinned base) at the maximum midspan displacement (140 mm) subjected in Wall-2 (fixed base) during the test. The maximum moment observed in Wall-2 (fixed base) was $1.2M_u$ at the base and $0.8M_u$ at midspan while in Wall-1 (pinned base) M_T was $0.9M_u$ at midspan. No reductions in M_2 were observed since the comparison was made at the same midspan displacement. However, an increment of 80% in out-of-plane capacity was observed in Wall-2 (fixed base) compared to Wall-1 (pinned base). After Wall-2 reached yielding (at 120 mm), the moment at the base remained essentially constant ($1.1M_u$) up to 140 mm of midspan displacement. While a small increase in moment of $0.1M_u$ was observed at midspan and $0.65h$, which is attributed to moment redistribution.

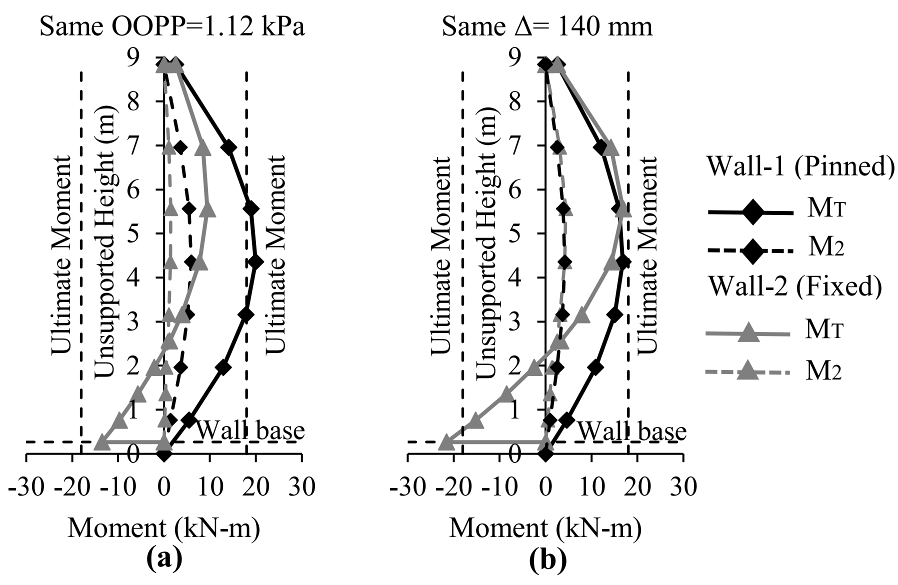

Figure 4.11 – MT and M2 profiles: (a) at same OOPP= 1.12 kPa; (b) at same Δ= 140 mm

In both cases, Wall-1 and Wall-2 exceeded the M_u without any sign of observable masonry damage (cracks/crushing) or instability. One of the main concerns in tall walls is the magnitude of the second-order effects due to the expected large deflections. Results here indicate that once the base stiffness on tall walls is accounted for, reductions in deflections and second-order effects are expected due to the change of moment distribution.

4.3.4. Damage analysis

Table 4.8 shows the maximum relative strains of the block face shells in compression and the steel reinforcement at the base of the wall, midspan, and $0.65h$ during the test of Wall-1 (pinned base) and Wall-2 (fixed base).

Table 4.8 – Maximum strain readings

Wall	Masonry (ε_{mu}= 3000με)			Steel reinforcement (ε_y= 2200με)		
	Base	Midspan	$0.65h$	Base	Midspan	$0.65h$
1	$0.01\varepsilon_{mu}$	$0.15\varepsilon_{mu}$	$0.16\varepsilon_{mu}$	$0.11\varepsilon_y$	$1.07\varepsilon_y$	$1.22\varepsilon_y$
2	$0.16\varepsilon_{mu}$	$0.12\varepsilon_{mu}$	$0.14\varepsilon_{mu}$	$1.05\varepsilon_y$	$0.70\varepsilon_y$	$1.12\varepsilon_y$

Note: ε_{mu}= ultimate compressive strain as per CSA S304-14 (2019);
ε_y= tensile yielding strain according to the material properties of 15M bars in Table 4.4

The strain response was consistent with the results presented in the load-displacement response section where the yielding was present at midspan for Wall-1 with pinned base, while Wall-2 with fixed base, was located at the base and $0.65h$ due to the change of moment distribution.

A visual inspection was done after every cycle of Wall-1 (pinned base) and Wall-2 (fixed base) to monitor the opening of joints at the walls. The maximum moment on Wall-1 with pinned base was expected at midspan, so a camera was placed facing the side of the wall at midspan to capture joint opening. Joints remained closed at 25 mm midspan displacement (Figure 4.12a). However, joint opening on the tension zone of the wall was observed when Wall-1 reached 48 mm of midspan displacement (Figure 4.12b), which became more pronounced when the midspan displacement was 200 mm (Figure 4.12c). Surface cracking at face shells was not observed in the compression zone of the wall after the test, which is consistent with the low compressive strain values captured at that region ($0.16\varepsilon_{mu}$).

For Wall-2 with fixed base, joints at midspan remained closed, up to 75 mm of midspan displacement (Figure 4.13). This was attributed to reduction of 27% of moments at midspan compared with Wall-1 with pinned base. Unfortunately, due to a camera malfunction, there was no photographic evidence after 75 mm of midspan displacement (cycle 19).

(a) (b) (c)

Figure 4.12 – Joint opening of Wall-1 at midspan: (a) Δ= 25 mm; (b) Δ= 48 mm; (c) Δ= 200 mm

(a) (b) (c)

Figure 4.13 – Joint opening of Wall-2 at C-22: (a) Δ= 25 mm, (b) Δ= 50 mm; (c) Δ= 75 mm

One of the main concerns was the potential material degradation at the wall base under out-of-plane cyclic loading when the base stiffness was accounted for in Wall-2. No joint opening was observed during the first six cycles of Wall-2. However, joint opening on the tension zone (back of the wall) at the base appeared and became more pronounced as the wall was subject to larger displacements (Figure 4.14).

(a) (b) (c)

Figure 4.14 – Joint opening of Wall-2 at base: (a) Δ= 25 mm; (b) Δ= 50 mm; (c) Δ= 140 mm

At the end of the test of Wall-2, a general inspection was done along the wall height to find any material degradation, mainly at $0.65h$ and the base of the wall. However, no signs of surface cracks were observed in the wall after the test, which is consistent with the low compressive strain values captured at midspan ($0.14\varepsilon_{mu}$) and at the base ($0.16\varepsilon_{mu}$) (Figure 4.15).

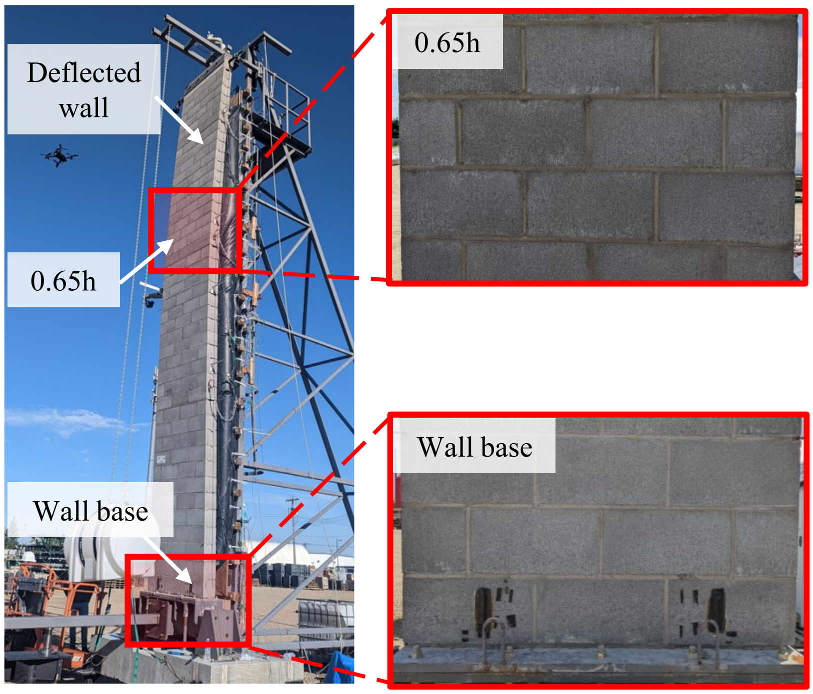

Figure 4.15 - Visual inspection along the height of Wall-2

The results were consistent with the findings by Pettit et al. (2021, 2022). However, it is noted that the tests of the walls were stopped before failure, and there was little plastic behaviour observed due to safety considerations and the risk of damaging the airbag if the wall fails. The cyclic damage observed in these walls is deemed valid for walls at the serviceability stage and yielding. More tests are required that investigate the behaviour at ultimate of full-scale specimens.

4.4. Implications for design

Engineers designing walls with $kh/t > 30$ designed per the CSA S304-14 (2019) standard are directed to the assumption that the base conditions are pinned. There is no equivalent clause in the U.S. masonry standard (TMS 402-16 2016). TMS 402-16 and North American reinforced-concrete standards (ACI 318-19 2019, CSA A23.3:19 2019) allow designers to consider the base fixity of walls of any height via rational analyses. The impact of this clause is twofold. First, it reduces the capacity of slender masonry walls under a given set of loads, requiring thicker blocks and/more reinforcement, which makes them uneconomical. Second, as shown by the analyses of Pettit and Cruz-Noguez (2021), relatively light foundations in soils with moderate capacity produce significant rotational stiffnesses; wall designs that neglect the presence of moments at the base may be potentially unsafe if the wall-base connection is not appropriately detailed. For example, an explosive, brittle failure mode in the bottom half of 2.4m high wallets was observed by Pettit and Cruz-Noguez (2021). This is concerning since the wall-foundation connection consists of lap splices where the maximum moment would be expected. Furthermore, the seismic design of these types of walls requires a specific level of ductility where neglecting the base stiffness is unconservative due to the reduction of deformation capacity and energy dissipation associated with walls featuring a rotational base stiffness (Pettit and Cruz-Noguez 2021).

4.5. Summary

Two slender-tall masonry walls were tested under different base conditions (pinned, partially fixed, and fixed) subjected to eccentric axial load and cyclic out-of-plane pressure, highlighting the following observations:

- An increase in out-of-plane capacity by 113% and 62% (at service and yielding stages, respectively) while decreasing the deflections by 77% (in both service and yielding stages) was observed when Wall-2 with fixed base was tested compared to Wall-1 with pinned base.
- A decrease of 61% in the M_T at midspan was observed when 1.12 kPa of out-of-plane pressure was applied to Wall-2 with fixed base compared to Wall-1 with pinned base, attributed to the change of moment distribution.
- When Wall-2 was subjected to 0.25 kPa of out-of-plane pressure under a partially fixed base condition, it developed a similar moment profile to a wall under a pinned base condition. However, when the out-of-plane pressure increased by 35%, the moment profile changed drastically to a similar moment profile of a wall under a fixed base condition.
- A decrease of 77% in M_2 and an increase of 80% in out-of-plane pressure was observed when Wall-2 (fixed base) and Wall-1 (pinned base) were compared at the same out-of-plane pressure (1.12 kPa) and at the same midspan displacement (140 mm), respectively.

- No visible material degradation was observed at the midspan ($0.15\varepsilon_{mu}$) and at the base of the wall ($0.16\varepsilon_{mu}$) during the test of both walls. Even though M_u was exceeded by 10% at the midspan of Wall-1 with pinned base and by 20% at the base of Wall-2 with fixed base.

It can be concluded that the presence of base stiffness enhances the out-of-plane performance of loadbearing masonry walls, increasing their capacity and decreasing their lateral deflections. The increase in capacity is attributed to the change of moment distribution along the wall height, while the reduction of second-order effects is attributed to the decrease in out-of-plane deflections. The wall-foundation interaction provides a rotational stiffness that resembles the behaviour of a fixed base condition after the cracked stage. Degradation at the wall base does not appear to be a factor since no visible material degradation was observed up to the yielding stage, suggesting a different mode of failure than expected for walls designed under pinned base conditions as required by CSA S304-14 for walls with a height-to-thickness ratio over 30.

Future research directions could focus on the development of rational methods to account for the rotational base stiffness in the design process of tall walls, such as:

- Using effective height factors (k) for different soil types and strip footing sizes, as it is allowed for walls with height-to-thickness ratios below 30 by the CSA S304-14.
- Obtaining pertinent equations for moments and deflections at crucial sections of the wall with the desired rotational base stiffness, using the principles of mechanics as the TMS 402-16 allows.
- Modelling the soil-structure interaction and the lap splices directly to the base of the wall, but this option could be less attractive for structural designers.

The benefits of base stiffness in the out-of-plane response presented in this study are limited to the yielding stage. Therefore, it is recommended to investigate the influence of base stiffness at the failure stage to prove if the level of fixity remains in the wall-foundation connection before failure and improve the effective flexural stiffness equation to obtain efficient wall designs.

Note: *Tasks 1.3 to 1.5 were addressed in this chapter to complete objective 1.*

5 THE EFFECT OF THE WALL-FOUNDATION INTERACTION ON THE OUT-OF-PLANE FLEXURAL RESPONSE OF SLENDER MASONRY WALLS [3]

Loadbearing masonry walls with a height-to-thickness ratio greater than 30 are typically employed in single-storey buildings such as warehouses, theatres, community centres, and school gymnasiums. When subjected to combined gravity and lateral loads, these walls are an effective structural system. North American masonry design standards (CSA S304-14 and TMS 402-16) set additional design criteria for these walls due to their perceived vulnerability to second-order effects. One of the CSA S304-14 design requirements is neglecting the base stiffness provided by the wall-foundation interaction, which impacts the strength and stiffness of slender masonry walls. However, the TMS 402-16 permits using different types of base support for any height-to-thickness ratio. This study aims to determine the out-of-plane flexural response of masonry walls subjected to combined gravity and lateral loads under various height-to-thickness ratios, types of soils, foundation geometry, and foundation depth. The parametric analysis showed increased flexural capacity and decreased deflections in the out-of-plane direction when the wall-foundation interaction was included in the push-over analysis of the wall. The foundation depth is one aspect that most affects the base stiffness. Even with weaker soils and small footing sizes, the flexural response of slender masonry walls can be similar to that of a fixed base. These findings imply that accounting for base rigidity in the analysis and design of slender masonry walls could be an untapped source of strength and stiffness, which may lead to more cost-effective masonry wall designs.

5.1. Introduction

Tall loadbearing masonry walls are popular in low-rise buildings such as industrial facilities, warehouses, retail stores, and school gymnasiums. Usually, strip footings are an efficient foundation solution for these types of walls because of the moderate gravity loads from the light roof system and the long continuous spans found in the exterior walls. The connection between the wall and the foundation is made by dowels fully anchored into the footing and spliced with the flexural steel reinforcement at the bottom of the wall, which can be considered a moment

[3] A version of Chapter 5 is in preparation as Alonso, A.; Gonzalez, R.; Elsayed, M.; Billota, M.; Deng, L.; Tomlinson, D.; and Cruz-Noguez, C. "The effect of the wall-foundation interaction on the out-of-plane flexural response of slender masonry walls", to be submitted in a journal paper.

connection. Moreover, the interaction between the flat base of the wall and the flat surface of the foundation when the wall tries to rock provides some level of fixity, according to Isfeld et al. (2019). Therefore, axial/shear forces and moments are transferred to the footing, which distributes the stresses into the soil, creating a semi-rigid base condition.

Despite the inherent base stiffness due to the wall-foundation interaction, when the masonry walls are slender ($kh/t \geq 30$) North American masonry design standards (TMS 402-16 2016, CSA S304-14 2019) set special design criteria for these masonry walls due to their perceived vulnerability to second-order effects. One of the CSA S304-14 (2019) design requirements is neglecting the base stiffness provided by the wall-foundation interaction. While the TMS 402-16 (2016) permits using different types of base support for any height-to-thickness ratio (h/t). The reluctance in the Canadian standard to account for the base stiffness could be due to the need for simplified and conservative design expressions before computers and specialized structural analysis software were more readily available and the lack of experimental data about the rapidly degrading wall-foundation interface due to cyclic loading.

Current code provisions for designing slender masonry walls are based on a small set of experimental programs, resulting in conservative design provisions. Since 1980, there has been no innovation in slender masonry walls since the American Concrete Institute (ACI) and the Structural Engineers Association of Southern California (SEASC) created a Test Report on Slender Walls (1982). This report was used as a reference to develop the following Canadian masonry design standard (CSA S304.1-M94 1994) until the current one (CSA S304-14 2019). Influenced by the AC-ASEC (1982) report, later studies on masonry walls did not explore walls featuring other base conditions but only with pinned base conditions (Liu et al. 1998, Liu and Dawe 2001, Liu and Hu 2007, Bean Popehn et al. 2008, Sparling et al. 2020, Sparling and Palermo 2023). Few studies (Mohsin 2005, Isfeld et al. 2019, Pettit and Cruz-Noguez 2021, Pettit et al. 2022) have addressed the effect of base stiffness on the out-of-plane behaviour of masonry walls after the ACI-SEASC (1982) report.

Even though the studies related to base stiffness have demonstrated the benefit of accounting for it, some important factors for the out-of-plane behaviour of slender walls have been neglected. To cover those aspects not entirely covered in previous experimental studies, two full-scale specimens were tested under a combination of gravity and lateral loads using different base stiffnesses, including a high slenderness ratio, realistic load combinations, and realistic support conditions in the experimental program of this research. Conclusions from the experimental study revealed that the presence of base stiffness improved the out-of-plane flexural behaviour of slender masonry walls. The increase in capacity and decrease in out-of-plane deflections are attributed to the change of moment distribution along the wall height, which reduces second-order effects. After the cracked stage, even a small value of base stiffness modified the wall behaviour to be similar to a wall with fixed base. No visible material degradation at the wall base was observed up to the yielding stage, suggesting a different failure mode than expected for walls designed under pinned base conditions. These benefits and observations are limited to the yielding stage since the walls were tested up to yielding due to safety concerns.

To overcome the economic, time, and practical constraints in experimental programs, finite element micro-modelling, macro-modelling, and simplified analytical approaches have been developed to predict the complex local or global behaviour of masonry structures. Micro-models explicitly model the interaction among the masonry units, mortar, and grout (Page 1978, Ali et al. 1986, Lotfi and Shing 1994, Sayed-Ahmed and Shrive 1995, Yi and Shrive 2001). This alternative effectively captures the local behaviour of masonry walls, but it is more computationally expensive. While macro-models treat the masonry assemblage as a homogeneous material – no distinction between the masonry units, mortar, and grout (Wang et al. 1997, Lopez et al. 1999, Pluijm 1999, Ma et al. 2001, Donà et al. 2018, Metwally et al. 2022). This alternative effectively captures the global behaviour of masonry walls with a lower computational cost, but it is limited when trying to capture detailed modes of failure. On the other hand, the simplified analytical models provide fast, stable, and exact solutions (Liu and Dawe 2003, Pettit 2019). However, they are restricted due to the number of modelling assumptions in ideal conditions, which rarely apply in reality.

When the soil-structure interaction is included in the numerical model, similar approaches are used to model the soil domain – micro and macro modelling (continuum). Depending on the level of detail of the required structural response, researchers opt to model the soil domain as a continuum (Masia Mark J. et al. 2004, Güllü and Jaf 2016, Piro et al. 2020, de Silva 2020, Fathi et al. 2020), while the macro-modelling approach is used more often to model the soil domain if the simplified model is enough for the required structural response. For instance, Petti et al. (2021,

2022) developed a linear-elastic Winkler model of a strip footing to obtain the out-of-plane rotational stiffness for different sizes of strip footings and soil types. The soil-foundation interaction was captured by defining elastic springs along the bottom edge of the foundation with a tributary vertical stiffness for each spring. Analyzing the possible combinations, the rotational stiffness values from the analysis provided range from 1,500 to 12,000 kN-m/rad. However, the superstructure was not included in the parametric analysis, the model did not account for the foundation depth properly, and the spring was modelled in the linear-elastic range.

This study aims to study the role of the wall-foundation interaction in the out-of-plane flexural response of slender masonry walls by developing a finite-element macro-model with static soil-structure interaction. A parametric analysis was performed, changing key parameters such as height-to-thickness ratios, types of soils, foundation geometry, and foundation depth. Results were analyzed in terms of flexural capacity, base stiffness intensity, and stability analysis to propose effective height factors (k) for different foundation conditions. Also, construction recommendations were proposed to improve the behaviour of the wall-foundation connection on strip footings in common soil types.

5.2. Slender masonry wall – typical configuration

5.2.1. Loading

Typically, the height of slender masonry walls ranges from 4 to 8 metres in single-storey buildings. The design of these types of walls is governed by flexure due to the combined gravity and out-of-plane loads. Due to the light roof systems used in these types of buildings, moderate gravity loads are expected, as well as small inertial forces in seismic events. Therefore, wind loads are the most critical when designing slender masonry walls due to the large spans and exposed areas in the out-of-plane direction. Figure 5.1 shows the typical external loading scenarios on exterior walls in single-storey buildings.

5.2.2. Steel reinforcement configurations and grout schemes

To resist the combined effects of gravity and out-of-plane loads, a steel reinforcement (flexural) configuration and grout scheme are selected when designing these types of walls. The rebar size and spacing are calculated and placed in the middle of selected cores. When only the reinforced cores are filled with grout, the wall is considered a partially grouted (PG) wall (Figure 5.2a), and when all the cores (reinforced and unreinforced) are filled with grout, the wall is known as a fully grouted (FG) wall (Figure 5.2b). Designers prefer PG walls over FG walls because they are lighter, reducing the self-weight, which has a significant impact on the calculation of second-order effects, reducing the inertial forces in seismic events, reducing the gravity load transmitted to the soil, making possible the use of small sizes of footings, and reducing the labour and material costs.

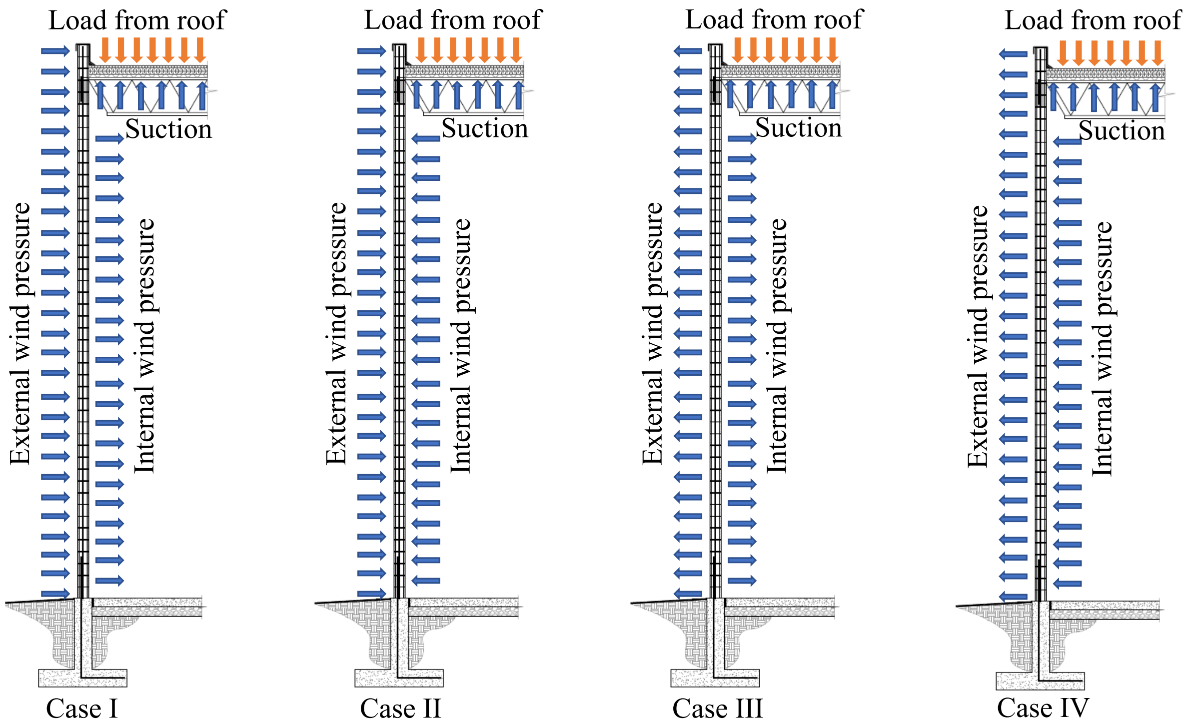

Figure 5.1 – Typical loading configuration in exterior walls

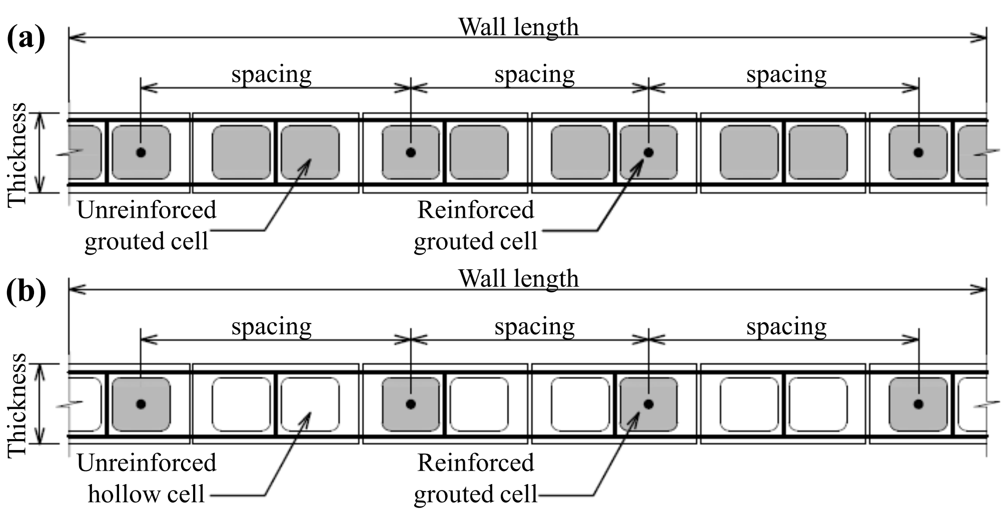

Figure 5.2 – Typical reinforced wall cross-section: (a) fully grouted; (b) partially grouted

5.2.3. Wall-foundation connection

Shallow foundations can be used on slender masonry walls if the soil is moderately competent. Strip footings are an efficient foundation solution for these types of walls because of the moderate gravity loads and the long continuous spans in the exterior walls. Strip footings are complemented by wall foundations from the footing slab to the ground level. In masonry construction, the wall foundations can be made of masonry (Figure 5.3a) or reinforced concrete (Figure 5.3b). The connection between the wall and the foundation is made by dowels fully anchored into the footing and spliced with the flexural steel reinforcement at the bottom of the wall, which can be considered a moment connection. Therefore, loads (vertical/lateral) and moments are transferred to the foundation, which distributes the stresses in the soil, creating a semi-rigid base for masonry walls.

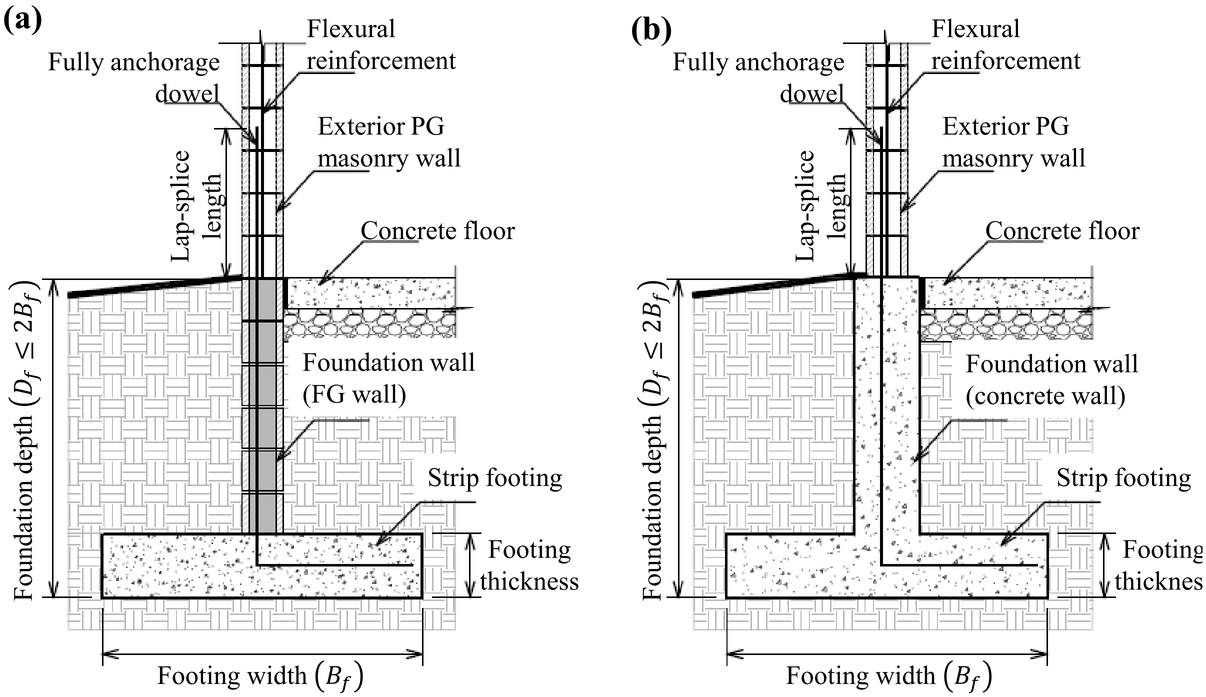

Figure 5.3 – Wall-foundation connection: (a) FG foundation wall; (b) Concrete foundation wall

5.3. Analysis model of slender masonry walls

Based on the typical configuration for slender masonry walls found in single-storey buildings, described in the previous section, the following characteristics were considered for the model:

- Loading Case IV from Figure 5.1, where internal and external wind pressures deflect the wall in the same direction as the moment created by the eccentric load from the roof – the suction on the roof was neglected.
- A conventionally reinforced PG wall of one-metre length (Figure 5.2b), founded on a reinforced concrete strip footing, and connected through fully anchored dowels spliced with the flexural reinforcement at the bottom of the wall (Figure 5.3b).

5.3.1. Numerical model

The model was developed using displacement-based beam-column type elements in an open-source FE software framework OpenSees (McKenna et al. 2000). A fibre cross-section was used to capture the material nonlinearity through distributed plasticity, using suitable uniaxial stress-strain constitutive relationships for each material. The homogenous behaviour of the masonry assemblage was simulated using the material C*oncrete02* based on the Kent-Scott-Park (1971) model. The steel reinforcement was simulated using the material *Steel02* with isotropic strain hardening based on the Guiffre-Menogoto-Pinto (1973) model. The model proposed by Barkhordary and Tariverdilo (2011) was used to account for bar slip in lap-splice located at the bottom of the wall, which consists of modifying the material stress-strain behaviour of the steel in tension while the stress-strain behaviour in compression remains intact. A *hysteretic* material model available in the OpenSees library was used to implement the modified stress-strain behaviour of the steel in lap-splice, with the maximum bar stress value calculated with the method proposed by Priestley et al. (1996). The geometric nonlinearity was considered by implementing the *corotational* geometric transformation rule in the OpenSees library. The top of the wall is free in the global Y direction but restrained in the global X direction while allowing rotation, emulating roller support. The model was divided into two modules to simulate the base of the wall. Module 1 consisted of simplified base conditions (pinned, partially fixed, or fixed). Module 2 explicitly modelled the soil-foundation interaction by using the beam-on-nonlinear-Winkler-foundation (BNWF) method, which distributes nonlinear springs along the width of the footing (Harden et al. 2005, Harden and Hutchinson 2009). Loading-wise, the macro model described was analyzed using a monotonic push-over analysis. The vertical axial load (P) with eccentricity (e) was modeled by the equivalent axial load and moment combination ($P,\ M = P \cdot e$) while the self weight was uniformly distributed along the height of the wall. The lateral pressure (ω) is applied along the height of the wall until the target displacement at midspan is achieved. The schematic drawing of the model described is shown in Figure 5.4.

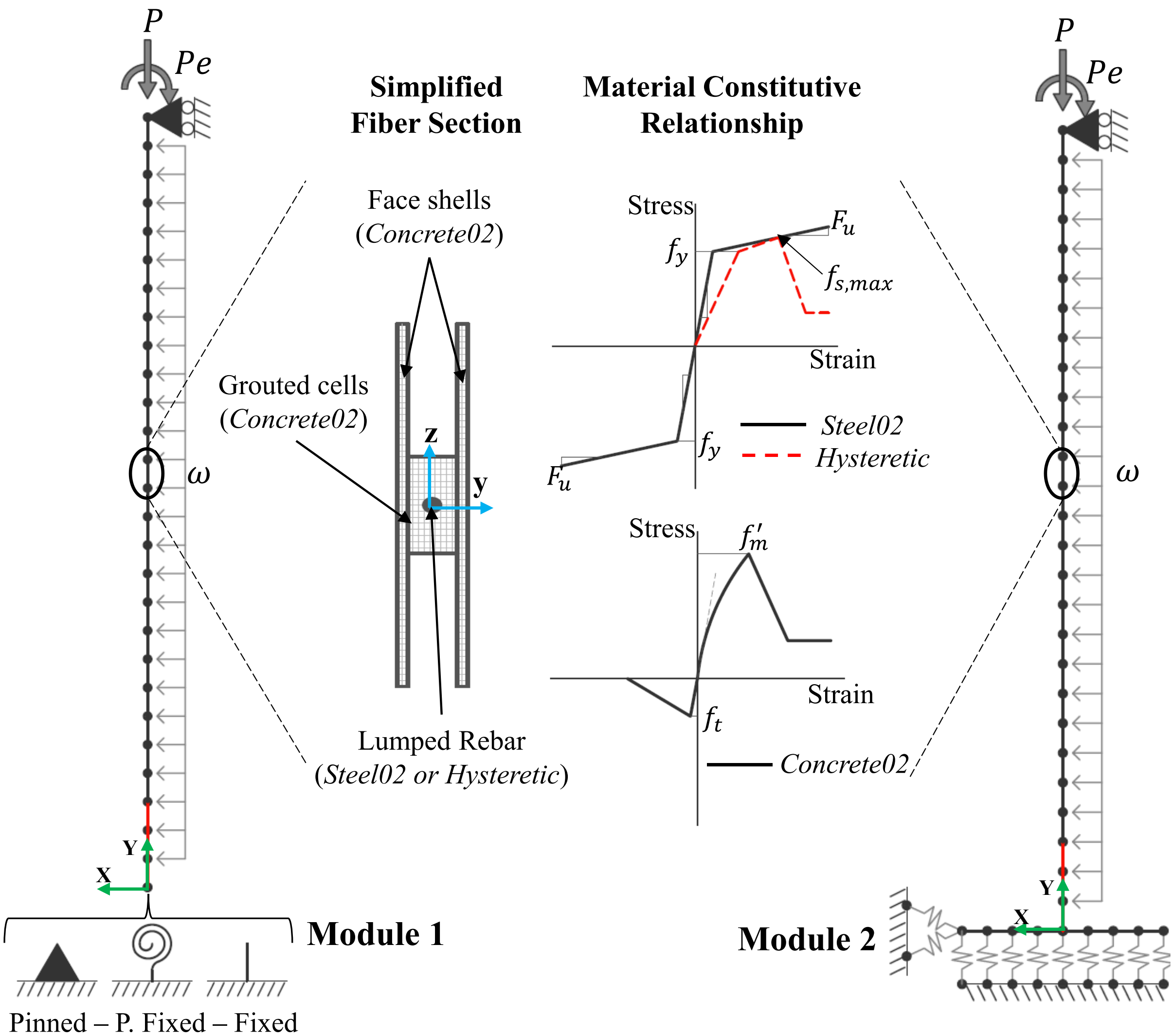

Figure 5.4 – FE macro model composition (global axes: green; local axes: blue)

The soil-foundation interaction introduced in Module 2 uses elastic beam-column elements to model the footing, while the nonlinear properties of the soil were modelled using zero-length soil elements (*q-z*, *p-y*, and *t-z*). The *q-z* elements capture the rocking, uplift, and settlement. The *p-y* elements capture the passive resistance of the soil surrounding the footing, and the *t-z* elements capture the friction resistance between the soil and foundation. Input parameters for the soil elements are the ultimate capacities (bearing capacity – Q_{ult}, horizontal passive resistance – P_{ult}, and horizontal sliding resistance – T_{ult}) and the displacements at half of the ultimate capacities (z_{50q}, y_{50p}, and z_{50t}). The ultimate capacities were obtained from conventional bearing capacity equations from the Canadian Foundation Engineering Manual (2006) and Coulomb's earth pressure. The static vertical and lateral stiffness of the soil were calculated using the equations given by Gazetas (1991) and Mylonakis et al. (2006), which depend on the secant shear modulus of the soil (G), Poisson's ratio (v), foundation geometry, and embedment depth (D_f). The rotational stiffness is captured by the variable distribution of the vertical nonlinear springs along the base footing. The footing is divided into two zones – end and middle zones. The end zones have a stiffness intensity greater than the middle zone to account for the higher reaction and the footing edges when subjected to combined vertical and rocking movements (Harden et al. 2005). The length end zone was obtained according to the equations proposed by Harden et al. (2005) that depend on the footing aspect ratio (B_f/L_f). The q-z element spacing was 0.01 m to provide numerical stability and reasonable accuracy, following the recommendation of Harden et al. (2005). The details of the soil-foundation interaction implemented in Module 2 are shown in Figure 5.5.

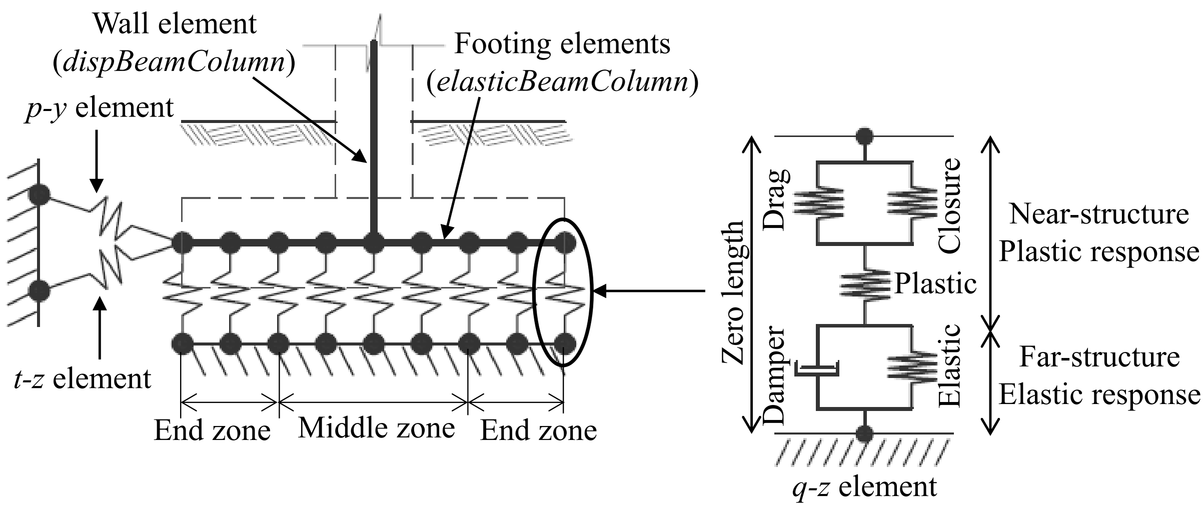

Figure 5.5 – Beam-on-nonlinear-Winkler-foundation (BNWF) model used in Module 2

5.3.2. Model validation

Results from the experimental program of this research were used to validate the model described. The experimental program consisted of two full-scale, partially grouted walls, tested under combined eccentric axial load and out-of-plane pressure. The walls were 8.75 m high, 1.19 m wide, and 0.19 m thick, with $h/t = 46$. The vertical reinforcement consists of 2-15M (ϕ=16.0 mm) bars at 600 mm. Wall-1 with pinned base was tested to 200 mm of midspan displacement (yielding), while Wall-2 with pinned, partially fixed, and fixed base was tested at 48 mm of midspan displacement (service limit) and 140 mm of midspan displacement (yielding) with a fixed base condition only.

Figure 5.6 compares the experimental load-displacement history from Wall-1 and -2 with the predicted capacity curve from the numerical model.

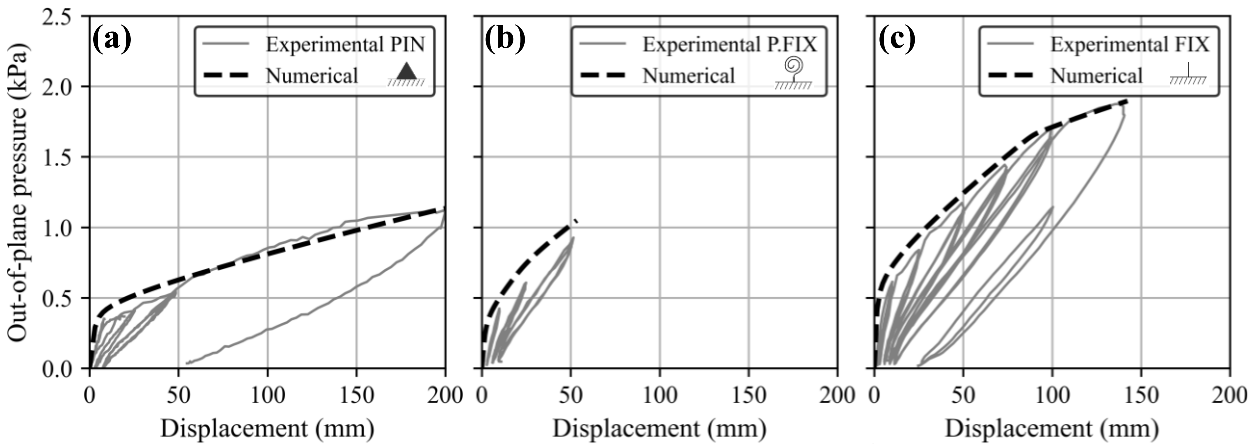

Figure 5.6 – Model validation - Global response: (a) Wall-1 (pinned base); (b) Wall-2 (partially fixed base); (c) Wall-2 (fixed base)

Since it is scarce to find a full-scale tall wall test with a real foundation, a pre-analysis was done to obtain an equivalent rotational base stiffness (RBS) using different soil types, foundation depth (D_f), and footing width (B_f), to match the RBS= 1,150 kN-m/rad used during the test of Wall-2 with a partially fixed base to validate the numerical model using Module 2.

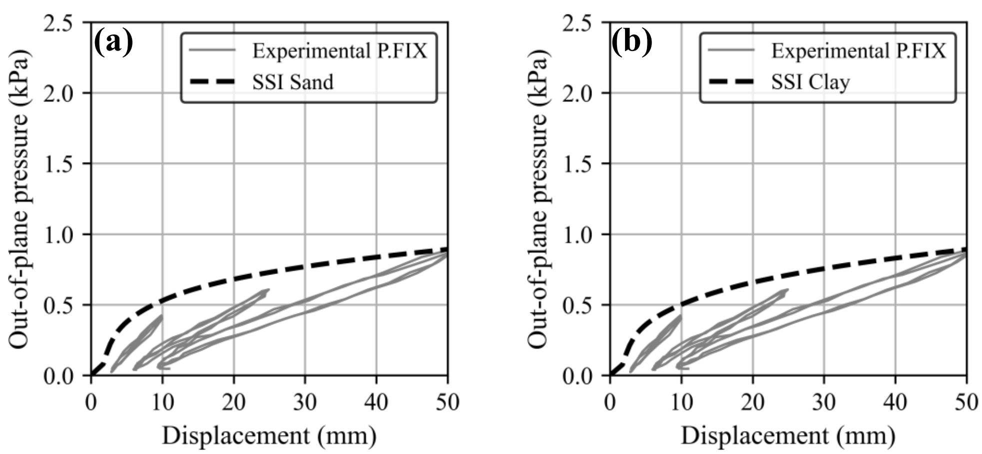

Figure 5.7 – Model validation (Module 2) - Global response of Wall-2 under partially fixed base: (a) SSI - sand; (b) SSI - clay

Figure 5.7 compares the experimental load-displacement history from Wall-2 under a partially fixed base (RBS= 1,150 kN-m/rad) with the predicted capacity curve from the numerical model using static soil-structure interaction – (a) Loose Sand, D_f=0.60 m, and B_f=0.60 m were used to obtain an equivalent RBS= 1,200 kN-m/rad; (b) Soft Clay, D_f=0.60 m, and B_f=0.70 m were used to obtain an equivalent RBS= 1,180 kN-m/rad.

Figure 5.8 compares the tensile (steel) and compressive (block) strains predicted in the numerical model with the strains captured during the test where maximum moments were located.

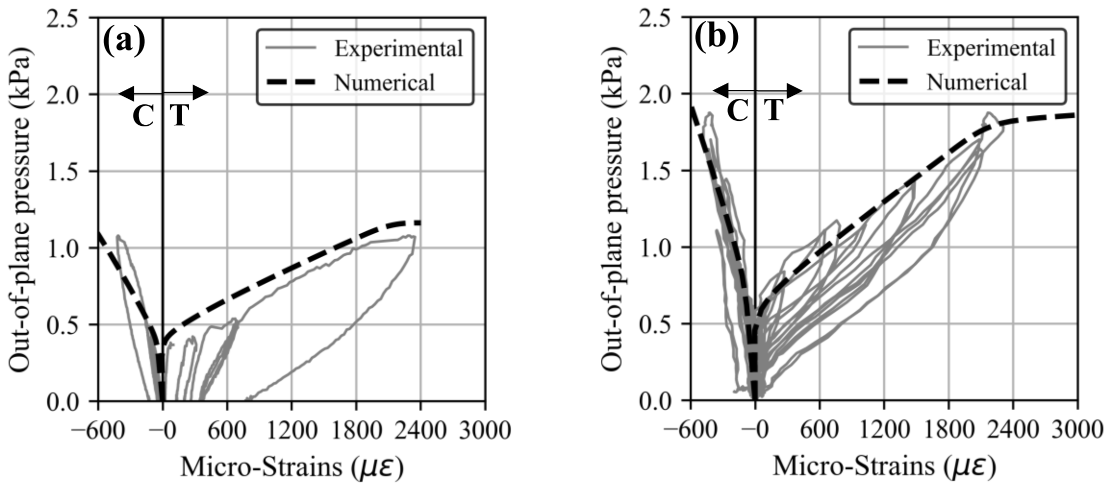

Figure 5.8 – Model validation - Local response: (a) Strains at midspan in Wall-1 (pinned base); (b) Strains at wall base in Wall-2 (fixed base)

The results show that the numerical model using Modules 1 and 2 achieved reasonable agreement in the global (predicted out-of-plane capacity) and local (predicted strains at critical locations) responses compared with the experimental results of both walls tested under different base conditions.

5.3.3. Limitations

The finite element model described was developed using a macro-modelling approach to capture the overall behaviour of loadbearing-slender masonry walls in the out-of-plane direction and the effect of the wall-foundation interaction. The model effectively predicted the global and local responses of slender masonry walls under different base conditions. However, the model has the following limitations:

- The model does not include the out-of-plane shear failure mechanism since walls with heights > 3.0 m are flexural-dominated, which is the primary focus of this research. If short walls want to be modelled, the shear failure mechanism must be added.

- The model can not predict detailed local responses such as crack propagation, material degradation, or join openings. A macro-modelling approach should be used if a more detailed response is required.
- The model does not account for dynamic loading (e.g., cyclic loading due to seismic events) nor material degradation. If dynamic loading wants to be included, degradation parameters in the out-of-plane direction must be used to modify the material models. Also, the static stiffness of the soil included in the model must be modified by dynamic factors that depend on the loading frequency to obtain the dynamic stiffness of the soil.

5.4. Parametric study

A parametric study was conducted to evaluate the effect of the wall-foundation interaction in the out-of-plane flexural response of loadbearing-slender masonry walls, including the out-of-plane capacity, equivalent rotational base stiffness, and stability analysis to obtain effective height factors.

5.4.1. Fixed parameters

Table 5.1 summarizes the fixed parameters that did not vary during the study. The walls analyzed were partially grouted (PG) with 15MPa–20cm concrete masonry units (CMU) and reinforced with 15M bars every 600 mm. The total axial load maintained a constant ratio of 0.9 with the maximum axial load allowed ($0.05f'_m A_e$) by the TMS 402-16 (2016) during the analyses.

Table 5.1 – Fixed parameters summary

Parameter	Value
Wall thickness	190 mm
Wall effective width	1000 mm
Total axial load ($P_f = P + P_w$)	40 kN/m
Load eccentricity (e)	63 mm
Compressive Masonry Strength (f'_m)	8.5 MPa
Tensile Masonry Strength (f_t)	0.55 MPa
Effective area of steel per metre (A_{s_m})	333 mm^2/m
Steel Yield Strength (f_y)	400 MPa
Steel Modulus of Elasticity (E_s)	200 GPa

5.4.2. Dependent parameters

The out-of-plane capacity of the loadbearing-slender masonry walls and the equivalent rotational base stiffness (RBS) were the dependent parameters of this study. These parameters were obtained from different cases of slenderness ratio, soil type, foundation depth, and footing width.

5.4.3. Independent parameters

Table 5.2 summarizes the independent parameters selected to investigate the effect on the dependent parameters: the wall height (h), the soil type (Table 5.3), foundation depth (D_f), and footing width (B_f). The height of the walls varied according to the usual range found in single-storey buildings, modifying the slenderness ratio (h/t), the initial imperfection at midspan ($0.1h$), and the self weight of the wall (P_w). The maximum foundation depth used in the analysis was 1.20 m, which is the minimum depth recommended for shallow foundations to prevent frost heaving in cold climates. The footing width range was based on the standard dimensions used in strip footing for long walls in single-storey buildings.

Table 5.2 – Simulation matrix

Parameter	Values
Wall height (h)	[4.8, 5.8, 6.8, 7.6] m
External axial load (P)	[31, 29, 26, 22] kN/m
Soil type: Sand	[Loose, Medium, Dense]
Soil type: Clay	[Soft, Medium, Stiff]
Foundation depth (D_f)	[0.30, 0.60, 0.90, 1.20] m
Footing width (B_f)	[0.60 – 1.60] every 0.10 m

Table 5.3 - Properties of typical soil types

Type of soil		Unit Weight (kN/m³)	Internal friction angle (degrees)	Cohesion (kPa)	Poisson's ratio	Modulus of Elasticity (MPa)
Sand	Loose	14.5	28	-----	0.30	20
	Medium	16.5	32	-----	0.33	25
	Dense	18.0	37	-----	0.38	45
Clay	Soft	11.5	-----	25	0.35	12
	Medium	14.5	-----	50	0.35	30
	Stiff	17.0	-----	100	0.35	70

Reference: *Principle of Foundation Engineering by Braja M. Das* (2023)

5.5. Results and discussion

5.5.1. Load-displacement curves

Load-displacement curves were plotted to evaluate the effect of slenderness (h/t), foundation depth (D_f), and footing width (B_f) in the out-of-plane wall capacity for each type of soil. The lateral pressure (LP) was normalized with the maximum lateral pressure (LP_{max}) from the wall with fixed base and plotted against the drift (Δ_{mid}/h). The capacity curves of the walls under pinned and fixed base conditions serve as lower and upper bound to compare the capacity curves with different foundation widths (B_f).

Figure 5.9 and 5.10 show the load-displacement curves for different slenderness ratios and foundation depths on loose sand and soft clay, respectively. It can be noticed how the wall-foundation interaction increases the out-of-plane capacity and is more pronounced as the walls become more slender. For instance, when the wall was simulated with the smallest footing width (B_f= 0.60 m), the smallest foundation depth (D_f= 0.30 m), and the least competent soils, the out-of-plane capacity increased by 41% (loose sand) and 50% (soft clay) when the h/t= 25 while the increment was about 100% (loose sand) and 126% (soft clay) when the h/t= 40, compared with the pinned base case.

The bearing capacity of the soil is one of the factors that most affect the base rotation and consequently increases the out-of-plane capacity on walls due to the wall-foundation interaction. Specifically, on sands, the internal friction angle and the foundation depth are the factors that most contribute to the bearing capacity, while in clays, the cohesion. For example, Figure 5.9 shows increase of 41%, 60%, 77%, and 80%, while Figure 5.10 shows increase of 48%, 50%, 52%, and 54% when the foundation depth increased by 0.30 m, 0.60 m, 0.90 m, and 1.20 m, respectively, compared with the pinned base condition. A more pronounced increase in the capacity curves can be observed among loose, medium, and dense sands or soft, medium, and stiff clays due to the increase of internal friction angle on sands and the cohesion on clays. All capacity curves for all types of soils studied here can be found in Appendix B.

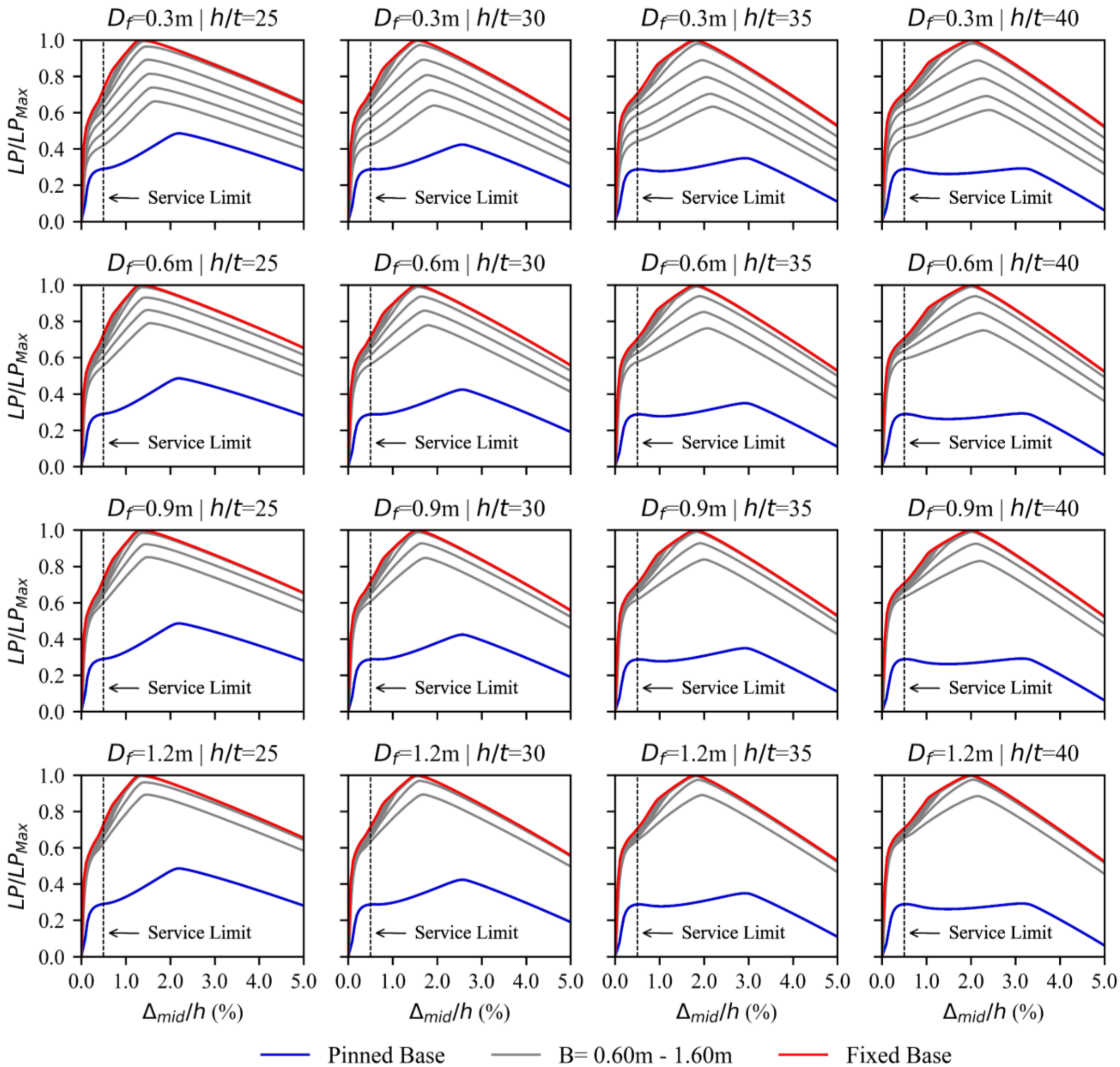

Figure 5.9 – Load-displacement curves on Loose Sand

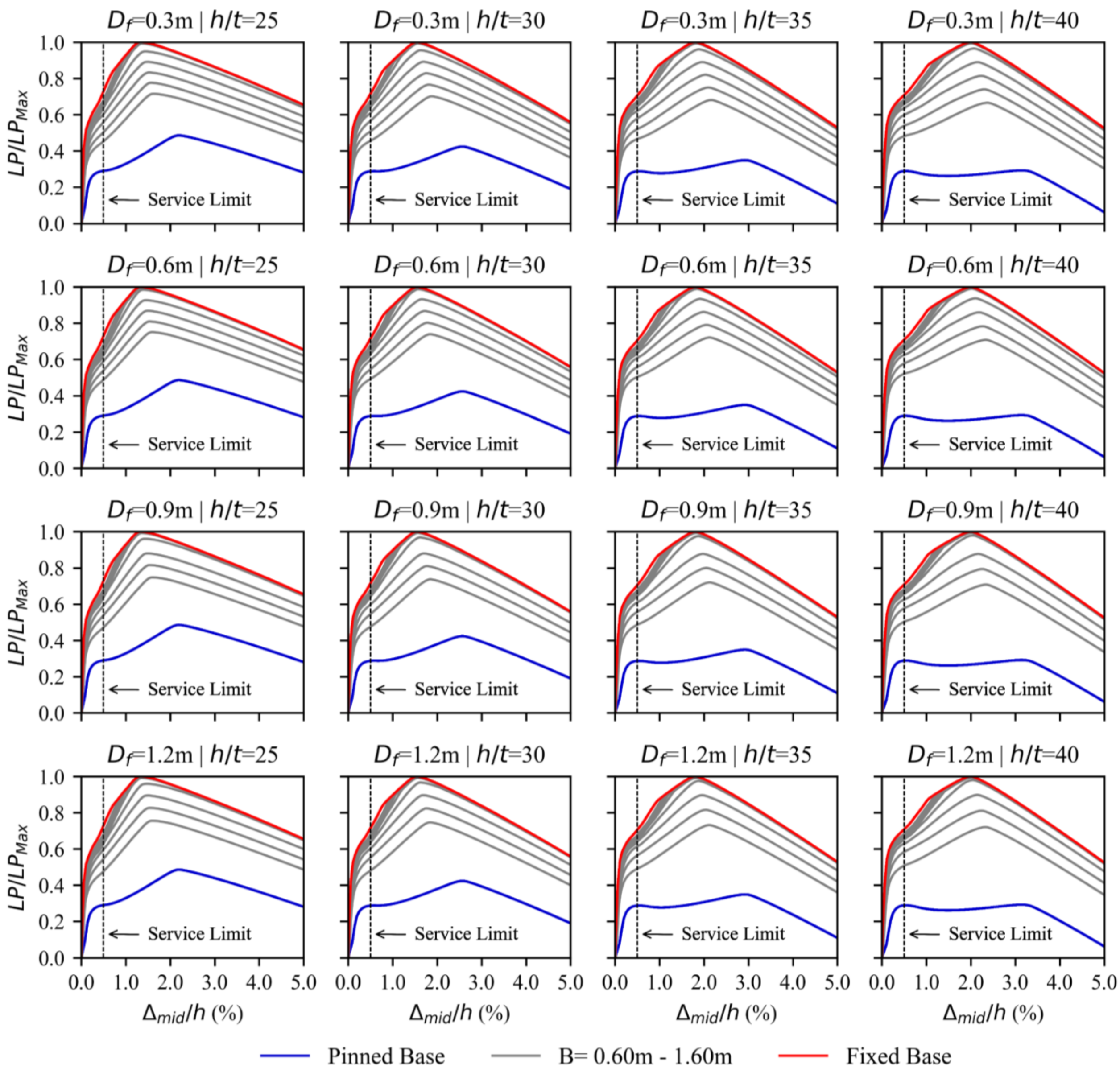

Figure 5.10 – Load-displacement curves on Soft Clay

5.5.2. Base rotation intensity and equivalent rotational base stiffness

The base rotation (θ) was normalized with the maximum base rotation (θ_{max}) from the wall with pinned base to show the level of fixity provided by the soil-foundation interaction according to the $^{D_f}/_{h}$ and $^{B_f}/_{h}$ ratios for each type of soil. The closer the relative rotation value to zero, the base will behave as fixed condition. However, the base will behave as pinned condition if the relative rotation value is close to one.

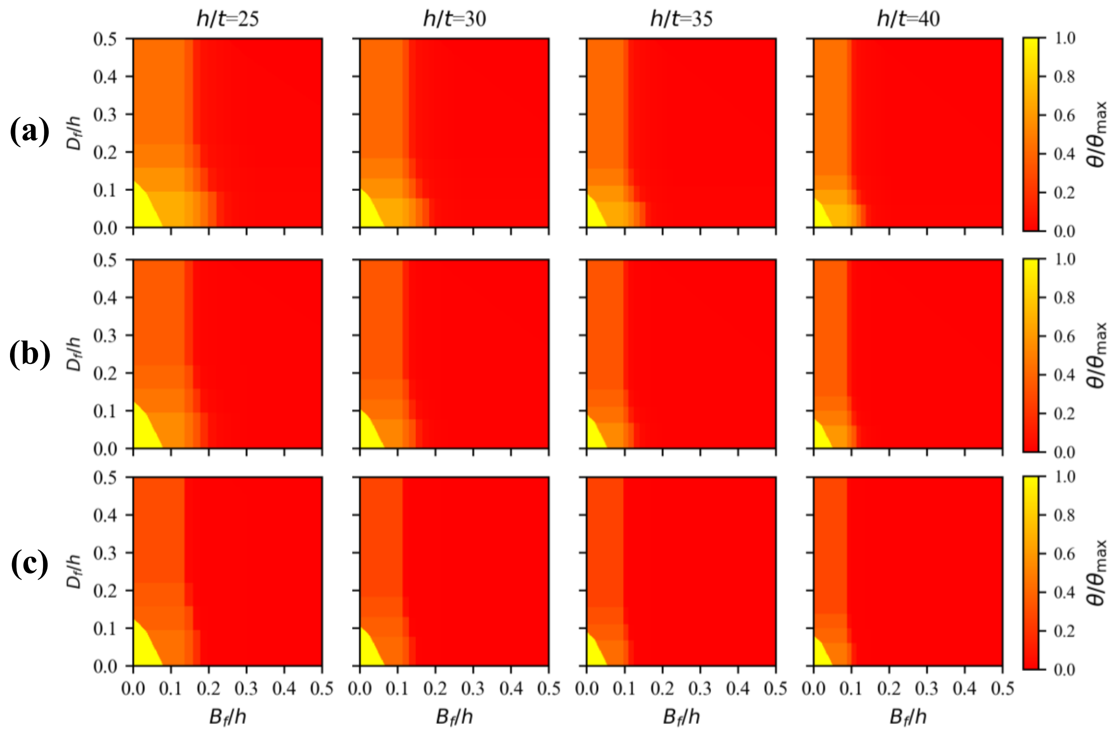

Figure 5.11 – Base rotation intensity on (a) Loose Sand; (b) Medium Sand; (c) Dense Sand

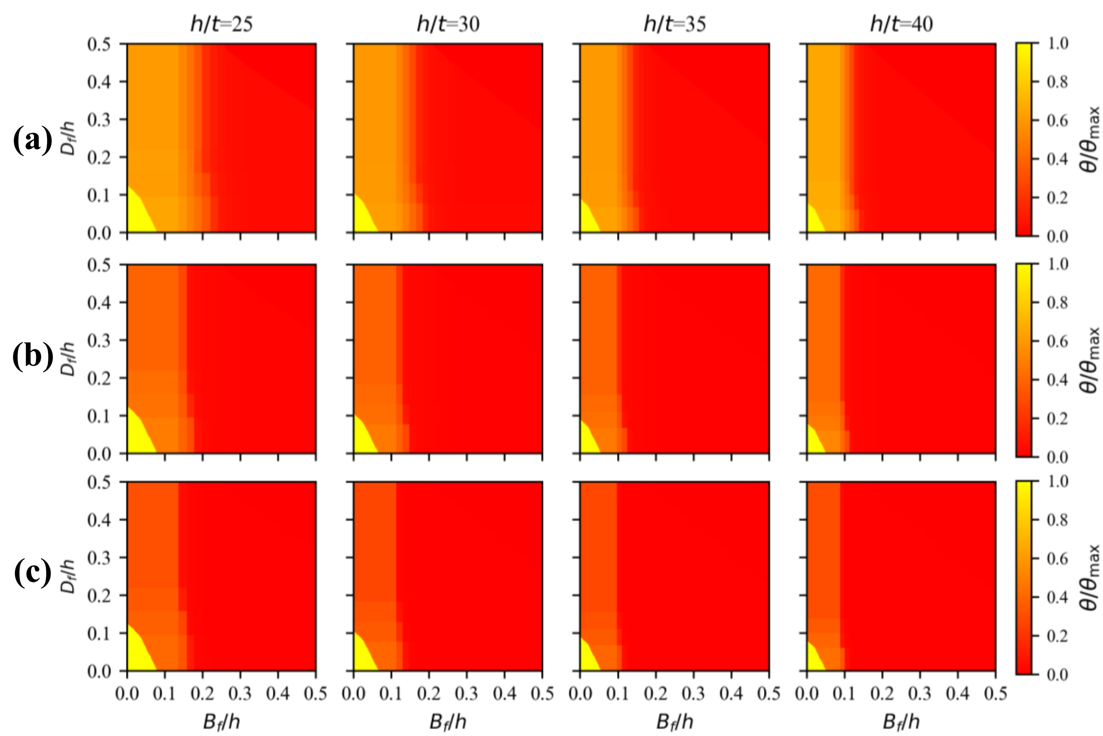

Figure 5.12 – Base rotation intensity on (a) Soft Clay; (b) Medium Clay; (c) Stiff Clay

Figure 5.11 and 5.12 show that the zone with greater rotation intensity is within ${D_f}/{h}$ and ${B_f}/{h} \leq 0.1$ and decreases with higher h/t ratio. Therefore, for ratios of ${D_f}/{h} > 0.1$ and $0 < {B_f}/{h} \leq 0.1$ a partially fixed base can be considered, while for ratios of ${D_f}/{h}$ and ${B_f}/{h} > 0.1$ a base closed to a fixed condition can be considered.

The equivalent rotational base stiffness (RBS) is a more practical interpretation of the base rotation intensity. Table 5.4 and 5.5 show the range of equivalent RBS values from different h/t ratios (25, 30, 35, and 40) obtained by using the base moment (M_b) and the base rotation (θ) at the peak lateral load resisted by the wall using Eq. (5.1). The complete database of the RBS values can be found in Appendix D.

$$RBS = \frac{M_b}{\theta} \tag{5.1}$$

Table 5.4 – Range of equivalent rotational base stiffness (RBS) per different type of sand

D_f (m)	B_f (m)	Loose	Medium	Dense
		RBS (kN-m/rad)		
0.3	0.6	80 – 95	200 – 290	320 – 460
0.3	0.8	210 – 300	530 – 730	1,500 – 2,260
0.3	1.0	720 – 840	4,800 – 5,600	40,600 – 41,550
0.3	1.2	4,600 – 5,300	14,000 – 14,960	56,200 – 56,400
0.6	0.6	170 – 250	300 – 430	420 – 600
0.6	0.8	490 – 650	1,300 – 1,780	10,400 – 19,950
0.6	1.0	3,000 – 3,400	9,800 – 10,600	43,600 – 44,050
0.6	1.2	7,250 – 7,500	24,800 – 26,600	56,800 – 56,900
0.9	0.6	250 – 400	350 – 550	510 – 700
0.9	0.8	950 – 1,170	3,800 – 4,850	28,800 – 30,550
0.9	1.0	5,200 – 5,500	17,800 – 19,600	45,250 – 45,450
0.9	1.2	8,700 – 9,070	28,350 – 28,500	57,200 – 57,250
1.2	0.6	360 – 500	490 – 660	700 – 870
1.2	0.8	2,100 – 2,500	8,500 – 9,500	32,300 – 33,100
1.2	1.0	6,250 – 6,500	22,100 – 22,250	45,800 – 45,900
1.2	1.2	11,700 – 12,300	28,800 – 28,900	57,500 – 57,550

Table 5.5 – Range of equivalent rotational base stiffness (RBS) per different type of clay

D_f (m)	B_f (m)	Soft	Medium	Stiff
		RBS (kN-m/rad)		
0.3	0.6	110 – 150	250 – 370	350 – 520
0.3	0.8	240 – 340	640 – 860	2,700 – 4,100
0.3	1.0	580 – 750	8,500 – 8,900	23,200 – 23,800
0.3	1.2	3,120 – 3,450	12,850 – 13,000	32,900 – 33,150
0.6	0.6	140 – 200	300 – 450	430 – 600
0.6	0.8	300 – 410	1,800 – 3,000	8,300 – 12,000
0.6	1.0	950 – 1,250	9,300 – 9,520	24,650 – 24,950
0.6	1.2	3,450 – 3,700	12,900 – 13,000	32,750 – 33,000
0.9	0.6	140 – 190	350 – 500	500 – 700
0.9	0.8	340 – 450	4,200 – 5,350	15,500 – 16,550
0.9	1.0	1,650 – 1950	9,700 – 9,850	25,200 – 25,500
0.9	1.2	3,800 – 4,000	13,000 – 13,150	33,050 – 33,300
1.2	0.6	150 – 200	390 – 570	650 – 850
1.2	0.8	400 – 480	5,750 – 6,150	17,150 – 17,650
1.2	1.0	1,500 – 1,800	9,700 – 9,850	25,200 – 25,350
1.2	1.2	4,050 – 4,200	13,150 – 13,250	33,350 – 33,600

5.5.3. Stability analysis and elastic effective height factors (k)

Stability analyses were performed in OpenSees on the slender masonry walls with different height-to-thickness ratios (25, 30, 35, and 40) using the lower bounds of RBS from Table 5.4 and 5.5. The walls were modelled using elastic beam-column elements. The top support of the wall was a roller, while the bottom support was modelled with a rotational spring. An initial imperfection of $0.1h$ at midspan was introduced, and a concentric axial load (P) was applied at the top of the wall and increased until elastic buckling failure. The load at the elastic buckling failure with an end-restrained (partially or completely) is known as elastic critical load (P_{cr}). While P_e is the Euler buckling load (load at the elastic buckling failure with pin-ended) that can be obtained by Eq. (5.2). Using P_{cr} and P_e the elastic effective height factors can be calculated by Eq. (5.3).

$$P_e = \frac{\pi^2 E_m I_{cr}}{h^2} \tag{5.2}$$

$$k = \sqrt{\frac{P_e}{P_{cr}}} \tag{5.3}$$

Where E_m is the modulus of elasticity of the masonry assembly, I_{cr} is the cracked moment of inertia, and h is the height of the wall.

Table 5.6 shows a summary of the elastic effective height factors obtained for different height-to-thickness ratios (h/t) with different ranges of RBS values. The complete database of the elastic effective height factors (k) calculated can be found in Appendix E.

Table 5.6 – Elastic effective height factors (k)

h/t	RBS (kN-m/rad)	P_e (kN)	P_{cr} (kN)	$k_{calculated}$	$k_{proposed}$
25	80 – 150	146	182 – 200	0.9	1.0
25	170 – 650	146	205 – 259	0.8	0.9
25	> 700	146	262 – 313	0.7	0.8
30	80 – 110	100	128 – 134	0.9	1.0
30	150 – 530	100	140 – 177	0.8	0.9
30	> 580	100	180 – 214	0.7	0.8
35	80	73	99	0.9	1.0
35	110 – 360	73	105 – 129	0.8	0.9
35	> 420	73	131 – 162	0.7	0.8
40	80	58	78	0.9	1.0
40	110 – 360	58	82 – 103	0.8	0.9
40	> 420	58	104 – 125	0.7	0.8

The elastic effective height factor obtained can not be used directly for design since ideal conditions are rarely achieved in practice. Therefore, the elastic effective height factors were increased by 10% (using as upper limit k=1.0) to account for uncertainties such as workmanship (out-of-plumbness, reinforcement location, etc.), the position of the loads, material strength, and degradation due to the life cycle of the structure. To get more detailed results from the proposed effective heigth factors, dynamic loads and creep should be considered during the analysis along with a respective reliability analysis to account for the uncertanties.

5.6. Design impact and construction recommendations

Structural engineers designing walls with kh/t > 30 following the CSA S304-14 (2019) standard must assume a pinned base condition. There is no such restriction in the American masonry standard (TMS 402-16 2016) nor the North American reinforced-concrete standards (ACI 318-19 2019, CSA A23.3:19 2019), allowing the designers to consider any base condition for walls of any height. The impact of this clause can be divided into two parts: (i) it underestimates the capacity of slender masonry walls, which makes them uneconomical compared with other structural systems, and (ii) slender masonry wall designs neglect the presence of moments at the base by using a not appropriate detailing in the bottom of the wall. If a brittle failure on the blocks occurs due to the concentrated moments at the base, the wall would reduce its axial capacity at the bottom making this unexpected failure unsafe.

The wall-foundation interaction is an untapped source of stiffness that can be used to reduce the impact of assuming a pinned base. The connection between the wall and the foundation is an important factor where the maximum moments are expected. Therefore, the following construction recommendations are to improve the wall-foundation interaction (Figure 5.13):

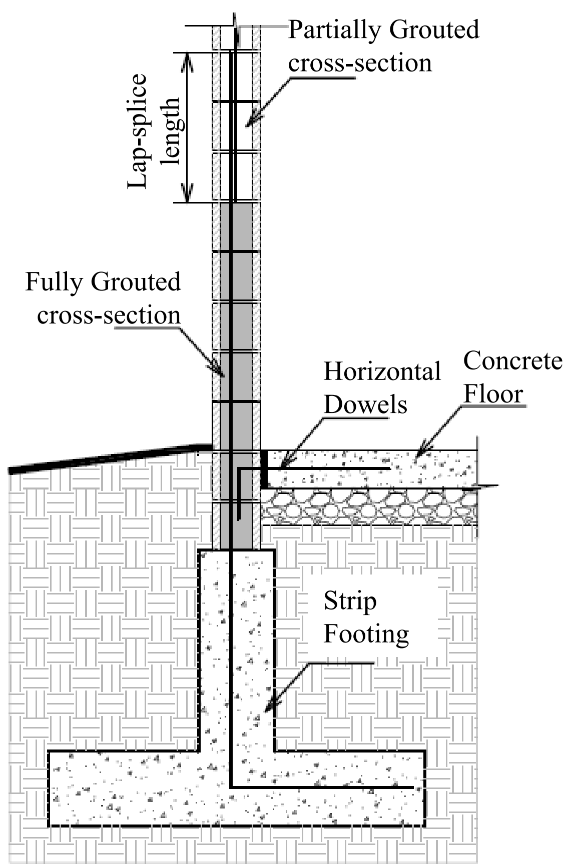

Figure 5.13 – Construction recommendations for wall-foundation connections

- Placing the lap-splice at a distance of $h/5$ from the bottom of the wall, closer to the zero moments based on the moment profile of a fixed base wall

- Using a fully grouted cross-section of the first courses ($h/5$) to increase the moment capacity and ductility at the wall base
- Placing horizontal dowels embedded into the indoor concrete floor to increase the base fixity, reducing the base rotation

5.7. Summary

An analysis model of a typical configuration of slender masonry walls was developed to investigate the effect of the wall-foundation interaction on the out-of-plane response by changing key parameters (wall height, soil types, foundation depth, and footing width), highlighting the following observations:

- The increment of out-of-plane capacity on walls with h/t= 25 was 41% (loose sand) and 50% (soft clay), while for walls with h/t= 40 the increment was 100% (loose sand) and 126% (soft clays) – using the same footing width and foundation depth.
- The out-of-plane capacity increased more significantly on sands (60%) compared with clays (6%) when the foundation depth was from 0.30m to 1.20m. However, the increment was similar (about 50%) when the soils changed from least competent to more competent (loose-soft, medium, dense-stiff).
- A semi-rigid (closed to fixed) base condition can be considered when ${}^{D_f}/_{h}$ and ${}^{B_f}/_{h} > 0.1$, making having a pinned base condition unrealistic – based on the practical shallow foundation solutions.
- A base condition close to a fix can be achieved if the $RBS \geq 700$ kN-m/rad for walls with h/t ratios of 25, 30, 35, and 40. This can be easily achieved with a minimum foundation depth of 0.30m, footing width of 1.0 m, and on loose sand or soft clay.

It can be concluded that the wall-foundation interaction is an untapped source of stiffness that enhances the performance of loadbearing masonry walls, increasing the out-of-plane capacity, and it is more pronounced as the wall is more slender. The increase in capacity is attributed to the change of moment distribution along the wall height due to the presence of base stiffness, which is inversely proportional to the base rotation and is mainly affected by the foundation depth and the bearing capacity of the soil. The base stiffness depends on the appropriate moment connection between the wall and foundation (location of the maximum moment), transferring the internal forces of the wall to the footing, which distributes the stresses into the soil creating a semi-rigid base condition. Therefore, a different failure mode is suggested than expected for walls designed under pinned base conditions, as required by CSA S304-14 for walls with $kh/t\ >30$. The use of elastic effective height factors (k) – as CSA S304-14 allows it for $kh/t < 30$, obtaining pertinent equations for moments and deflections using principles of mechanics – as TMS 402-16 allows it for any h/t ratio, or directly modelling the soil-foundation-structure interaction can be options to account for the presence of base stiffness in the design of slender masonry walls and reduce the impact of assuming a pinned base.

The benefits of the wall-foundation interaction on the out-of-plane response presented in this study are limited to strip footings and monotonic loadings. Therefore, it is recommended to investigate the degradation of the wall-foundation connection under dynamic loadings to prove if the level of fixity remains before failure.

Note: *Tasks 2.1 to 2.4 and Tasks 3.1 to 3.3 were addressed in this chapter to complete objectives 2 and 3.*

6 CONCLUSIONS AND RECOMMENDATIONS

This chapter provides a summary, conclusions, and recommendations for future research projects on loadbearing-slender masonry walls.

6.1. Summary

The primary objective of determining the influence of foundation rigidity on the out-of-plane flexural response of slender masonry walls was achieved by the following steps:

1. Pre-test analysis of the full-scale specimens to predict the adequate applied loads, expected deflected shapes, and failure modes:
    - A finite element model using a macro-modelling approach was developed in OpenSees for different base conditions (pinned, partially fixed, or fixed).
    - Validation of the model was conducted by comparing the numerical results with two experimental programs (ACI-SEASC 1982, Mohsin 2005).
    - It was concluded from the parametric analysis that the adequate eccentric axial load obtained was 15 kN, expecting a maximum lateral pressure of 0.90 kPa, and a buckling failure was expected at 300 mm of midspan displacement.
2. Experimental testing of two full-scale slender masonry walls with different rotational base stiffnesses:
    - Design the offsite experimental setup needed to test the full-scale specimens since the Morrison Structural Laboratory was temporarily closed due to the expansion project.
    - Two full-scale specimens were 8.75 m tall, 1.19 m wide, and 0.19 m thick, resulting in $h/t = 46$. Certified masons build the specimens using 15 MPa standard 20 cm blocks in a running bond pattern.
    - The vertical reinforcement consists of 2-15M bars at 600 mm. Bond beams with a single 10M bar at 2400 mm. Ladder-type, 9-gauge joint reinforcement at 400 mm was provided along the height of the wall.
    - The walls were built over a base plate, in which two 15M bars were welded to simulate a satisfactory wall-foundation connection, which is attached to a steel fixture used to simulate different rotational base stiffness (0, 1,150, ∞ kN-m/rad).

- The walls were tested under combined eccentric axial load ($P = 15$ kN, $e = 170$ mm) and cyclic lateral uniform pressure – applied using an airbag.
- Wall-1 was tested under fixed and pinned base conditions up to yielding and served as the control wall. Wall-2 was tested under pinned, partially fixed, and fixed base conditions at the service limit and under fixed base condition up to yielding. In both cases, the test was stopped at yielding due to safety concerns about sudden failure due to buckling.
- Data collected from the experimental program include out-of-plane displacements, strains on concrete blocks and steel reinforcement, rotations at the top and bottom, the lateral pressure applied, the axial load applied, and weather conditions.

3. Develop a finite element model to predict the out-of-plane flexural response of slender masonry walls, including the soil-foundation-structure interaction:
   - Developing a finite element model using a macro-modelling approach to capture the overall response of slender masonry walls with different base stiffnesses.
   - Validation of the model was conducted by comparing the numerical results with the results from the experimental program of this study – the global and local responses.
   - The static soil-structure interaction (SSI) was implemented using the beam-on-nonlinear-Winkler-foundation (BNWF) approach on strip footing and common soil types.
   - A parametric analysis was performed using the validated model that included the static SSI interaction to create a database by changing key parameters such as wall height, footing width, foundation depth, and soil type.
   - The database was used to obtain the equivalent rotational base stiffness (RBS) for different wall heights and foundation conditions.
4. Assessment of the collected data from the experimental program and parametric analysis to recommend the inclusion of base stiffness in the design of slender masonry walls:
   - Assessing the collected data from the experimental program and the parametric analysis.
   - The equivalent RBS values obtained were used to perform stability analyses on different wall heights to obtain the elastic effective height factors (k) according to the foundation conditions.
   - Proposing construction recommendations to improve the behaviour of the wall-foundation connection on typical strip footings and common soil types.

6.2. Conclusions

Conclusions drawn from the experimental program and numerical modelling on the study of the influence of foundation rigidity on the out-of-plane flexural response of slender masonry walls are as follows:

- The wall-foundation interaction is an untapped source of stiffness that enhances the out-of-plane performance of loadbearing, slender masonry walls, increasing their capacity and decreasing their lateral deflections.
- The increase in capacity is attributed to the change of moment distribution along the wall height, and it is more pronounced as the wall is more slender.
- The reduction of second-order effects is attributed to the decrease in out-of-plane deflections.
- The presence of base stiffness makes the wall deflect in double curvature, creating a maximum negative moment at the wall and a maximum positive moment above the wall midspan (approximately $0.65h$).
- The wall-foundation interaction provides a base stiffness that acts more actively after the wall is cracked.
- Degradation at the wall base does not appear to be a factor since no visible material degradation was observed under cyclic loading – up to the yielding stage.
- A different failure mode is suggested than expected for walls designed under pinned base conditions, as required by CSA S304-14 with $kh/t >$30.
- The analysis model of the typical configuration of slender masonry wall developed to investigate the effect of the wall-foundation interaction showed a reasonable agreement when predicting the global and local responses of the experimental program of this study.
- The base stiffness is inversely proportional to the base rotation and is mainly affected by the foundation depth and the bearing capacity of the soil.
- The base stiffness depends on the appropriate moment connection between the wall and the foundation (location of the maximum moment), transferring the internal forces of the wall to the footing, which distributes the stresses into the soil, creating a semi-rigid base condition.

- Construction recommendations are suggested to improve the behaviour of the wall-foundation connection.
- The use of elastic effective height factors (k) – as CSA S304-14 allows it for $kh/t < 30$, obtaining pertinent equations for moments and deflections using principles of mechanics – as TMS 402-16 allows it for any h/t ratio, or directly modelling the soil-foundation-structure interaction can be options to account for the presence of base stiffness in the design of slender masonry walls and reduce the impact of assuming a pinned base.

The conclusions and benefits of foundation rigidity on the out-of-plane flexural response of slender masonry walls presented in this study are limited to (1) the yielding for the experimental program and (2) strip footings and monotonic loadings in the analysis model.

6.3. Recommendations for future research

This study is part of a research campaign at the Masonry Research Centre at the University of Alberta to improve the performance of slender masonry walls using different techniques. Specifically, this thesis aimed to determine the influence of base rigidity on the out-of-plane flexural response of slender masonry walls and was limited in various aspects. Recommendations for future research work are suggested as follows:

- Future experimental programs should explore testing slender masonry walls with base stiffness subjected to combined eccentric axial loads and cyclic lateral pressure to failure, taking the necessary safety measures. It is crucial to capture the failure mode with base stiffness since this study suggested that it could differ from what is expected for walls with pinned base.
- Future experimental programs should explore the testing of slender masonry walls with a more significant number of cycles to capture material degradation at the wall base up to failure since this study was tested up to yielding in 25 cycles and no visual material degradation was observed.
- Future experimental programs should explore the testing of slender masonry walls, changing the load eccentricity (e) and increasing the axial load (P) – simulating different ways to connect the roof system (which changes e) with the wall and capturing the effect

of large P on the flexural stiffness since slender walls are susceptible to second-order effects.

- Future experimental programs should explore the testing of slender masonry walls with different reinforcement configurations and ratios. It is important to capture their influence on the global and local responses, ductility, and failure modes of the wall.
- Future numerical analysis should explore the degradation of the wall-foundation connection under dynamic loads (e.g., seismic, wind) – calibrating material models with damage parameters and using dynamic soil-structure interaction.
- Future numerical analysis should explore the effect of yield strain penetration on the out-of-plane flexural response of slender masonry walls since the dowels have a full anchorage into the foundation.
- Future numerical analysis should explore the detailed local response (e.g., crack propagation, material degradation, join openings) to predict the actual failure mode for slender masonry walls that account for the foundation rigidity.
- Future parametric analysis should explore the influence of creep and the axial load effect on the effective flexural stiffness because significantly impacts the design of slender masonry walls subjected to combined axial and gravity loads.

REFERENCES

(ACI) American Concrete Institute. 2019. Building Code Requirements for Structural Concrete and Commentary (Reapproved 2022) ACI 318-19. ACI Committee 318, Farmington Hills, MI, USA.

ACI-SEASC Task Committee on Slender Walls. 1982. Test Report on Slender Walls. ACI-SEASC (American Concrete Institute - Structural Engineers Association of Southern California).

(ACI-TMS) American Concrete Institute and The Masonry Society. 1995. TMS 602-95 Building Code Requirements for Masonry Structures. ACI-TMS, New York, NY.

Ali, S., Page, A., and Kleeman, P.W. 1986. Non-Linear Finite Element Model for Concrete Masonry with Particular Reference to Concentrated Loads. *In* 4th Canadian Masonry Symposium. pp. 137–148.

American Association State Highway and Transportation Officials Standard (AASHTO). 2004. ASTM-A-615M-04a Standard Specification for Deformed and Plain Carbon Steel Bars for Concrete Reinforcement. American Society for Testing and Materials, West Conshohocken, PA.

Amrhein, J.E. 1998. Constructing Tall Slender Walls - How to maximize their height, strength, and performance. Masonry Institute of America.

Babatunde, S.A. 2017. Review of strengthening techniques for masonry using fiber reinforced polymers. Composite Structures, **161**: 246–255. Elsevier. doi:10.1016/j.compstruct.2016.10.132.

Bapir, B., Abrahamczyk, L., Wichtmann, T., and Prada-Sarmiento, L.F. 2023. Soil-structure interaction: A state-of-the-art review of modeling techniques and studies on seismic response of building structures. Frontiers in Built Environment, **9**. doi:10.3389/fbuil.2023.1120351.

Barkhordary, M., and Tariverdilo, S. 2011. Vulnerability of ordinary moment resistant concrete frames. Earthquake Engineering and Engineering Vibration, **10**(4): 519–533. doi:10.1007/s11803-011-0086-9.

Bean Popehn, J.R., Schultz, A.E., Lu, M., Stolarski, H.K., and Ojard, N.J. 2008. Influence of transverse loading on the stability of slender unreinforced masonry walls. Engineering Structures, **30**(10): 2830–2839. Elsevier. doi:10.1016/j.engstruct.2008.02.016.

Canadian Foundation Engineering Manual. 2006. Canadian Geothecnical Society.

(CSA) Canadian Standard Associaton. 2019. Design of concrete standards. Standard CSA A23.3:19. CSA Group, Rexdale, ON.

(CSA) Canadian Standards Association. 1994. Design of Masonry Structures. Standard CSA S304.1-M94. CSA Group, Rexdale, ON.

(CSA) Canadian Standards Association. 2014. Mortar and Grout Unit Masonry CSA A179-14. CSA Group, Rexdale, ON.

(CSA) Canadian Standards Association. 2019. Design of masonry structures. Standard CSA S304-14 (R2019). CSA Group, Rexdale, ON.

Das, B.M. 2023. Principles of foundation engineering. Cengage Learning.

De Santis, S., De Canio, G., de Felice, G., Meriggi, P., and Roselli, I. 2019. Out-of-plane seismic retrofitting of masonry walls with Textile Reinforced Mortar composites. Bulletin of Earthquake Engineering, **17**(11): 6265–6300. Springer. doi:10.1007/s10518-019-00701-5.

Donà, M., Tecchio, G., and da Porto, F. 2018. Verification of second-order effects in slender reinforced masonry walls. Materials and Structures, **51**(3): 69. doi:10.1617/s11527-018-1196-x.

Drysdale, R.G., and Hamid, A.A. 2005. Masonry Structures Behaviour and Design. *Edited by* D.W. Stubbs. Canada Masonry Design Centre.

Entz, J. 2019. Development of Innovative in-Line Stiffening Element for Out-of-Plane Masonry Walls. MSc, University of Alberta.

Fathi, A., Sadeghi, A., Emami Azadi, M.R., and Hoveidae, N. 2020. Assessing the soil-structure interaction effects by direct method on the out-of-plane behavior of masonry structures (case study: Arge-Tabriz). Bulletin of Earthquake Engineering, **18**(14): 6429–6443. doi:10.1007/s10518-020-00933-w.

Fortes, E.S., Parsekian, G.A., Fonseca, F.S., and Camacho, J.S. 2018. High-strength concrete masonry walls under concentric and eccentric loadings. Journal of Structural Engineering , **144**(6): 04018055. American Society of Civil Engineers (ASCE). doi:10.1061/(asce)st.1943-541x.0001978.

Gazetas, G. 1991. Formulas and Charts for Impedances of Surface and Embedded Foundations. ASEC - J. Geotech. Engrg., **117**(9): 1363–1381.

Güllü, H., and Jaf, H.S. 2016. Full 3D nonlinear time history analysis of dynamic soil–structure interaction for a historical masonry arch bridge. Environmental Earth Sciences, **75**(21): 1421. doi:10.1007/s12665-016-6230-0.

Harden, C., Hutchinson, T., Martin, G.R., and Kutter, B.L. 2005. Numerical Modeling of the Nonlinear Cyclic Response of Shallow Foundations. Pacific Earthquake Engineering Research (PEER) Center.

Harden, C.W., and Hutchinson, T.C. 2009. Beam-on-Nonlinear-Winkler-Foundation Modeling of Shallow, Rocking-Dominated Footings. Earthquake Spectra, **25**(2): 277–300. SAGE Publications Ltd STM. doi:10.1193/1.3110482.

Hatzinikolas, M., Longworth, J., and Warwaruk, J. 1978a. Experimental Data for Concrete Masonry Walls. University of Alberta.

Hatzinikolas, M., Longworth, J., and Warwaruk, J. 1978b. Concrete Masonry Walls. University of Alberta.

Isfeld, A.C., Müller, A.L., Hagel, M., and Shrive, N.G. 2019. Analysis of safety of slender concrete masonry walls in relation to CSA S304-14. Canadian Journal of Civil Engineering, **46**(5): 424–438. Canadian Science Publishing. doi:10.1139/cjce-2018-0210.

Kent, D.C., and Park, R. 1971. Flexural members with confined concrete. Journal of the Structural Division, **97**(7): 1969–1990.

Liu, Y., Aridru, G.G., and Dawe, J.L. 1998. Effective Flexural Rigidity of Concrete Masonry Walls. *In* 8th Canadian Masonry Symposium. pp. 18–24.

Liu, Y., and Dawe, J.L. 2001. Experimental determination of masonry beam-column behaviour. Canadian Journal of Civil Engineering, **28**(5): 794–803. Canadian Science Publishing. doi:10.1139/cjce-28-5-794.

Liu, Y., and Dawe, J.L. 2003. Analytical modeling of masonry load-bearing walls. Canadian Journal of Civil Engineering, **30**(5): 795–806. Canadian Science Publishing. doi:10.1139/l03-036.

Liu, Y., and Hu, K. 2007. Experimental study of reinforced masonry walls subjected to combined axial load and out-of-plane bendingThis article is one of a selection of papers published in this Special Issue on Masonry. Canadian Journal of Civil Engineering, **34**(11): 1486–1494. Canadian Science Publishing. doi:10.1139/l06-167.

Lopez, J., Oller, S., Onate, E., and Lubliner, J. 1999. A Homogeneous Constitutive Model for Masonry. Int. J. Numer. Meth. Engng., **46**: 1651–1671. doi:10.1002/(SICI)1097-0207(19991210)46:10.

Lotfi, H.R., and Shing, P.B. 1994. Interface Model Applied to Fracture of Masonry Structures. Journal of Structural Engineering , **120**(1): 63–80.

Ma, G., Hao, H., and Lu, Y. 2001. Homogenization of Masonry Using Numerical Simulations. Journal of Engineering Mechanics, **127**(5): 421–431.

MacGregor, J.G., Breen, J.E., and Pfrang, A.E. 0. 1970. Design of slender concrete columns. Journal of American Concrete Institute, **67**(1): 6–28. American Concrete Institute. doi:10.14359/7254.

Masia Mark J., Kleeman Peter W., and Melchers Robert E. 2004. Modeling Soil/Structure Interaction for Masonry Structures. Journal of Structural Engineering , **130**(4): 641–649. American Society of Civil Engineers. doi:10.1061/(ASCE)0733-9445(2004)130:4(641).

McKenna, F., Scott, M.H., and Jeremic, B. 2000. Open System for Earthaquake Engineering Simulation (OpenSees) [Computer Software]. Pacifi Earthquake Engineering Research Centre, University of California Berkley, California, USA.

Menegotto, M., and Pinto, P.E. 1973. Method of analysis for cyclically loaded reinforced concrete plane force and bending. Proceedings, IABSE Symposium on Resistance and,.

Metwally, Z., Zeng, B., and Li, Y. 2022. Probabilistic Behavior and Variance-Based Sensitivity Analysis of Reinforced Concrete Masonry Walls Considering Slenderness Effect. ASCE-ASME Journal of Risk and Uncertainty in Engineering Systems, Part A: Civil Engineering, **8**(4): 04022051. American Society of Civil Engineers. doi:10.1061/AJRUA6.0001273.

Mohsin, E. 2005. Support Stiffness Effect on Tall Load Bearing Masonry Walls. PhD, University of Alberta.

Mylonakis, G., Nikolaou, S., and Gazetas, G. 2006. Footings under seismic loading: Analysis and design issues with emphasis on bridge foundations. Soil Dynamics and Earthquake Engineering, **26**(9): 824–853. doi:10.1016/j.soildyn.2005.12.005.

National Earthquake Hazards Reduction Program (NEHRP) and National Institute of Standards and Technology (NIST). 2012. Soil-Structure Interaction for Building Structures. NEHRP-NIST.

Page, A.W. 1978. Finite Element Model for Masonry. ASEC - Journal of the Structural Division, **104**(8): 1267–1285.

Pettit, C. 2019. Effect of Rotational Base Stiffness on the Behaviour of Loadbearing Masonry Walls. MSc, University of Alberta.

Pettit, C., and Cruz-Noguez, C. 2021. Effect of Rotational Base Stiffness on the Behavior of Load-Bearing Masonry Walls. Journal of Structural Engineering , **147**(12): 04021215. American Society of Civil Engineers. doi:10.1061/(ASCE)ST.1943-541X.0003209.

Pettit, C., Mohsin, E., Cruz-Noguez, C., and Elwi, A. 2022. Experimental testing of slender load-bearing masonry walls with realistic support conditions. Canadian Journal of Civil Engineering, **49**(1): 95–108. Canadian Science Publishing. doi:10.1139/cjce-2020-0297.

Piro, A., de Silva, F., Parisi, F., Scotto di Santolo, A., and Silvestri, F. 2020. Effects of soil-foundation-structure interaction on fundamental frequency and radiation damping ratio of historical masonry building sub-structures. Bulletin of Earthquake Engineering, **18**(4): 1187–1212. doi:10.1007/s10518-019-00748-4.

Pluijm, R.R. van der. 1999. Out-of-plane bending of masonry : behaviour and strength. Phd, Eindhoven University of Technology.

Priestley, M.J.N., and Elder, D.M. 1983. Stress-strain curves for unconfined and confined concrete masonry. Journal of American Concrete Institute, **80**(3): 192–201. American Concrete Institute. doi:10.14359/10834.

Priestley, M.J.N., Seible, F., and Calvi, G.M. 1996. Seismic Design and Retrofit of Reinforced Concrete Bridges. John Wiley & Sons, Inc, 605 Third Avenue, New York, NY .

Sayed-Ahmed, E.Y., and Shrive, N.G. 1995. Numerical analysis of face-shell bedded hollow masonry walls subject to concentrated loads. Canadian Journal of Civil Engineering, **22**(4): 802–818. Canadian Science Publishing. doi:10.1139/l95-090.

de Silva, F. 2020. Influence of soil-structure interaction on the site-specific seismic demand to masonry towers. Soil Dynamics and Earthquake Engineering, **131**: 106023. doi:10.1016/j.soildyn.2019.106023.

Sparling, A., and Palermo, D. 2023. Response of full-scale slender masonry walls with conventional and NSM steel reinforcement subjected to axial and out-of-plane loads. Journal of Structural Engineering , **149**(1): 04022208. American Society of Civil Engineers (ASCE). doi:10.1061/jsendh/steng-11364.

Sparling, A., Palermo, D., and Hashemian, F. 2020. Out-of-plane flexural testing and stiffness response of concrete masonry walls with NSM steel reinforcement. Canadian Journal of Civil Engineering, (cjce-2019-0685): 1–14. Canadian Science Publishing. doi:10.1139/cjce-2019-0685.

(TMS) The Masonry Society. 2016. TMS 402/602-16 Building code requirements and specification for masonry structures. MJSC, Longmont, CO.

Wang, R., Elwi, A.E., Hatzinikolas, M.A., and Warwaruk, J. 1997. Test of Tall Cavity Walls Subjected to Eccentric Loading. Journal of Structural Engineering , **123**(7): 912–919.

Yi, J., and Shrive, N.G. 2001. 3D Finite Element Models of Plain and Bond-Beamed Hollow Masonry Walls Subjected to Concentric and Eccentric Concentrated Loads. *In* 9th Canadian Masonry Symposium.

Yokel, F.Y., Mathey, R.G., and Dikkers, R.D. 1970. Compressive Strength of Slender Concrete Masonry Walls. National Bureau of Standards, Washington, DC.

Yokel, F.Y., Mathey, R.G., and Dikkers, R.D. 1971. Strength of Masonry Walls Under Compressive and Transverse Loads. National Bureau of Standards.

Appendix A – Construction process of specimens

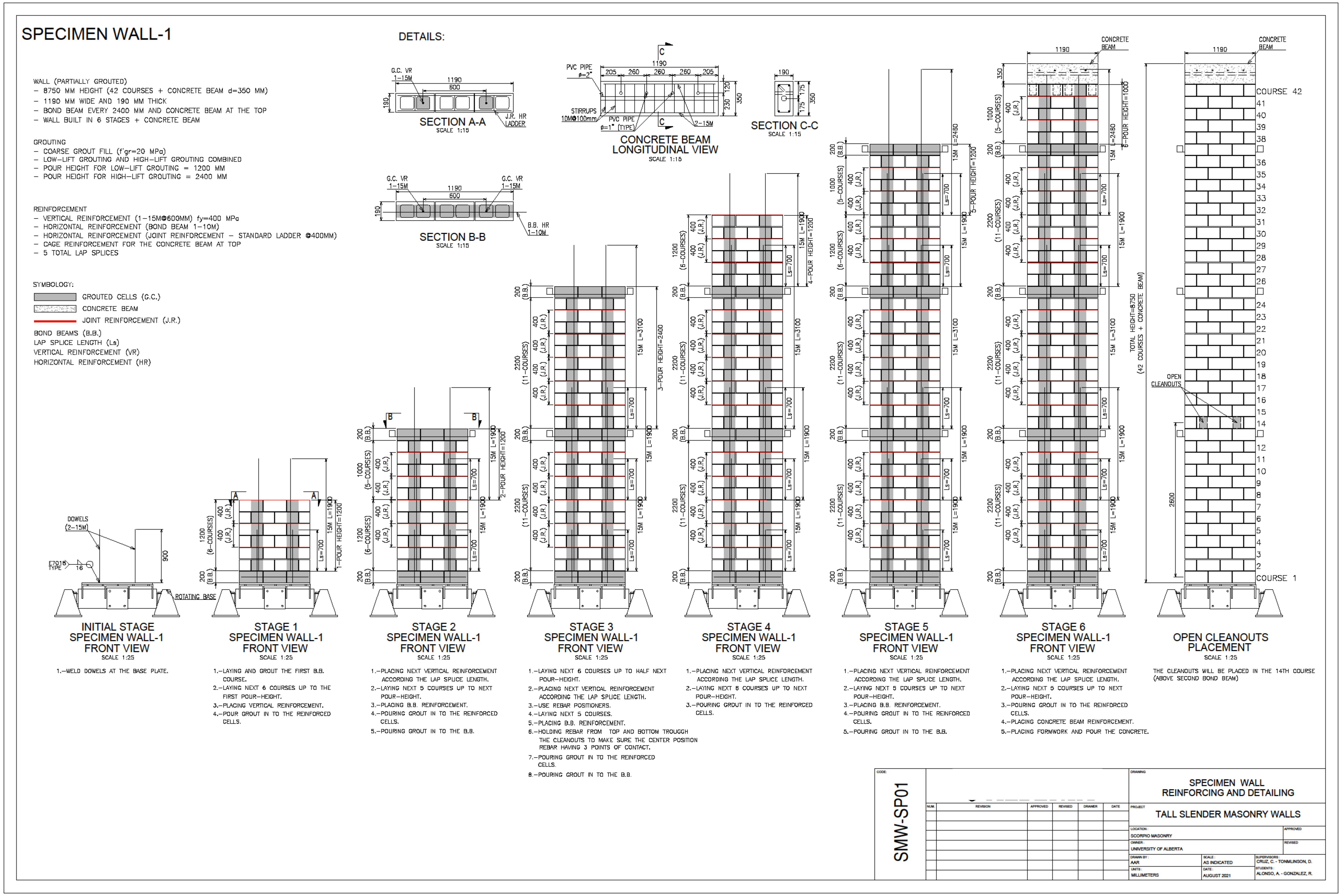

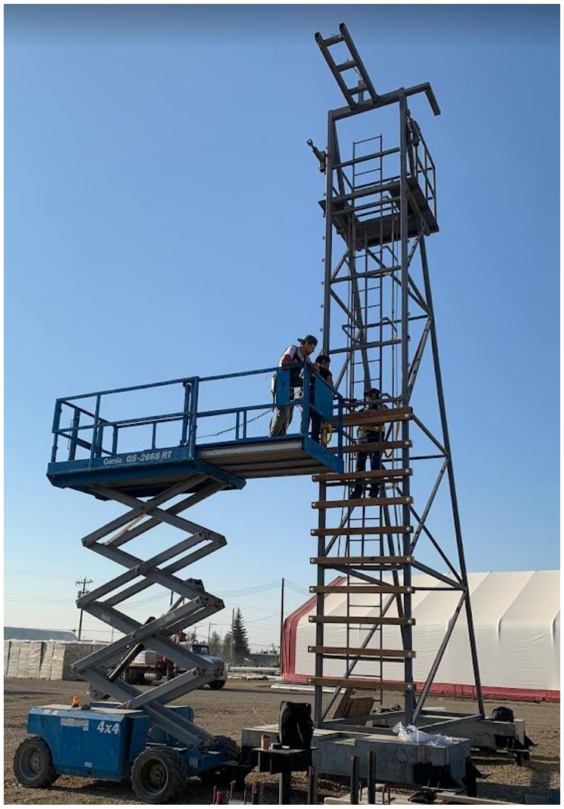
Genie GS-2668 RT
4x4


Save
COURSE 1

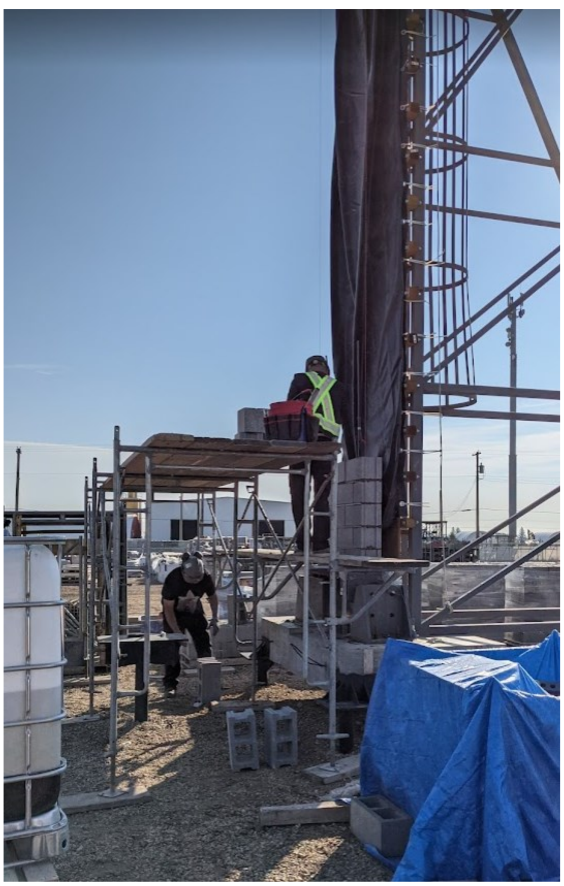

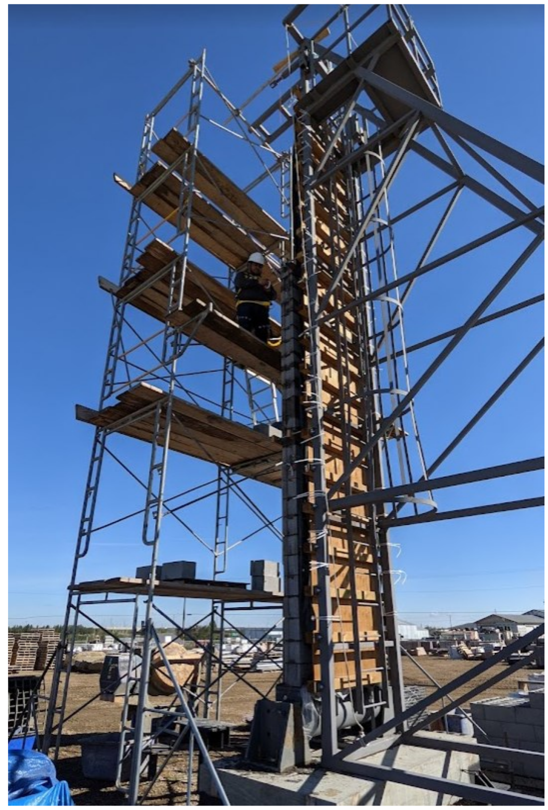

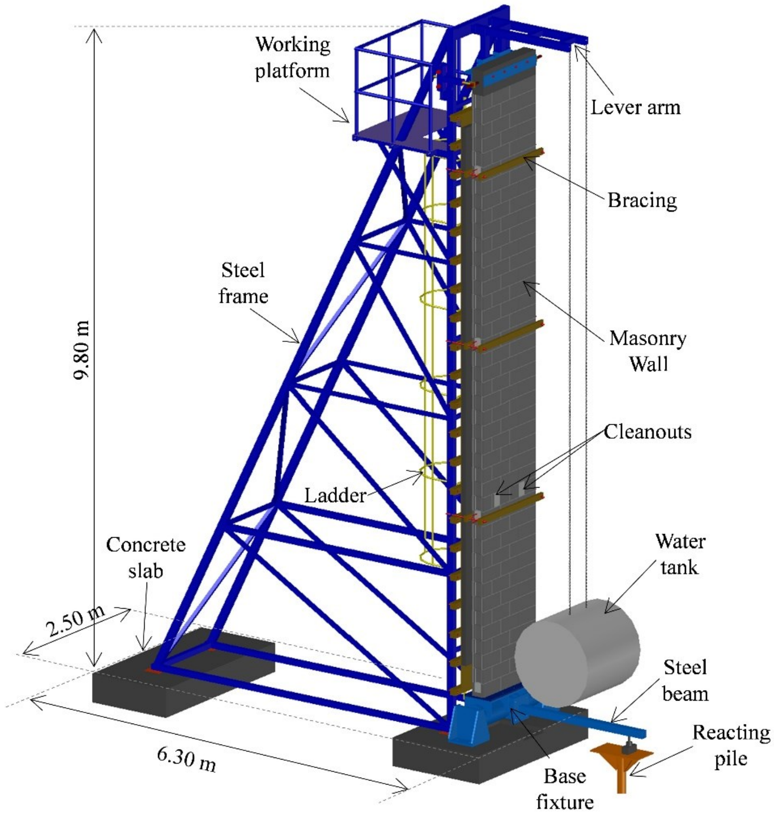
Working
platform
Lever arm
Bracing
Steel
frame
9.80 m
Masonry
Wall
Cleanouts
Ladder
Concrete
slab
Water
tank
2.50 m
Steel
beam
Reacting
pile
6.30 m
Base
fixture

Appendix B – Load-Displacement curves per soil type

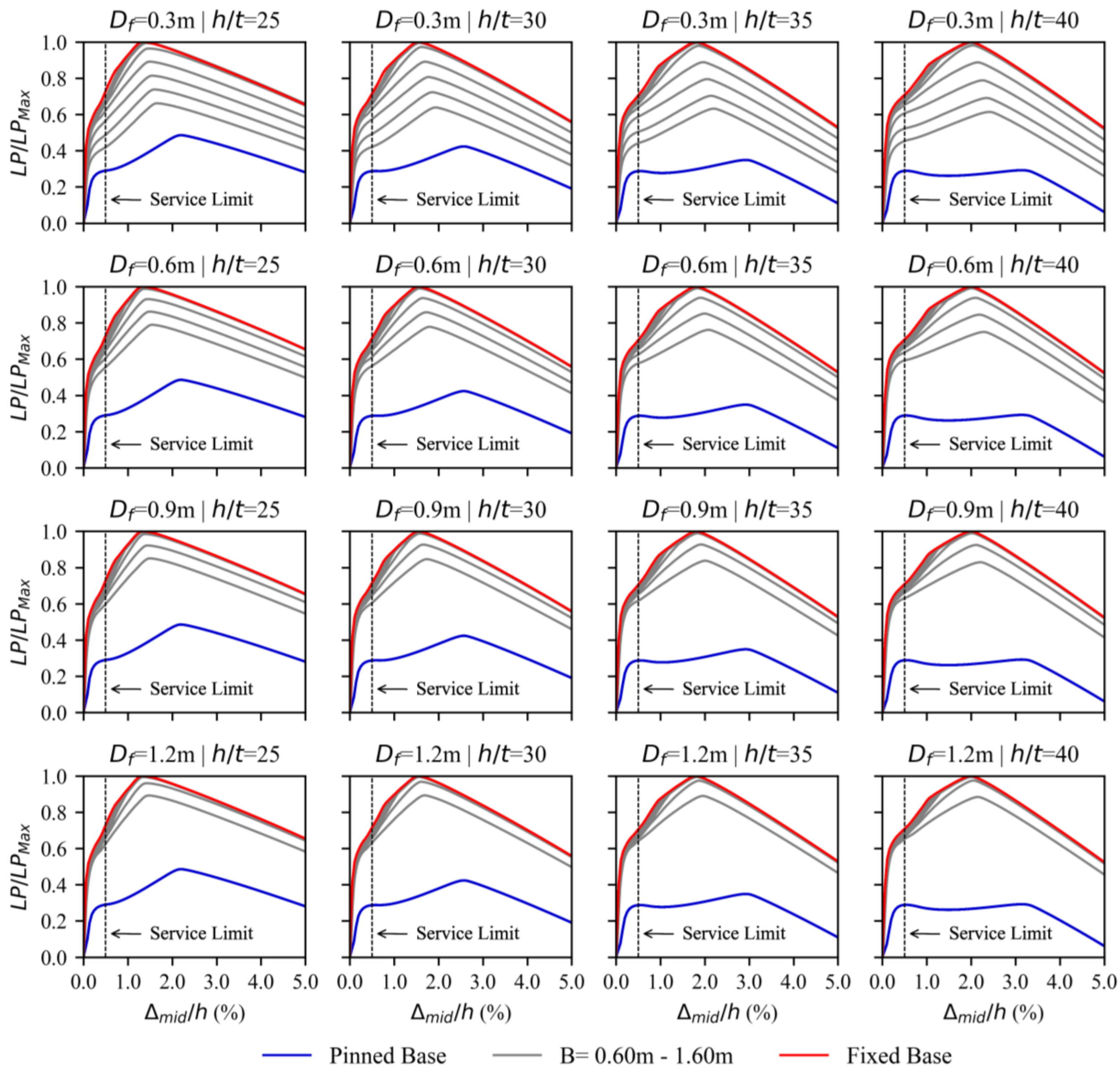

Figure B1 – Load-displacement curves on Loose Sand

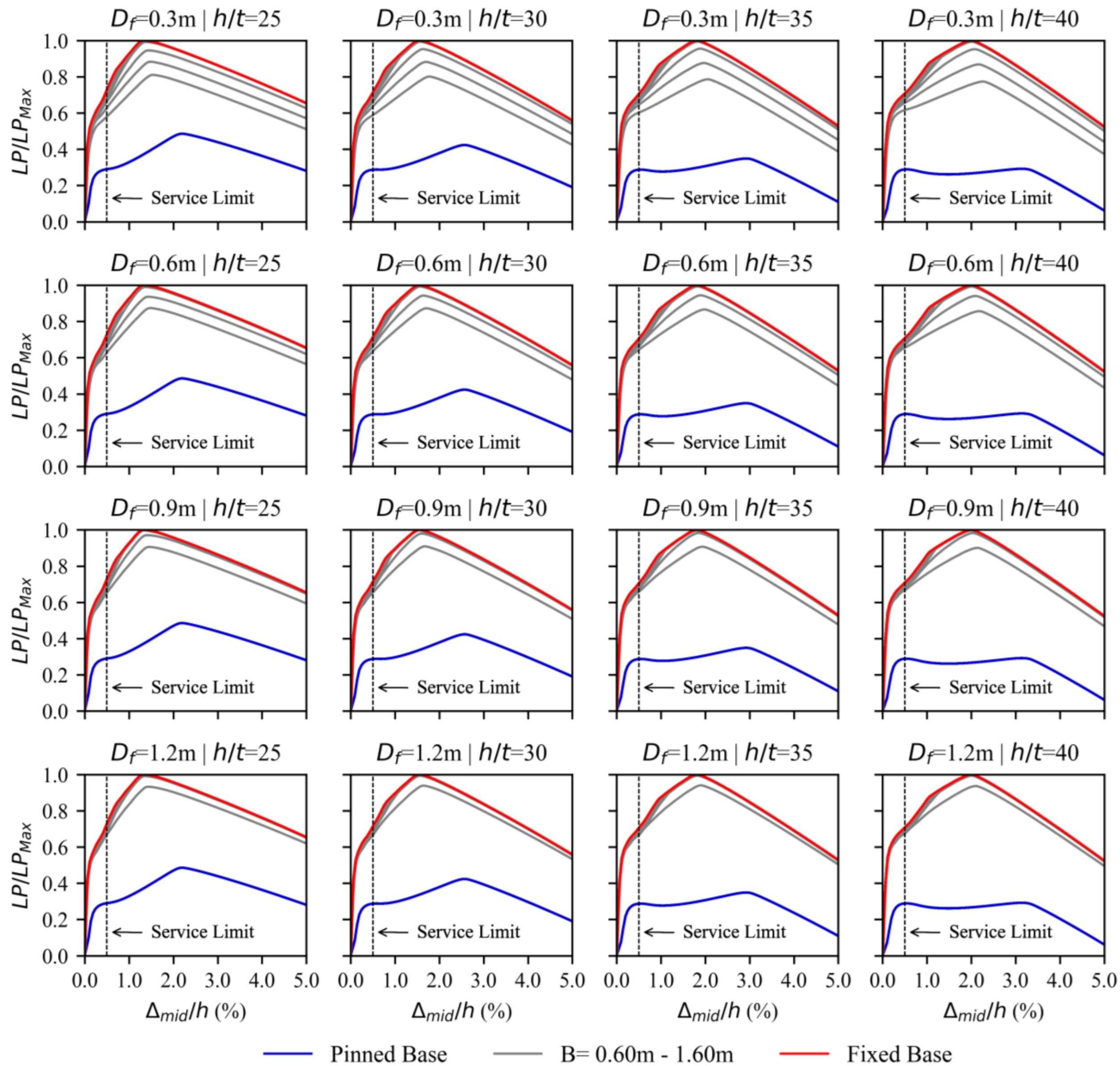

Figure B2 – Load-displacement curves on Medium Sand

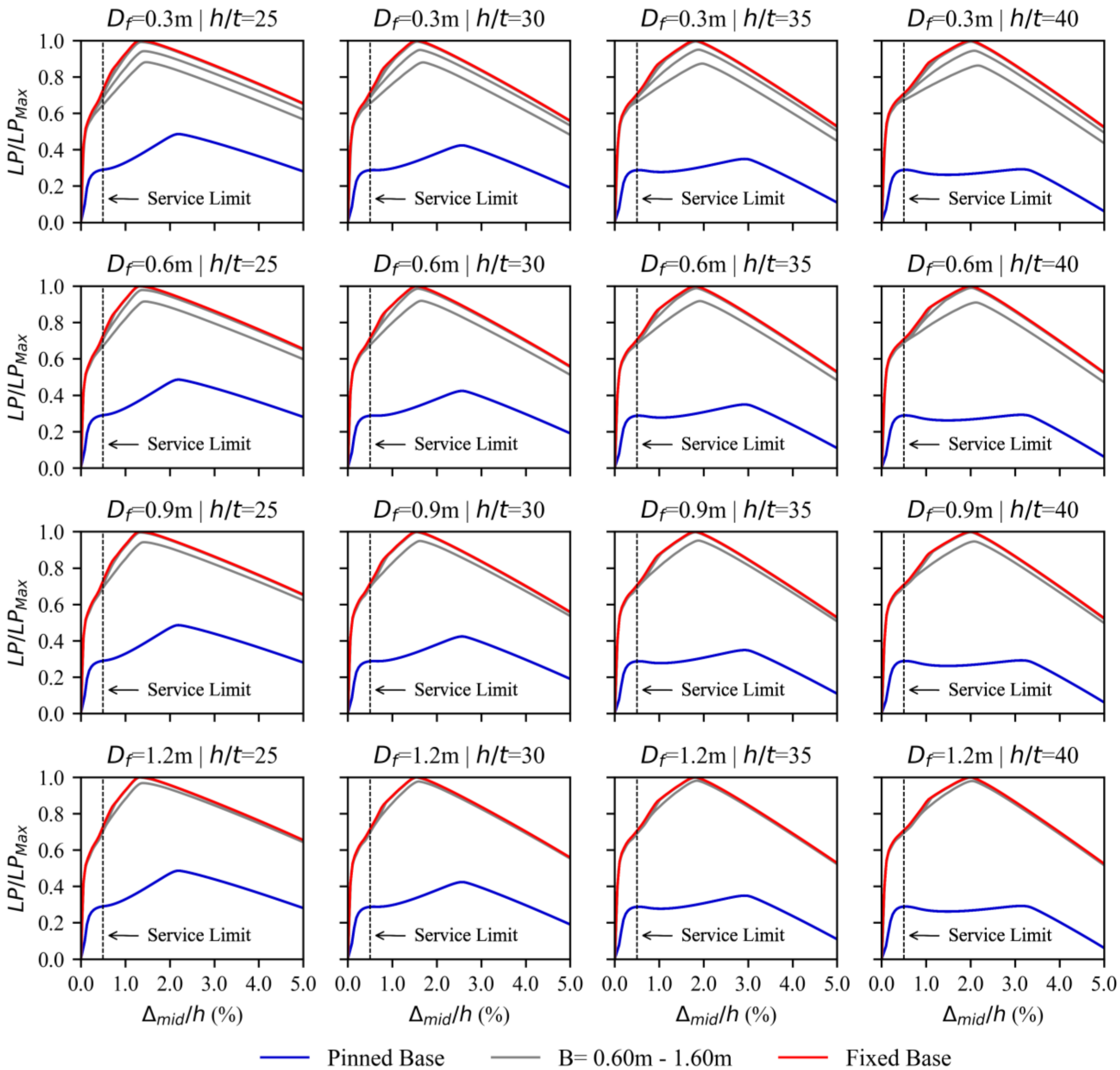

Figure B3 – Load-displacement curves on Stiff Sand

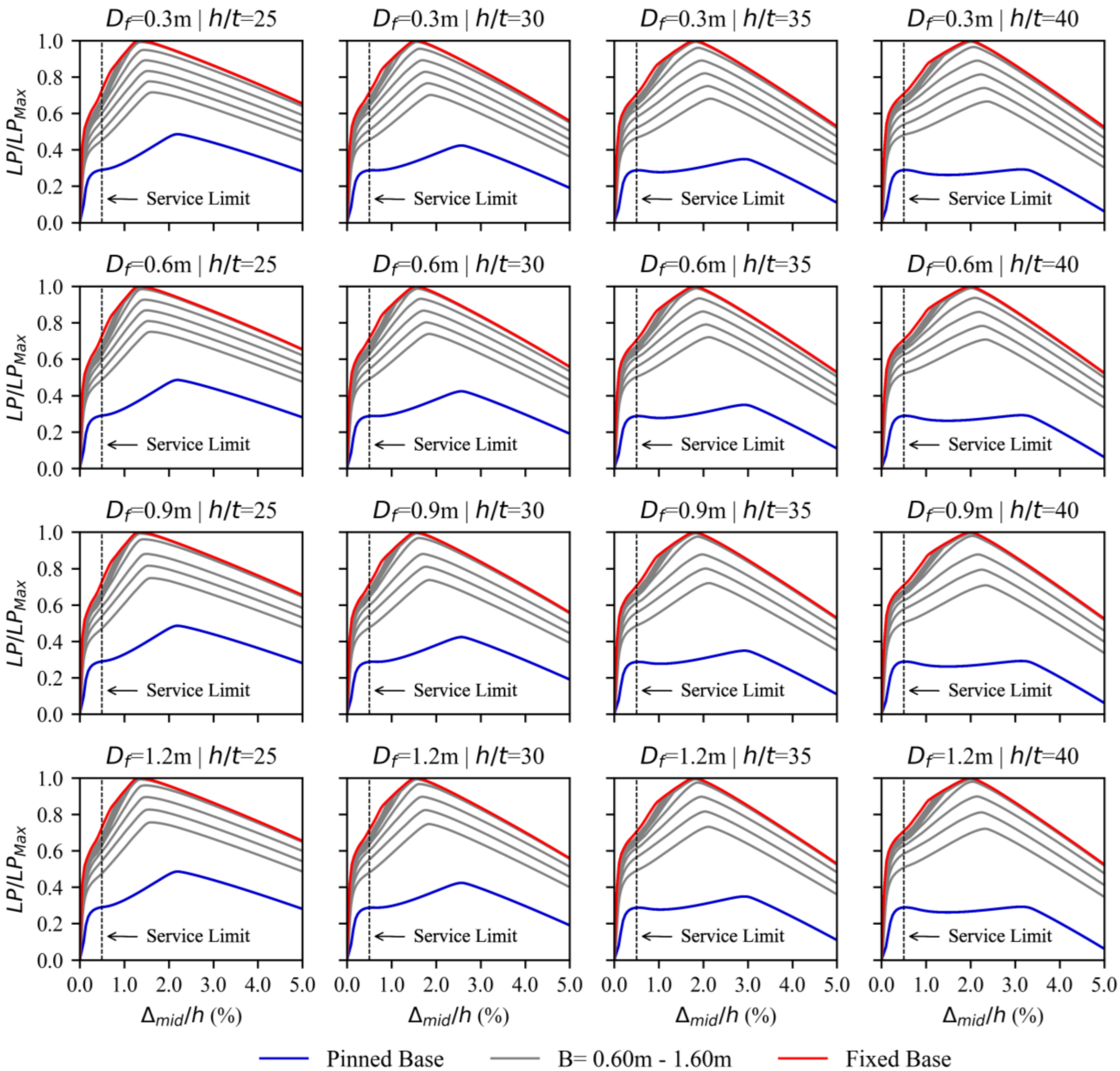

Figure B4 – Load-displacement curves on Soft Clay

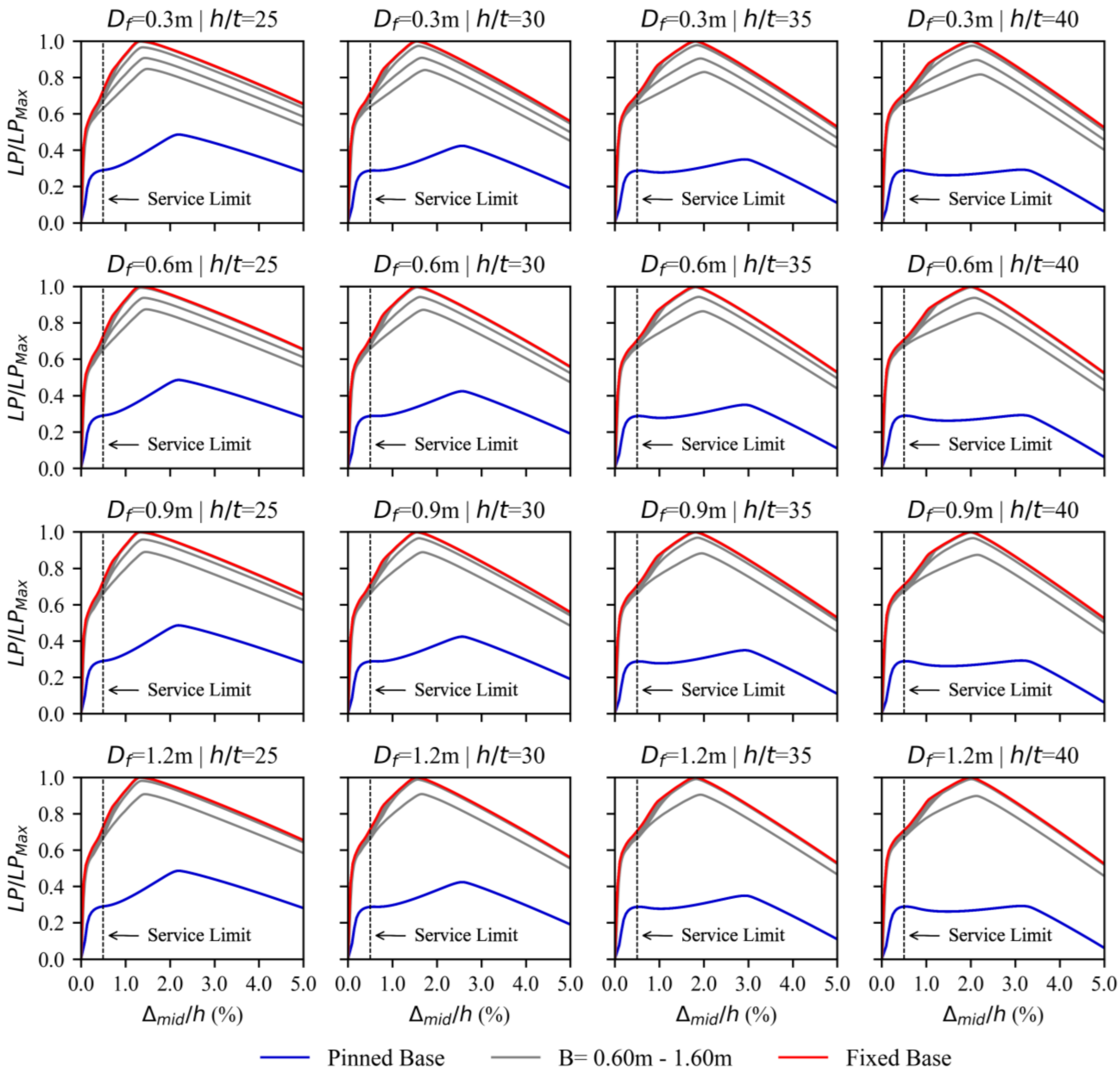

Figure B5 – Load-displacement curves on Medium Clay

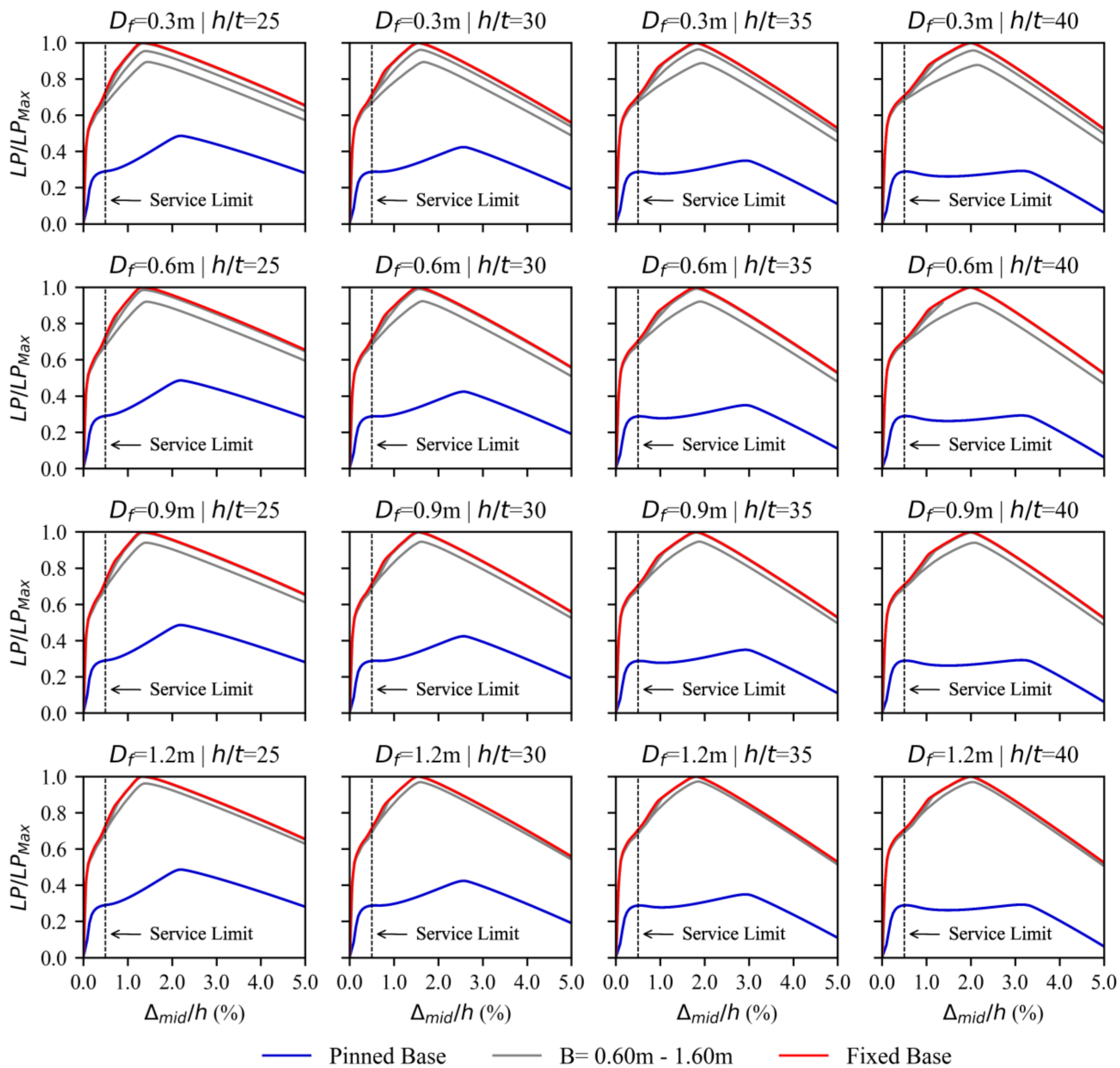

Figure B6 – Load-displacement curves on Stiff Clay

Appendix C – Moment – Rotation curves per soil type

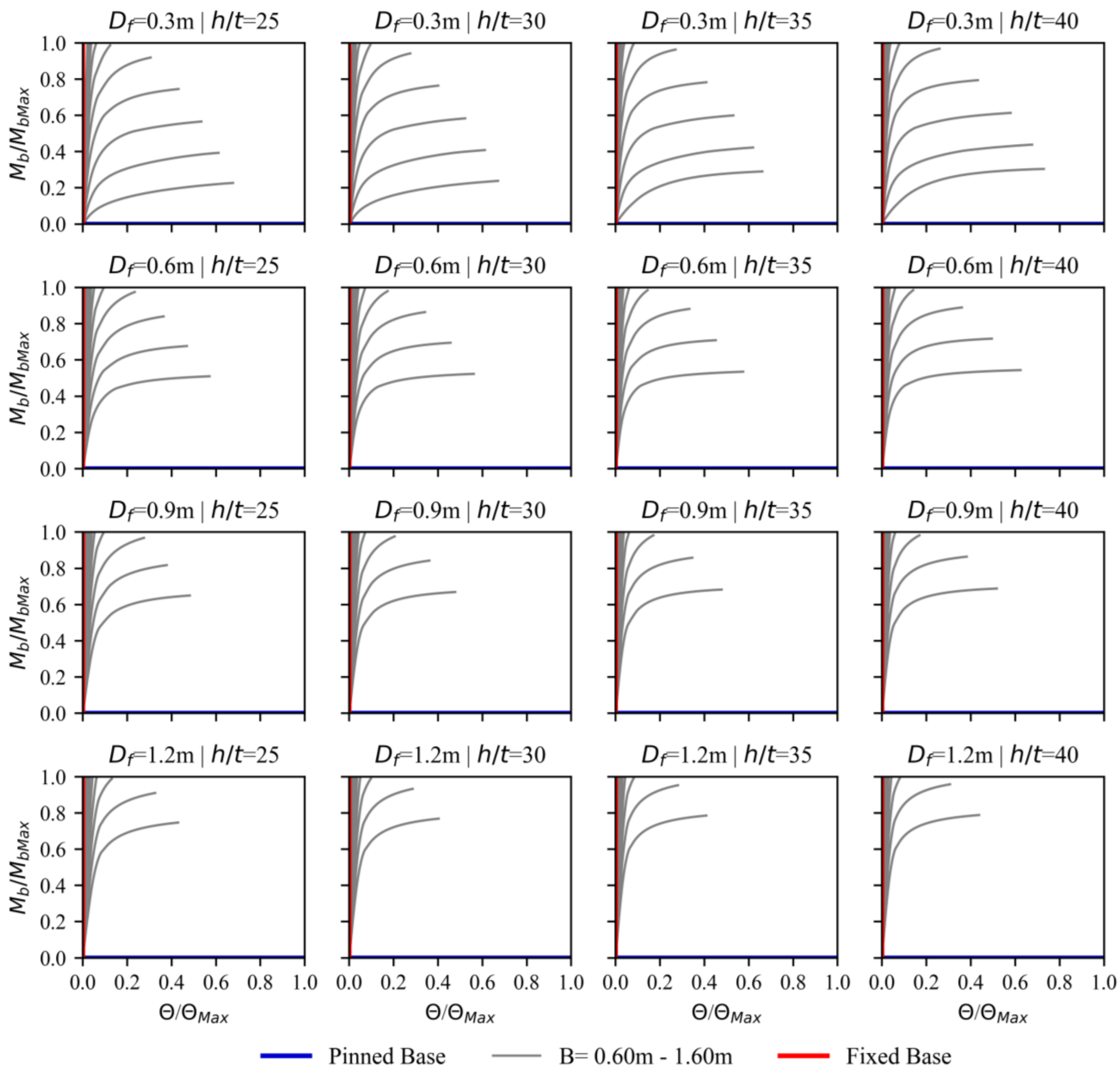

Figure C1 – Moment-rotation curves on Loose Sand

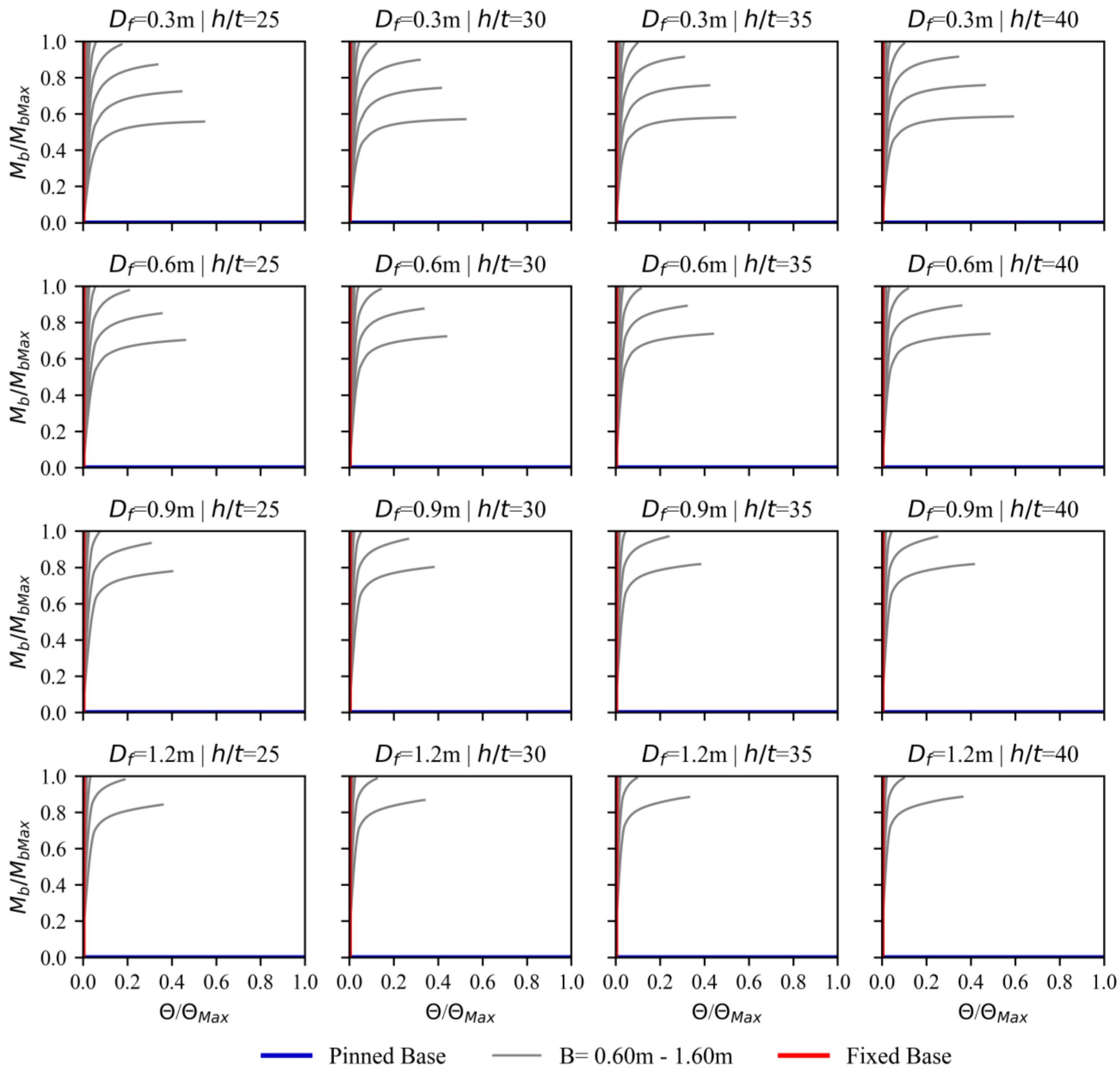

Figure C2 – Moment-rotation curves on Medium Sand

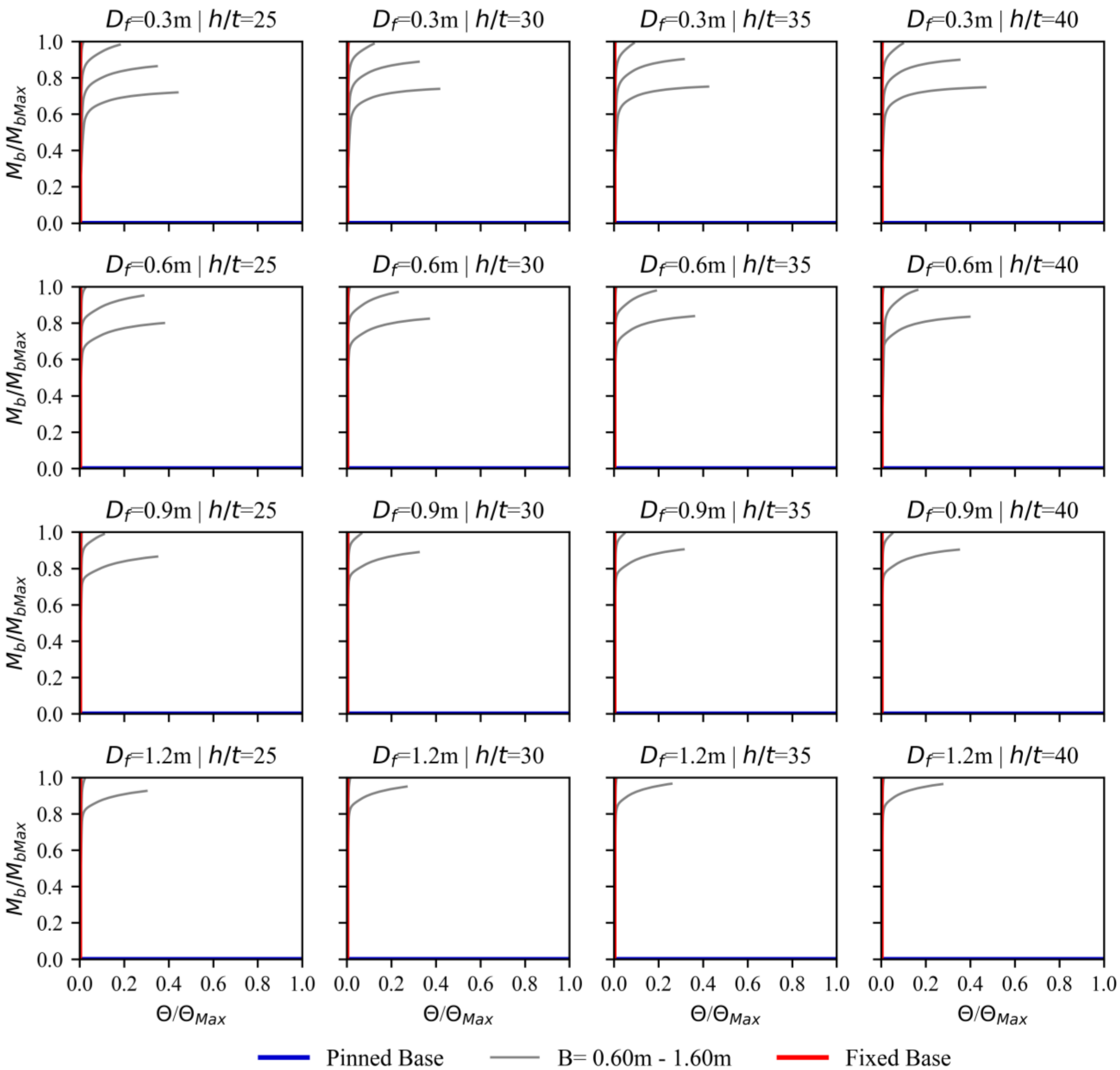

Figure C3 – Moment-rotation curves on Dense Sand

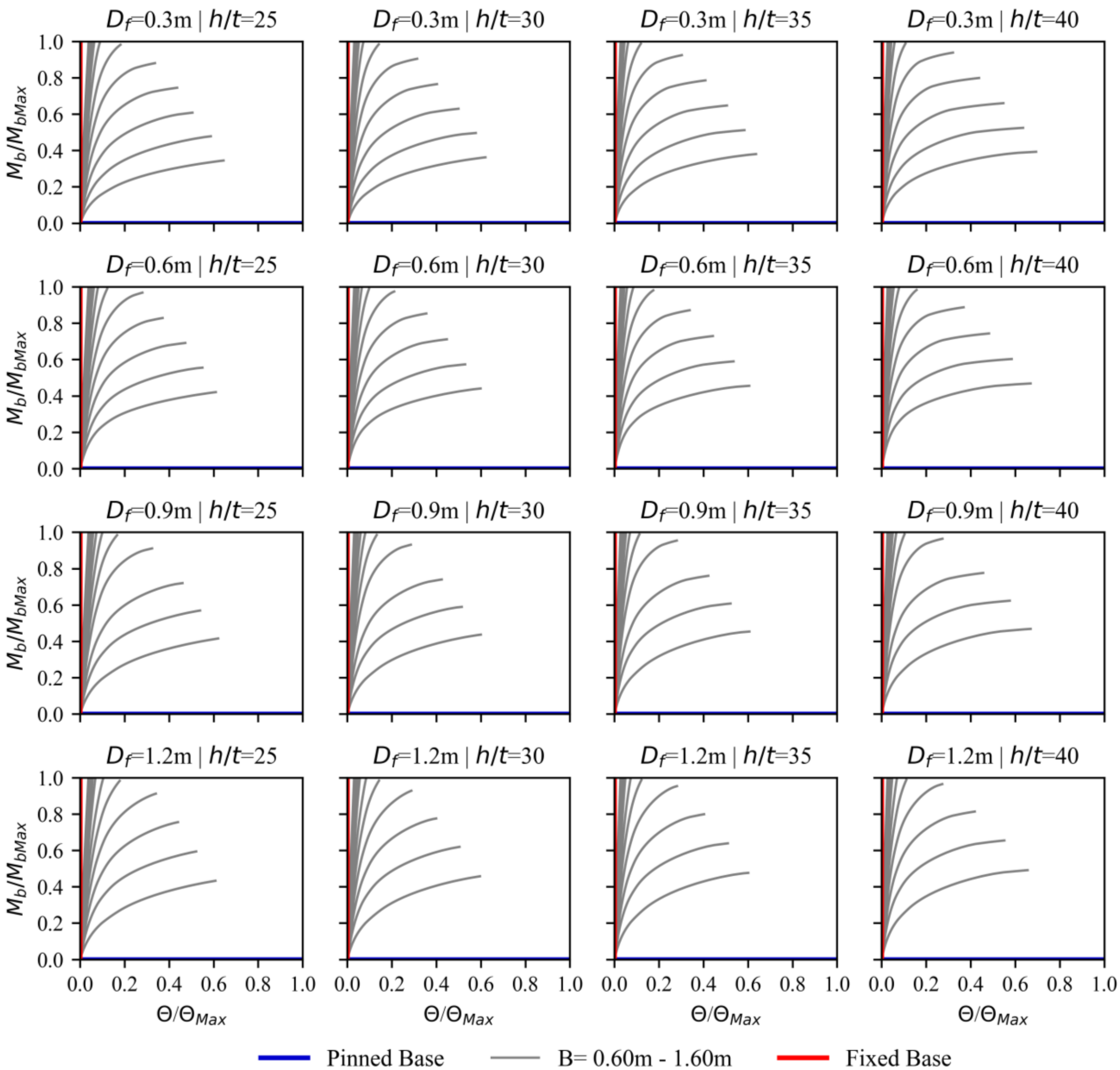

Figure C4 – Moment-rotation curves on Soft Clay

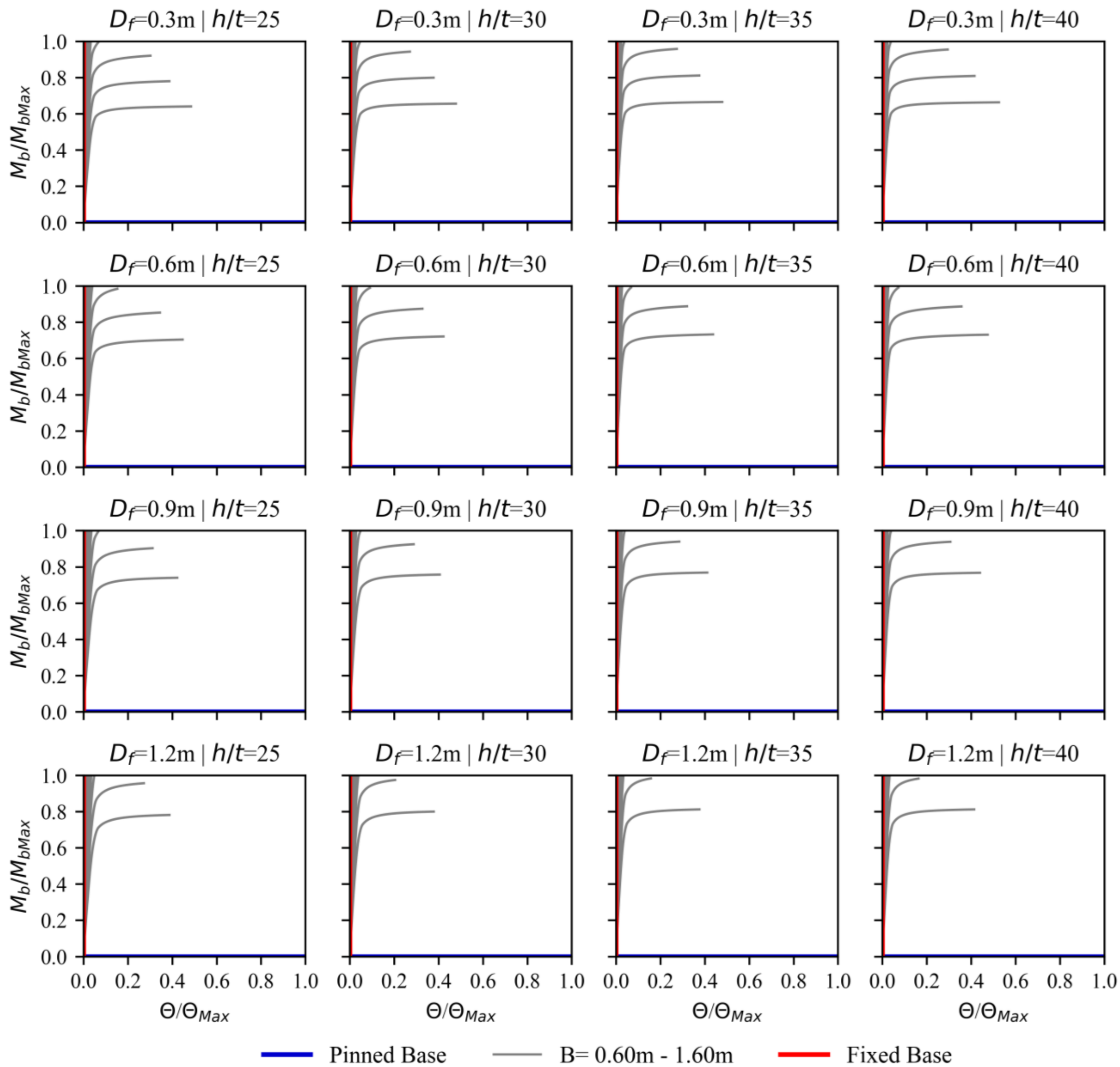

Figure C5 – Moment-rotation curves on Medium Clay

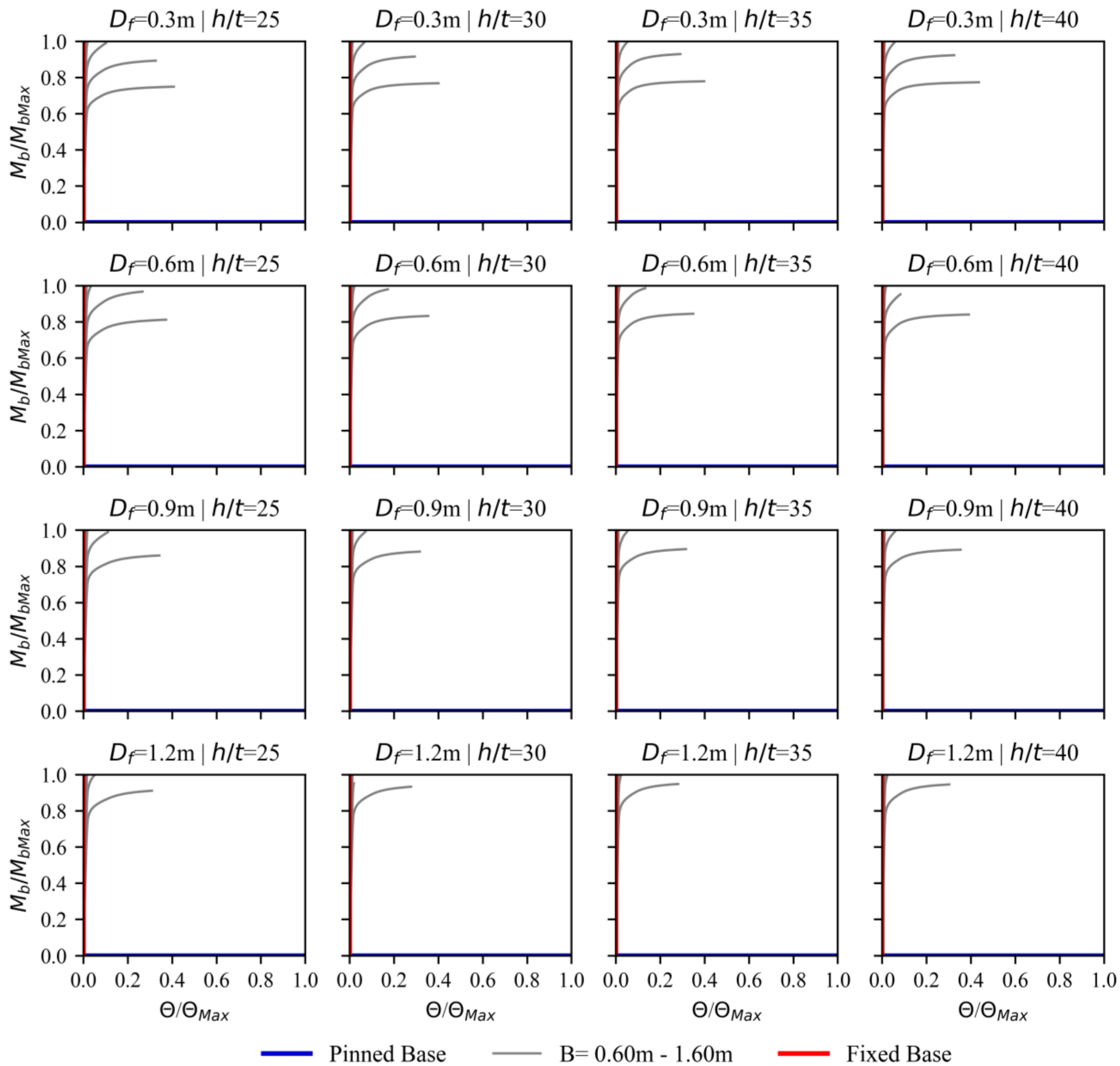

Figure C6 – Moment-rotation curves on Medium Clay

Appendix D – Equivalent rotational base stiffness (RBS)

ID	Soil Type	h/t	D_f (m)	B_f (m)	θ (rad)	M_b (kN-m)	RBS (kN-m/rad)
1	Loose Sand	25	0.30	0.60	0.0415	3.9	93
2	Loose Sand	25	0.30	0.70	0.0375	6.7	179
3	Loose Sand	25	0.30	0.80	0.0328	9.7	296
4	Loose Sand	25	0.30	0.90	0.0265	12.8	482
5	Loose Sand	25	0.30	1.00	0.0188	15.7	839
6	Loose Sand	25	0.30	1.10	0.0076	16.9	2,227
7	Loose Sand	25	0.30	1.20	0.0036	17.0	4,666
8	Loose Sand	25	0.30	1.30	0.0023	17.0	7,283
9	Loose Sand	25	0.30	1.40	0.0018	17.0	9,247
10	Loose Sand	25	0.30	1.50	0.0015	17.0	11,139
11	Loose Sand	25	0.30	1.60	0.0013	17.1	12,933
12	Loose Sand	25	0.60	0.60	0.0350	8.7	249
13	Loose Sand	25	0.60	0.70	0.0288	11.6	403
14	Loose Sand	25	0.60	0.80	0.0224	14.4	644
15	Loose Sand	25	0.60	0.90	0.0144	16.7	1,163
16	Loose Sand	25	0.60	1.00	0.0056	17.0	3,012
17	Loose Sand	25	0.60	1.10	0.0031	17.0	5,420
18	Loose Sand	25	0.60	1.20	0.0023	17.0	7,269
19	Loose Sand	25	0.60	1.30	0.0019	17.1	8,971
20	Loose Sand	25	0.60	1.40	0.0016	17.1	10,733
21	Loose Sand	25	0.60	1.50	0.0013	17.1	13,401
22	Loose Sand	25	0.60	1.60	0.0010	17.1	16,958
23	Loose Sand	25	0.90	0.60	0.0296	11.1	376
24	Loose Sand	25	0.90	0.70	0.0232	14.0	603
25	Loose Sand	25	0.90	0.80	0.0169	16.6	980
26	Loose Sand	25	0.90	0.90	0.0056	17.0	3,018
27	Loose Sand	25	0.90	1.00	0.0033	17.0	5,221
28	Loose Sand	25	0.90	1.10	0.0025	17.0	6,834
29	Loose Sand	25	0.90	1.20	0.0019	17.1	8,782
30	Loose Sand	25	0.90	1.30	0.0015	17.1	11,207
31	Loose Sand	25	0.90	1.40	0.0012	17.1	14,314
32	Loose Sand	25	0.90	1.50	0.0009	17.1	18,759
33	Loose Sand	25	0.90	1.60	0.0007	17.1	25,410
34	Loose Sand	25	1.20	0.60	0.0264	12.8	485
35	Loose Sand	25	1.20	0.70	0.0200	15.6	779
36	Loose Sand	25	1.20	0.80	0.0080	16.9	2,107
37	Loose Sand	25	1.20	0.90	0.0038	17.0	4,462

38	Loose Sand	25	1.20	1.00	0.0027	17.0	6,259
39	Loose Sand	25	1.20	1.10	0.0020	17.1	8,405
40	Loose Sand	25	1.20	1.20	0.0015	17.1	11,763
41	Loose Sand	25	1.20	1.30	0.0011	17.1	15,579
42	Loose Sand	25	1.20	1.40	0.0008	17.1	21,303
43	Loose Sand	25	1.20	1.50	0.0006	17.1	30,046
44	Loose Sand	25	1.20	1.60	0.0005	17.1	34,380
45	Loose Sand	30	0.30	0.60	0.0490	4.0	82
46	Loose Sand	30	0.30	0.70	0.0447	6.9	154
47	Loose Sand	30	0.30	0.80	0.0382	9.8	257
48	Loose Sand	30	0.30	0.90	0.0293	12.9	438
49	Loose Sand	30	0.30	1.00	0.0201	15.9	788
50	Loose Sand	30	0.30	1.10	0.0070	16.7	2,387
51	Loose Sand	30	0.30	1.20	0.0034	16.7	4,931
52	Loose Sand	30	0.30	1.30	0.0023	16.7	7,396
53	Loose Sand	30	0.30	1.40	0.0018	16.7	9,318
54	Loose Sand	30	0.30	1.50	0.0015	16.8	11,176
55	Loose Sand	30	0.30	1.60	0.0013	16.8	12,942
56	Loose Sand	30	0.60	0.60	0.0410	8.8	215
57	Loose Sand	30	0.60	0.70	0.0334	11.7	351
58	Loose Sand	30	0.60	0.80	0.0250	14.6	582
59	Loose Sand	30	0.60	0.90	0.0127	16.5	1,301
60	Loose Sand	30	0.60	1.00	0.0052	16.7	3,215
61	Loose Sand	30	0.60	1.10	0.0030	16.7	5,552
62	Loose Sand	30	0.60	1.20	0.0023	16.7	7,338
63	Loose Sand	30	0.60	1.30	0.0019	16.8	9,010
64	Loose Sand	30	0.60	1.40	0.0016	16.8	10,711
65	Loose Sand	30	0.60	1.50	0.0013	16.8	13,346
66	Loose Sand	30	0.60	1.60	0.0010	16.8	16,910
67	Loose Sand	30	0.90	0.60	0.0349	11.3	323
68	Loose Sand	30	0.90	0.70	0.0264	14.2	537
69	Loose Sand	30	0.90	0.80	0.0150	16.4	1096
70	Loose Sand	30	0.90	0.90	0.0052	16.7	3232
71	Loose Sand	30	0.90	1.00	0.0032	16.7	5311
72	Loose Sand	30	0.90	1.10	0.0024	16.7	6885
73	Loose Sand	30	0.90	1.20	0.0019	16.8	8782
74	Loose Sand	30	0.90	1.30	0.0015	16.8	11178
75	Loose Sand	30	0.90	1.40	0.0012	16.8	14296
76	Loose Sand	30	0.90	1.50	0.0009	16.8	18763
77	Loose Sand	30	0.90	1.60	0.0007	16.8	25495
78	Loose Sand	30	1.20	0.60	0.0295	12.9	439
79	Loose Sand	30	1.20	0.70	0.0209	15.7	751

80	Loose Sand	30	1.20	0.80	0.0072	16.7	2325
81	Loose Sand	30	1.20	0.90	0.0037	16.7	4555
82	Loose Sand	30	1.20	1.00	0.0027	16.7	6297
83	Loose Sand	30	1.20	1.10	0.0020	16.8	8418
84	Loose Sand	30	1.20	1.20	0.0014	16.8	11769
85	Loose Sand	30	1.20	1.30	0.0011	16.8	15622
86	Loose Sand	30	1.20	1.40	0.0008	16.8	21414
87	Loose Sand	30	1.20	1.50	0.0006	16.8	30188
88	Loose Sand	30	1.20	1.60	0.0005	16.8	34393
89	Loose Sand	35	0.30	0.60	0.0542	4.8	89
90	Loose Sand	35	0.30	0.70	0.0507	7.0	138
91	Loose Sand	35	0.30	0.80	0.0435	9.9	229
92	Loose Sand	35	0.30	0.90	0.0335	13.0	387
93	Loose Sand	35	0.30	1.00	0.0222	16.0	721
94	Loose Sand	35	0.30	1.10	0.0066	16.4	2504
95	Loose Sand	35	0.30	1.20	0.0032	16.5	5151
96	Loose Sand	35	0.30	1.30	0.0022	16.5	7487
97	Loose Sand	35	0.30	1.40	0.0018	16.5	9389
98	Loose Sand	35	0.30	1.50	0.0015	16.5	11231
99	Loose Sand	35	0.30	1.60	0.0013	16.5	12981
100	Loose Sand	35	0.60	0.60	0.0471	8.9	188
101	Loose Sand	35	0.60	0.70	0.0370	11.8	318
102	Loose Sand	35	0.60	0.80	0.0273	14.6	536
103	Loose Sand	35	0.60	0.90	0.0119	16.3	1378
104	Loose Sand	35	0.60	1.00	0.0049	16.4	3349
105	Loose Sand	35	0.60	1.10	0.0029	16.5	5644
106	Loose Sand	35	0.60	1.20	0.0022	16.5	7402
107	Loose Sand	35	0.60	1.30	0.0018	16.5	9058
108	Loose Sand	35	0.60	1.40	0.0015	16.5	10760
109	Loose Sand	35	0.60	1.50	0.0012	16.5	13424
110	Loose Sand	35	0.60	1.60	0.0010	16.5	17053
111	Loose Sand	35	0.90	0.60	0.0391	11.3	289
112	Loose Sand	35	0.90	0.70	0.0283	14.2	503
113	Loose Sand	35	0.90	0.80	0.0140	16.3	1165
114	Loose Sand	35	0.90	0.90	0.0049	16.5	3376
115	Loose Sand	35	0.90	1.00	0.0031	16.5	5378
116	Loose Sand	35	0.90	1.10	0.0024	16.5	6935
117	Loose Sand	35	0.90	1.20	0.0019	16.5	8843
118	Loose Sand	35	0.90	1.30	0.0015	16.5	11251
119	Loose Sand	35	0.90	1.40	0.0011	16.5	14434
120	Loose Sand	35	0.90	1.50	0.0009	16.5	18993
121	Loose Sand	35	0.90	1.60	0.0006	16.5	25967

122	Loose Sand	35	1.20	0.60	0.0335	13.0	389
123	Loose Sand	35	1.20	0.70	0.0231	15.8	685
124	Loose Sand	35	1.20	0.80	0.0067	16.4	2461
125	Loose Sand	35	1.20	0.90	0.0036	16.5	4620
126	Loose Sand	35	1.20	1.00	0.0026	16.5	6359
127	Loose Sand	35	1.20	1.10	0.0019	16.5	8486
128	Loose Sand	35	1.20	1.20	0.0014	16.5	11885
129	Loose Sand	35	1.20	1.30	0.0010	16.5	15838
130	Loose Sand	35	1.20	1.40	0.0008	16.5	21820
131	Loose Sand	35	1.20	1.50	0.0005	16.5	30482
132	Loose Sand	35	1.20	1.60	0.0005	16.5	34404
133	Loose Sand	40	0.30	0.60	0.0597	5.0	83
134	Loose Sand	40	0.30	0.70	0.0554	7.2	129
135	Loose Sand	40	0.30	0.80	0.0475	10.0	211
136	Loose Sand	40	0.30	0.90	0.0354	13.0	367
137	Loose Sand	40	0.30	1.00	0.0213	15.8	745
138	Loose Sand	40	0.30	1.10	0.0063	16.2	2578
139	Loose Sand	40	0.30	1.20	0.0031	16.3	5233
140	Loose Sand	40	0.30	1.30	0.0022	16.3	7564
141	Loose Sand	40	0.30	1.40	0.0017	16.3	9473
142	Loose Sand	40	0.30	1.50	0.0014	16.3	11322
143	Loose Sand	40	0.30	1.60	0.0012	16.3	13096
144	Loose Sand	40	0.60	0.60	0.0511	8.9	174
145	Loose Sand	40	0.60	0.70	0.0405	11.7	289
146	Loose Sand	40	0.60	0.80	0.0295	14.6	493
147	Loose Sand	40	0.60	0.90	0.0115	16.1	1396
148	Loose Sand	40	0.60	1.00	0.0048	16.2	3391
149	Loose Sand	40	0.60	1.10	0.0029	16.3	5703
150	Loose Sand	40	0.60	1.20	0.0022	16.3	7468
151	Loose Sand	40	0.60	1.30	0.0018	16.3	9130
152	Loose Sand	40	0.60	1.40	0.0015	16.3	11005
153	Loose Sand	40	0.60	1.50	0.0012	16.3	13816
154	Loose Sand	40	0.60	1.60	0.0009	16.3	17659
155	Loose Sand	40	0.90	0.60	0.0424	11.3	266
156	Loose Sand	40	0.90	0.70	0.0313	14.1	452
157	Loose Sand	40	0.90	0.80	0.0138	16.1	1161
158	Loose Sand	40	0.90	0.90	0.0048	16.2	3413
159	Loose Sand	40	0.90	1.00	0.0030	16.3	5428
160	Loose Sand	40	0.90	1.10	0.0023	16.3	7011
161	Loose Sand	40	0.90	1.20	0.0018	16.3	9059
162	Loose Sand	40	0.90	1.30	0.0014	16.3	11565
163	Loose Sand	40	0.90	1.40	0.0011	16.3	14919

164	Loose Sand	40	0.90	1.50	0.0008	16.3	19797
165	Loose Sand	40	0.90	1.60	0.0006	16.3	27447
166	Loose Sand	40	1.20	0.60	0.0359	12.9	360
167	Loose Sand	40	1.20	0.70	0.0251	15.7	624
168	Loose Sand	40	1.20	0.80	0.0065	16.2	2478
169	Loose Sand	40	1.20	0.90	0.0035	16.2	4665
170	Loose Sand	40	1.20	1.00	0.0025	16.3	6499
171	Loose Sand	40	1.20	1.10	0.0019	16.3	8701
172	Loose Sand	40	1.20	1.20	0.0013	16.3	12271
173	Loose Sand	40	1.20	1.30	0.0010	16.3	16496
174	Loose Sand	40	1.20	1.40	0.0007	16.3	23007
175	Loose Sand	40	1.20	1.50	0.0005	16.3	30977
176	Loose Sand	40	1.20	1.60	0.0005	16.3	34410
177	Medium Sand	25	0.30	0.60	0.0335	9.6	286
178	Medium Sand	25	0.30	0.70	0.0272	12.4	457
179	Medium Sand	25	0.30	0.80	0.0205	15.0	729
180	Medium Sand	25	0.30	0.90	0.0106	16.8	1590
181	Medium Sand	25	0.30	1.00	0.0035	17.0	4840
182	Medium Sand	25	0.30	1.10	0.0019	17.1	9023
183	Medium Sand	25	0.30	1.20	0.0012	17.1	14084
184	Medium Sand	25	0.30	1.30	0.0008	17.1	21476
185	Medium Sand	25	0.30	1.40	0.0005	17.1	32231
186	Medium Sand	25	0.30	1.50	0.0004	17.1	38203
187	Medium Sand	25	0.30	1.60	0.0004	17.1	41943
188	Medium Sand	25	0.60	0.60	0.0282	12.1	429
189	Medium Sand	25	0.60	0.70	0.0217	14.6	673
190	Medium Sand	25	0.60	0.80	0.0126	16.8	1326
191	Medium Sand	25	0.60	0.90	0.0033	17.0	5150
192	Medium Sand	25	0.60	1.00	0.0017	17.1	9895
193	Medium Sand	25	0.60	1.10	0.0011	17.1	15493
194	Medium Sand	25	0.60	1.20	0.0007	17.1	24854
195	Medium Sand	25	0.60	1.30	0.0005	17.1	31490
196	Medium Sand	25	0.60	1.40	0.0005	17.1	35006
197	Medium Sand	25	0.60	1.50	0.0004	17.1	38723
198	Medium Sand	25	0.60	1.60	0.0004	17.1	42561
199	Medium Sand	25	0.90	0.60	0.0246	13.4	542
200	Medium Sand	25	0.90	0.70	0.0187	16.0	858
201	Medium Sand	25	0.90	0.80	0.0044	17.0	3824
202	Medium Sand	25	0.90	0.90	0.0016	17.1	10464
203	Medium Sand	25	0.90	1.00	0.0010	17.1	17821
204	Medium Sand	25	0.90	1.10	0.0007	17.1	24993
205	Medium Sand	25	0.90	1.20	0.0006	17.1	28397

206	Medium Sand	25	0.90	1.30	0.0005	17.1	31877
207	Medium Sand	25	0.90	1.40	0.0005	17.1	35510
208	Medium Sand	25	0.90	1.50	0.0004	17.1	39283
209	Medium Sand	25	0.90	1.60	0.0004	17.1	43179
210	Medium Sand	25	1.20	0.60	0.0220	14.4	657
211	Medium Sand	25	1.20	0.70	0.0115	16.8	1468
212	Medium Sand	25	1.20	0.80	0.0020	17.1	8511
213	Medium Sand	25	1.20	0.90	0.0010	17.1	16527
214	Medium Sand	25	1.20	1.00	0.0008	17.1	22194
215	Medium Sand	25	1.20	1.10	0.0007	17.1	25386
216	Medium Sand	25	1.20	1.20	0.0006	17.1	28818
217	Medium Sand	25	1.20	1.30	0.0005	17.1	32352
218	Medium Sand	25	1.20	1.40	0.0005	17.1	36043
219	Medium Sand	25	1.20	1.50	0.0004	17.1	39877
220	Medium Sand	25	1.20	1.60	0.0004	17.1	43838
221	Medium Sand	30	0.30	0.60	0.0382	9.6	252
222	Medium Sand	30	0.30	0.70	0.0301	12.5	416
223	Medium Sand	30	0.30	0.80	0.0231	15.1	655
224	Medium Sand	30	0.30	0.90	0.0088	16.6	1891
225	Medium Sand	30	0.30	1.00	0.0032	16.7	5288
226	Medium Sand	30	0.30	1.10	0.0018	16.8	9185
227	Medium Sand	30	0.30	1.20	0.0012	16.8	14226
228	Medium Sand	30	0.30	1.30	0.0008	16.8	21608
229	Medium Sand	30	0.30	1.40	0.0005	16.8	32437
230	Medium Sand	30	0.30	1.50	0.0004	16.8	38213
231	Medium Sand	30	0.30	1.60	0.0004	16.8	41942
232	Medium Sand	30	0.60	0.60	0.0318	12.2	383
233	Medium Sand	30	0.60	0.70	0.0244	14.8	606
234	Medium Sand	30	0.60	0.80	0.0103	16.6	1610
235	Medium Sand	30	0.60	0.90	0.0029	16.7	5685
236	Medium Sand	30	0.60	1.00	0.0017	16.8	10073
237	Medium Sand	30	0.60	1.10	0.0011	16.8	15659
238	Medium Sand	30	0.60	1.20	0.0007	16.8	25162
239	Medium Sand	30	0.60	1.30	0.0005	16.8	31500
240	Medium Sand	30	0.60	1.40	0.0005	16.8	35005
241	Medium Sand	30	0.60	1.50	0.0004	16.8	38726
242	Medium Sand	30	0.60	1.60	0.0004	16.8	42568
243	Medium Sand	30	0.90	0.60	0.0277	13.5	488
244	Medium Sand	30	0.90	0.70	0.0193	16.1	836
245	Medium Sand	30	0.90	0.80	0.0038	16.7	4430
246	Medium Sand	30	0.90	0.90	0.0016	16.8	10728
247	Medium Sand	30	0.90	1.00	0.0009	16.8	18105

248	Medium Sand	30	0.90	1.10	0.0007	16.8	25040
249	Medium Sand	30	0.90	1.20	0.0006	16.8	28397
250	Medium Sand	30	0.90	1.30	0.0005	16.8	31880
251	Medium Sand	30	0.90	1.40	0.0005	16.8	35517
252	Medium Sand	30	0.90	1.50	0.0004	16.8	39294
253	Medium Sand	30	0.90	1.60	0.0004	16.8	43195
254	Medium Sand	30	1.20	0.60	0.0247	14.6	591
255	Medium Sand	30	1.20	0.70	0.0090	16.6	1846
256	Medium Sand	30	1.20	0.80	0.0019	16.8	8898
257	Medium Sand	30	1.20	0.90	0.0010	16.8	16868
258	Medium Sand	30	1.20	1.00	0.0008	16.8	22202
259	Medium Sand	30	1.20	1.10	0.0007	16.8	25388
260	Medium Sand	30	1.20	1.20	0.0006	16.8	28824
261	Medium Sand	30	1.20	1.30	0.0005	16.8	32362
262	Medium Sand	30	1.20	1.40	0.0005	16.8	36057
263	Medium Sand	30	1.20	1.50	0.0004	16.8	39897
264	Medium Sand	30	1.20	1.60	0.0004	16.8	43864
265	Medium Sand	35	0.30	0.60	0.0440	9.6	219
266	Medium Sand	35	0.30	0.70	0.0345	12.6	364
267	Medium Sand	35	0.30	0.80	0.0252	15.2	602
268	Medium Sand	35	0.30	0.90	0.0080	16.4	2053
269	Medium Sand	35	0.30	1.00	0.0030	16.5	5563
270	Medium Sand	35	0.30	1.10	0.0018	16.5	9338
271	Medium Sand	35	0.30	1.20	0.0011	16.5	14452
272	Medium Sand	35	0.30	1.30	0.0008	16.5	21994
273	Medium Sand	35	0.30	1.40	0.0005	16.5	32898
274	Medium Sand	35	0.30	1.50	0.0004	16.5	38222
275	Medium Sand	35	0.30	1.60	0.0004	16.5	41954
276	Medium Sand	35	0.60	0.60	0.0358	12.2	341
277	Medium Sand	35	0.60	0.70	0.0262	14.8	565
278	Medium Sand	35	0.60	0.80	0.0092	16.4	1776
279	Medium Sand	35	0.60	0.90	0.0027	16.5	6026
280	Medium Sand	35	0.60	1.00	0.0016	16.5	10265
281	Medium Sand	35	0.60	1.10	0.0010	16.5	15947
282	Medium Sand	35	0.60	1.20	0.0006	16.5	25688
283	Medium Sand	35	0.60	1.30	0.0005	16.5	31508
284	Medium Sand	35	0.60	1.40	0.0005	16.5	35015
285	Medium Sand	35	0.60	1.50	0.0004	16.5	38740
286	Medium Sand	35	0.60	1.60	0.0004	16.5	42586
287	Medium Sand	35	0.90	0.60	0.0312	13.6	435
288	Medium Sand	35	0.90	0.70	0.0195	16.1	827
289	Medium Sand	35	0.90	0.80	0.0034	16.5	4810

290	Medium Sand	35	0.90	0.90	0.0015	16.5	10995
291	Medium Sand	35	0.90	1.00	0.0009	16.5	18559
292	Medium Sand	35	0.90	1.10	0.0007	16.5	25093
293	Medium Sand	35	0.90	1.20	0.0006	16.5	28406
294	Medium Sand	35	0.90	1.30	0.0005	16.5	31892
295	Medium Sand	35	0.90	1.40	0.0005	16.5	35533
296	Medium Sand	35	0.90	1.50	0.0004	16.5	39315
297	Medium Sand	35	0.90	1.60	0.0004	16.5	43222
298	Medium Sand	35	1.20	0.60	0.0271	14.7	542
299	Medium Sand	35	1.20	0.70	0.0078	16.4	2101
300	Medium Sand	35	1.20	0.80	0.0018	16.5	9196
301	Medium Sand	35	1.20	0.90	0.0010	16.5	17258
302	Medium Sand	35	1.20	1.00	0.0007	16.5	22209
303	Medium Sand	35	1.20	1.10	0.0007	16.5	25398
304	Medium Sand	35	1.20	1.20	0.0006	16.5	28839
305	Medium Sand	35	1.20	1.30	0.0005	16.5	32380
306	Medium Sand	35	1.20	1.40	0.0005	16.5	36081
307	Medium Sand	35	1.20	1.50	0.0004	16.5	39926
308	Medium Sand	35	1.20	1.60	0.0004	16.5	43900
309	Medium Sand	40	0.30	0.60	0.0483	9.6	198
310	Medium Sand	40	0.30	0.70	0.0379	12.4	328
311	Medium Sand	40	0.30	0.80	0.0280	15.0	535
312	Medium Sand	40	0.30	0.90	0.0081	16.2	1989
313	Medium Sand	40	0.30	1.00	0.0029	16.3	5564
314	Medium Sand	40	0.30	1.10	0.0017	16.3	9559
315	Medium Sand	40	0.30	1.20	0.0011	16.3	14957
316	Medium Sand	40	0.30	1.30	0.0007	16.3	23077
317	Medium Sand	40	0.30	1.40	0.0005	16.3	33707
318	Medium Sand	40	0.30	1.50	0.0004	16.3	38225
319	Medium Sand	40	0.30	1.60	0.0004	16.3	41994
320	Medium Sand	40	0.60	0.60	0.0396	12.1	305
321	Medium Sand	40	0.60	0.70	0.0292	14.6	501
322	Medium Sand	40	0.60	0.80	0.0095	16.2	1694
323	Medium Sand	40	0.60	0.90	0.0027	16.3	6057
324	Medium Sand	40	0.60	1.00	0.0015	16.3	10566
325	Medium Sand	40	0.60	1.10	0.0010	16.3	16617
326	Medium Sand	40	0.60	1.20	0.0006	16.3	26594
327	Medium Sand	40	0.60	1.30	0.0005	16.3	31512
328	Medium Sand	40	0.60	1.40	0.0005	16.3	35050
329	Medium Sand	40	0.60	1.50	0.0004	16.3	38780
330	Medium Sand	40	0.60	1.60	0.0004	16.3	42633
331	Medium Sand	40	0.90	0.60	0.0339	13.4	396

332	Medium Sand	40	0.90	0.70	0.0203	15.9	783
333	Medium Sand	40	0.90	0.80	0.0034	16.2	4799
334	Medium Sand	40	0.90	0.90	0.0014	16.3	11391
335	Medium Sand	40	0.90	1.00	0.0008	16.3	19542
336	Medium Sand	40	0.90	1.10	0.0006	16.3	25143
337	Medium Sand	40	0.90	1.20	0.0006	16.3	28436
338	Medium Sand	40	0.90	1.30	0.0005	16.3	31927
339	Medium Sand	40	0.90	1.40	0.0005	16.3	35574
340	Medium Sand	40	0.90	1.50	0.0004	16.3	39362
341	Medium Sand	40	0.90	1.60	0.0004	16.3	43276
342	Medium Sand	40	1.20	0.60	0.0296	14.5	490
343	Medium Sand	40	1.20	0.70	0.0080	16.2	2017
344	Medium Sand	40	1.20	0.80	0.0017	16.3	9507
345	Medium Sand	40	1.20	0.90	0.0009	16.3	17817
346	Medium Sand	40	1.20	1.00	0.0007	16.3	22232
347	Medium Sand	40	1.20	1.10	0.0006	16.3	25426
348	Medium Sand	40	1.20	1.20	0.0006	16.3	28873
349	Medium Sand	40	1.20	1.30	0.0005	16.3	32421
350	Medium Sand	40	1.20	1.40	0.0005	16.3	36128
351	Medium Sand	40	1.20	1.50	0.0004	15.5	40062
352	Medium Sand	40	1.20	1.60	0.0004	16.3	43964
353	Dense Sand	25	0.30	0.60	0.0269	12.3	458
354	Dense Sand	25	0.30	0.70	0.0212	14.8	697
355	Dense Sand	25	0.30	0.80	0.0110	16.8	1526
356	Dense Sand	25	0.30	0.90	0.0010	17.1	16636
357	Dense Sand	25	0.30	1.00	0.0004	17.1	40629
358	Dense Sand	25	0.30	1.10	0.0004	17.1	48574
359	Dense Sand	25	0.30	1.20	0.0003	17.1	56227
360	Dense Sand	25	0.30	1.30	0.0003	17.1	62893
361	Dense Sand	25	0.30	1.40	0.0002	17.1	68356
362	Dense Sand	25	0.30	1.50	0.0002	17.1	74359
363	Dense Sand	25	0.30	1.60	0.0002	17.1	80308
364	Dense Sand	25	0.60	0.60	0.0232	13.7	591
365	Dense Sand	25	0.60	0.70	0.0175	16.3	931
366	Dense Sand	25	0.60	0.80	0.0016	17.1	10465
367	Dense Sand	25	0.60	0.90	0.0005	17.1	35607
368	Dense Sand	25	0.60	1.00	0.0004	17.1	43685
369	Dense Sand	25	0.60	1.10	0.0003	17.1	50400
370	Dense Sand	25	0.60	1.20	0.0003	17.1	56868
371	Dense Sand	25	0.60	1.30	0.0003	17.1	62839
372	Dense Sand	25	0.60	1.40	0.0002	17.1	68858
373	Dense Sand	25	0.60	1.50	0.0002	17.1	74872

374	Dense Sand	25	0.60	1.60	0.0002	17.1	80832
375	Dense Sand	25	0.90	0.60	0.0214	14.8	695
376	Dense Sand	25	0.90	0.70	0.0067	17.0	2536
377	Dense Sand	25	0.90	0.80	0.0006	17.1	28870
378	Dense Sand	25	0.90	0.90	0.0004	17.1	38428
379	Dense Sand	25	0.90	1.00	0.0004	17.1	45264
380	Dense Sand	25	0.90	1.10	0.0003	17.1	51328
381	Dense Sand	25	0.90	1.20	0.0003	17.1	57219
382	Dense Sand	25	0.90	1.30	0.0003	17.1	63206
383	Dense Sand	25	0.90	1.40	0.0002	17.1	69240
384	Dense Sand	25	0.90	1.50	0.0002	17.1	75269
385	Dense Sand	25	0.90	1.60	0.0002	17.1	81242
386	Dense Sand	25	1.20	0.60	0.0184	15.9	862
387	Dense Sand	25	1.20	0.70	0.0015	17.1	11668
388	Dense Sand	25	1.20	0.80	0.0005	17.1	32340
389	Dense Sand	25	1.20	0.90	0.0004	17.1	39894
390	Dense Sand	25	1.20	1.00	0.0004	17.1	45846
391	Dense Sand	25	1.20	1.10	0.0003	17.1	51608
392	Dense Sand	25	1.20	1.20	0.0003	17.1	57515
393	Dense Sand	25	1.20	1.30	0.0003	17.1	63519
394	Dense Sand	25	1.20	1.40	0.0002	17.1	69568
395	Dense Sand	25	1.20	1.50	0.0002	17.1	75611
396	Dense Sand	25	1.20	1.60	0.0002	17.1	81598
397	Dense Sand	30	0.30	0.60	0.0303	12.4	411
398	Dense Sand	30	0.30	0.70	0.0236	15.0	635
399	Dense Sand	30	0.30	0.80	0.0088	16.6	1886
400	Dense Sand	30	0.30	0.90	0.0007	16.8	22483
401	Dense Sand	30	0.30	1.00	0.0004	16.8	41251
402	Dense Sand	30	0.30	1.10	0.0003	16.8	48820
403	Dense Sand	30	0.30	1.20	0.0003	16.8	56267
404	Dense Sand	30	0.30	1.30	0.0003	16.8	62930
405	Dense Sand	30	0.30	1.40	0.0002	16.8	68372
406	Dense Sand	30	0.30	1.50	0.0002	16.8	74374
407	Dense Sand	30	0.30	1.60	0.0002	16.8	80326
408	Dense Sand	30	0.60	0.60	0.0269	13.9	516
409	Dense Sand	30	0.60	0.70	0.0167	16.4	980
410	Dense Sand	30	0.60	0.80	0.0010	16.8	16767
411	Dense Sand	30	0.60	0.90	0.0005	16.8	36277
412	Dense Sand	30	0.60	1.00	0.0004	16.8	43912
413	Dense Sand	30	0.60	1.10	0.0003	16.8	50432
414	Dense Sand	30	0.60	1.20	0.0003	16.8	56883
415	Dense Sand	30	0.60	1.30	0.0003	16.8	62856

416	Dense Sand	30	0.60	1.40	0.0002	16.8	68875
417	Dense Sand	30	0.60	1.50	0.0002	16.8	74891
418	Dense Sand	30	0.60	1.60	0.0002	16.8	80853
419	Dense Sand	30	0.90	0.60	0.0236	15.0	636
420	Dense Sand	30	0.90	0.70	0.0047	16.7	3524
421	Dense Sand	30	0.90	0.80	0.0006	16.8	30071
422	Dense Sand	30	0.90	0.90	0.0004	16.8	38717
423	Dense Sand	30	0.90	1.00	0.0004	16.8	45303
424	Dense Sand	30	0.90	1.10	0.0003	16.8	51343
425	Dense Sand	30	0.90	1.20	0.0003	16.8	57235
426	Dense Sand	30	0.90	1.30	0.0003	16.8	63224
427	Dense Sand	30	0.90	1.40	0.0002	16.8	69260
428	Dense Sand	30	0.90	1.50	0.0002	16.8	75291
429	Dense Sand	30	0.90	1.60	0.0002	16.8	81266
430	Dense Sand	30	1.20	0.60	0.0196	16.0	817
431	Dense Sand	30	1.20	0.70	0.0011	16.8	15449
432	Dense Sand	30	1.20	0.80	0.0005	16.8	32818
433	Dense Sand	30	1.20	0.90	0.0004	16.8	39994
434	Dense Sand	30	1.20	1.00	0.0004	16.8	45860
435	Dense Sand	30	1.20	1.10	0.0003	16.8	51624
436	Dense Sand	30	1.20	1.20	0.0003	16.8	57534
437	Dense Sand	30	1.20	1.30	0.0003	16.8	63540
438	Dense Sand	30	1.20	1.40	0.0002	16.8	69591
439	Dense Sand	30	1.20	1.50	0.0002	16.8	75636
440	Dense Sand	30	1.20	1.60	0.0002	16.8	81625
441	Dense Sand	35	0.30	0.60	0.0346	12.5	360
442	Dense Sand	35	0.30	0.70	0.0256	15.0	584
443	Dense Sand	35	0.30	0.80	0.0073	16.4	2259
444	Dense Sand	35	0.30	0.90	0.0006	16.5	25843
445	Dense Sand	35	0.30	1.00	0.0004	16.5	41535
446	Dense Sand	35	0.30	1.10	0.0003	16.5	48943
447	Dense Sand	35	0.30	1.20	0.0003	16.5	56304
448	Dense Sand	35	0.30	1.30	0.0003	16.5	62981
449	Dense Sand	35	0.30	1.40	0.0002	16.5	68379
450	Dense Sand	35	0.30	1.50	0.0002	16.5	74383
451	Dense Sand	35	0.30	1.60	0.0002	16.5	80334
452	Dense Sand	35	0.60	0.60	0.0294	13.9	473
453	Dense Sand	35	0.60	0.70	0.0154	16.2	1055
454	Dense Sand	35	0.60	0.80	0.0008	16.5	19935
455	Dense Sand	35	0.60	0.90	0.0005	16.5	36570
456	Dense Sand	35	0.60	1.00	0.0004	16.5	44018
457	Dense Sand	35	0.60	1.10	0.0003	16.5	50473

458	Dense Sand	35	0.60	1.20	0.0003	16.5	56891
459	Dense Sand	35	0.60	1.30	0.0003	16.5	62864
460	Dense Sand	35	0.60	1.40	0.0002	16.5	68885
461	Dense Sand	35	0.60	1.50	0.0002	16.5	74902
462	Dense Sand	35	0.60	1.60	0.0002	16.5	80864
463	Dense Sand	35	0.90	0.60	0.0256	15.0	587
464	Dense Sand	35	0.90	0.70	0.0038	16.5	4312
465	Dense Sand	35	0.90	0.80	0.0005	16.5	30538
466	Dense Sand	35	0.90	0.90	0.0004	16.5	38861
467	Dense Sand	35	0.90	1.00	0.0004	16.5	45347
468	Dense Sand	35	0.90	1.10	0.0003	16.5	51352
469	Dense Sand	35	0.90	1.20	0.0003	16.5	57245
470	Dense Sand	35	0.90	1.30	0.0003	16.5	63235
471	Dense Sand	35	0.90	1.40	0.0002	16.5	69272
472	Dense Sand	35	0.90	1.50	0.0002	16.5	75303
473	Dense Sand	35	0.90	1.60	0.0002	16.5	81279
474	Dense Sand	35	1.20	0.60	0.0211	16.0	759
475	Dense Sand	35	1.20	0.70	0.0009	16.5	17522
476	Dense Sand	35	1.20	0.80	0.0005	16.5	33055
477	Dense Sand	35	1.20	0.90	0.0004	16.5	40038
478	Dense Sand	35	1.20	1.00	0.0004	16.5	45869
479	Dense Sand	35	1.20	1.10	0.0003	16.5	51634
480	Dense Sand	35	1.20	1.20	0.0003	16.5	57545
481	Dense Sand	35	1.20	1.30	0.0003	16.5	63552
482	Dense Sand	35	1.20	1.40	0.0002	16.5	69605
483	Dense Sand	35	1.20	1.50	0.0002	16.5	75651
484	Dense Sand	35	1.20	1.60	0.0002	16.5	81642
485	Dense Sand	40	0.30	0.60	0.0383	12.2	320
486	Dense Sand	40	0.30	0.70	0.0287	14.7	512
487	Dense Sand	40	0.30	0.80	0.0080	16.2	2028
488	Dense Sand	40	0.30	0.90	0.0007	16.3	24995
489	Dense Sand	40	0.30	1.00	0.0004	16.3	41377
490	Dense Sand	40	0.30	1.10	0.0003	16.3	48929
491	Dense Sand	40	0.30	1.20	0.0003	16.3	56376
492	Dense Sand	40	0.30	1.30	0.0003	16.3	63045
493	Dense Sand	40	0.30	1.40	0.0002	16.3	68373
494	Dense Sand	40	0.30	1.50	0.0002	16.3	74377
495	Dense Sand	40	0.30	1.60	0.0002	16.3	80328
496	Dense Sand	40	0.60	0.60	0.0324	13.7	421
497	Dense Sand	40	0.60	0.70	0.0133	16.1	1210
498	Dense Sand	40	0.60	0.80	0.0009	16.3	18529
499	Dense Sand	40	0.60	0.90	0.0004	16.3	36449

500	Dense Sand	40	0.60	1.00	0.0004	16.3	44037
501	Dense Sand	40	0.60	1.10	0.0003	16.3	50548
502	Dense Sand	40	0.60	1.20	0.0003	16.3	56888
503	Dense Sand	40	0.60	1.30	0.0003	16.3	62861
504	Dense Sand	40	0.60	1.40	0.0002	16.3	68881
505	Dense Sand	40	0.60	1.50	0.0002	16.3	74898
506	Dense Sand	40	0.60	1.60	0.0002	16.3	80861
507	Dense Sand	40	0.90	0.60	0.0285	14.8	518
508	Dense Sand	40	0.90	0.70	0.0041	16.2	4006
509	Dense Sand	40	0.90	0.80	0.0005	16.3	30362
510	Dense Sand	40	0.90	0.90	0.0004	16.3	38881
511	Dense Sand	40	0.90	1.00	0.0004	16.3	45423
512	Dense Sand	40	0.90	1.10	0.0003	16.3	51350
513	Dense Sand	40	0.90	1.20	0.0003	16.3	57244
514	Dense Sand	40	0.90	1.30	0.0003	16.3	63234
515	Dense Sand	40	0.90	1.40	0.0002	16.3	69271
516	Dense Sand	40	0.90	1.50	0.0002	16.3	75302
517	Dense Sand	40	0.90	1.60	0.0002	16.3	81279
518	Dense Sand	40	1.20	0.60	0.0225	15.8	702
519	Dense Sand	40	1.20	0.70	0.0010	16.3	16601
520	Dense Sand	40	1.20	0.80	0.0005	16.3	33044
521	Dense Sand	40	1.20	0.90	0.0004	16.3	40109
522	Dense Sand	40	1.20	1.00	0.0004	16.3	45868
523	Dense Sand	40	1.20	1.10	0.0003	16.3	51634
524	Dense Sand	40	1.20	1.20	0.0003	16.3	57545
525	Dense Sand	40	1.20	1.30	0.0003	16.3	63552
526	Dense Sand	40	1.20	1.40	0.0002	16.3	69605
527	Dense Sand	40	1.20	1.50	0.0002	16.3	75653
528	Dense Sand	40	1.20	1.60	0.0002	16.3	81644
529	Soft Clay	25	0.30	0.60	0.0395	5.9	150
530	Soft Clay	25	0.30	0.70	0.0360	8.2	228
531	Soft Clay	25	0.30	0.80	0.0310	10.4	337
532	Soft Clay	25	0.30	0.90	0.0267	12.8	478
533	Soft Clay	25	0.30	1.00	0.0206	15.1	732
534	Soft Clay	25	0.30	1.10	0.0111	16.8	1511
535	Soft Clay	25	0.30	1.20	0.0054	17.0	3144
536	Soft Clay	25	0.30	1.30	0.0039	17.0	4387
537	Soft Clay	25	0.30	1.40	0.0032	17.0	5283
538	Soft Clay	25	0.30	1.50	0.0027	17.0	6294
539	Soft Clay	25	0.30	1.60	0.0023	17.0	7263
540	Soft Clay	25	0.60	0.60	0.0374	7.2	193
541	Soft Clay	25	0.60	0.70	0.0337	9.5	282

542	Soft Clay	25	0.60	0.80	0.0290	11.9	409
543	Soft Clay	25	0.60	0.90	0.0227	14.2	625
544	Soft Clay	25	0.60	1.00	0.0172	16.6	967
545	Soft Clay	25	0.60	1.10	0.0075	16.9	2271
546	Soft Clay	25	0.60	1.20	0.0049	17.0	3489
547	Soft Clay	25	0.60	1.30	0.0038	17.0	4518
548	Soft Clay	25	0.60	1.40	0.0031	17.0	5487
549	Soft Clay	25	0.60	1.50	0.0027	17.0	6416
550	Soft Clay	25	0.60	1.60	0.0023	17.0	7343
551	Soft Clay	25	0.90	0.60	0.0380	7.1	187
552	Soft Clay	25	0.90	0.70	0.0331	9.8	295
553	Soft Clay	25	0.90	0.80	0.0282	12.3	438
554	Soft Clay	25	0.90	0.90	0.0198	15.6	788
555	Soft Clay	25	0.90	1.00	0.0102	16.9	1654
556	Soft Clay	25	0.90	1.10	0.0060	17.0	2820
557	Soft Clay	25	0.90	1.20	0.0044	17.0	3822
558	Soft Clay	25	0.90	1.30	0.0036	17.0	4743
559	Soft Clay	25	0.90	1.40	0.0030	17.0	5632
560	Soft Clay	25	0.90	1.50	0.0026	17.0	6513
561	Soft Clay	25	0.90	1.60	0.0023	17.0	7408
562	Soft Clay	25	1.20	0.60	0.0373	7.4	199
563	Soft Clay	25	1.20	0.70	0.0320	10.2	319
564	Soft Clay	25	1.20	0.80	0.0270	13.0	480
565	Soft Clay	25	1.20	0.90	0.0209	15.6	749
566	Soft Clay	25	1.20	1.00	0.0109	16.8	1544
567	Soft Clay	25	1.20	1.10	0.0063	17.0	2700
568	Soft Clay	25	1.20	1.20	0.0042	17.0	4064
569	Soft Clay	25	1.20	1.30	0.0035	17.0	4913
570	Soft Clay	25	1.20	1.40	0.0030	17.0	5747
571	Soft Clay	25	1.20	1.50	0.0026	17.0	6595
572	Soft Clay	25	1.20	1.60	0.0023	17.0	7465
573	Soft Clay	30	0.30	0.60	0.0453	6.1	135
574	Soft Clay	30	0.30	0.70	0.0422	8.4	198
575	Soft Clay	30	0.30	0.80	0.0365	10.6	291
576	Soft Clay	30	0.30	0.90	0.0294	12.9	438
577	Soft Clay	30	0.30	1.00	0.0229	15.2	664
578	Soft Clay	30	0.30	1.10	0.0103	16.6	1602
579	Soft Clay	30	0.30	1.20	0.0052	16.7	3202
580	Soft Clay	30	0.30	1.30	0.0038	16.7	4410
581	Soft Clay	30	0.30	1.40	0.0032	16.7	5293
582	Soft Clay	30	0.30	1.50	0.0027	16.7	6298
583	Soft Clay	30	0.30	1.60	0.0023	16.7	7264

584	Soft Clay	30	0.60	0.60	0.0437	7.4	170
585	Soft Clay	30	0.60	0.70	0.0387	9.7	250
586	Soft Clay	30	0.60	0.80	0.0327	12.0	367
587	Soft Clay	30	0.60	0.90	0.0259	14.4	554
588	Soft Clay	30	0.60	1.00	0.0154	16.4	1065
589	Soft Clay	30	0.60	1.10	0.0071	16.7	2333
590	Soft Clay	30	0.60	1.20	0.0047	16.7	3517
591	Soft Clay	30	0.60	1.30	0.0037	16.7	4531
592	Soft Clay	30	0.60	1.40	0.0030	16.7	5494
593	Soft Clay	30	0.60	1.50	0.0026	16.7	6418
594	Soft Clay	30	0.60	1.60	0.0023	16.7	7344
595	Soft Clay	30	0.90	0.60	0.0438	7.4	168
596	Soft Clay	30	0.90	0.70	0.0376	9.9	264
597	Soft Clay	30	0.90	0.80	0.0310	12.5	402
598	Soft Clay	30	0.90	0.90	0.0209	15.7	752
599	Soft Clay	30	0.90	1.00	0.0097	16.6	1717
600	Soft Clay	30	0.90	1.10	0.0058	16.7	2858
601	Soft Clay	30	0.90	1.20	0.0044	16.7	3836
602	Soft Clay	30	0.90	1.30	0.0035	16.7	4754
603	Soft Clay	30	0.90	1.40	0.0030	16.7	5636
604	Soft Clay	30	0.90	1.50	0.0026	16.7	6515
605	Soft Clay	30	0.90	1.60	0.0023	16.7	7409
606	Soft Clay	30	1.20	0.60	0.0435	7.7	177
607	Soft Clay	30	1.20	0.70	0.0368	10.4	283
608	Soft Clay	30	1.20	0.80	0.0292	13.1	448
609	Soft Clay	30	1.20	0.90	0.0210	15.6	743
610	Soft Clay	30	1.20	1.00	0.0104	16.6	1591
611	Soft Clay	30	1.20	1.10	0.0061	16.7	2731
612	Soft Clay	30	1.20	1.20	0.0041	16.7	4077
613	Soft Clay	30	1.20	1.30	0.0034	16.7	4918
614	Soft Clay	30	1.20	1.40	0.0029	16.7	5751
615	Soft Clay	30	1.20	1.50	0.0025	16.7	6597
616	Soft Clay	30	1.20	1.60	0.0022	16.7	7467
617	Soft Clay	35	0.30	0.60	0.0521	6.3	121
618	Soft Clay	35	0.30	0.70	0.0478	8.5	178
619	Soft Clay	35	0.30	0.80	0.0414	10.7	260
620	Soft Clay	35	0.30	0.90	0.0335	13.0	389
621	Soft Clay	35	0.30	1.00	0.0248	15.3	619
622	Soft Clay	35	0.30	1.10	0.0097	16.4	1686
623	Soft Clay	35	0.30	1.20	0.0050	16.4	3281
624	Soft Clay	35	0.30	1.30	0.0037	16.5	4461
625	Soft Clay	35	0.30	1.40	0.0031	16.5	5334

626	Soft Clay	35	0.30	1.50	0.0026	16.5	6329
627	Soft Clay	35	0.30	1.60	0.0023	16.5	7291
628	Soft Clay	35	0.60	0.60	0.0496	7.6	152
629	Soft Clay	35	0.60	0.70	0.0438	9.8	223
630	Soft Clay	35	0.60	0.80	0.0362	12.1	334
631	Soft Clay	35	0.60	0.90	0.0277	14.5	522
632	Soft Clay	35	0.60	1.00	0.0143	16.3	1138
633	Soft Clay	35	0.60	1.10	0.0068	16.4	2408
634	Soft Clay	35	0.60	1.20	0.0046	16.5	3573
635	Soft Clay	35	0.60	1.30	0.0036	16.5	4572
636	Soft Clay	35	0.60	1.40	0.0030	16.5	5526
637	Soft Clay	35	0.60	1.50	0.0026	16.5	6446
638	Soft Clay	35	0.60	1.60	0.0022	16.5	7368
639	Soft Clay	35	0.90	0.60	0.0496	7.5	152
640	Soft Clay	35	0.90	0.70	0.0427	10.1	236
641	Soft Clay	35	0.90	0.80	0.0345	12.6	365
642	Soft Clay	35	0.90	0.90	0.0229	15.8	690
643	Soft Clay	35	0.90	1.00	0.0092	16.4	1786
644	Soft Clay	35	0.90	1.10	0.0056	16.4	2917
645	Soft Clay	35	0.90	1.20	0.0042	16.5	3878
646	Soft Clay	35	0.90	1.30	0.0034	16.5	4790
647	Soft Clay	35	0.90	1.40	0.0029	16.5	5664
648	Soft Clay	35	0.90	1.50	0.0025	16.5	6539
649	Soft Clay	35	0.90	1.60	0.0022	16.5	7432
650	Soft Clay	35	1.20	0.60	0.0492	7.9	161
651	Soft Clay	35	1.20	0.70	0.0417	10.6	254
652	Soft Clay	35	1.20	0.80	0.0330	13.3	402
653	Soft Clay	35	1.20	0.90	0.0230	15.8	688
654	Soft Clay	35	1.20	1.00	0.0099	16.4	1651
655	Soft Clay	35	1.20	1.10	0.0059	16.4	2785
656	Soft Clay	35	1.20	1.20	0.0040	16.5	4113
657	Soft Clay	35	1.20	1.30	0.0033	16.5	4947
658	Soft Clay	35	1.20	1.40	0.0029	16.5	5775
659	Soft Clay	35	1.20	1.50	0.0025	16.5	6670
660	Soft Clay	35	1.20	1.60	0.0022	16.5	7488
661	Soft Clay	40	0.30	0.60	0.0568	6.4	113
662	Soft Clay	40	0.30	0.70	0.0520	8.6	165
663	Soft Clay	40	0.30	0.80	0.0448	10.8	241
664	Soft Clay	40	0.30	0.90	0.0358	13.1	365
665	Soft Clay	40	0.30	1.00	0.0262	15.4	585
666	Soft Clay	40	0.30	1.10	0.0088	16.2	1843
667	Soft Clay	40	0.30	1.20	0.0047	16.2	3432

668	Soft Clay	40	0.30	1.30	0.0035	16.2	4582
669	Soft Clay	40	0.30	1.40	0.0030	16.3	5440
670	Soft Clay	40	0.30	1.50	0.0025	16.3	6420
671	Soft Clay	40	0.30	1.60	0.0022	16.3	7371
672	Soft Clay	40	0.60	0.60	0.0548	7.7	140
673	Soft Clay	40	0.60	0.70	0.0478	9.9	206
674	Soft Clay	40	0.60	0.80	0.0395	12.2	308
675	Soft Clay	40	0.60	0.90	0.0302	14.5	481
676	Soft Clay	40	0.60	1.00	0.0129	16.1	1250
677	Soft Clay	40	0.60	1.10	0.0063	16.2	2559
678	Soft Clay	40	0.60	1.20	0.0044	16.2	3698
679	Soft Clay	40	0.60	1.30	0.0035	16.2	4678
680	Soft Clay	40	0.60	1.40	0.0029	16.3	5617
681	Soft Clay	40	0.60	1.50	0.0025	16.3	6526
682	Soft Clay	40	0.60	1.60	0.0022	16.3	7441
683	Soft Clay	40	0.90	0.60	0.0548	7.7	140
684	Soft Clay	40	0.90	0.70	0.0471	10.2	217
685	Soft Clay	40	0.90	0.80	0.0373	12.7	340
686	Soft Clay	40	0.90	0.90	0.0224	15.8	705
687	Soft Clay	40	0.90	1.00	0.0084	16.2	1923
688	Soft Clay	40	0.90	1.10	0.0053	16.2	3038
689	Soft Clay	40	0.90	1.20	0.0041	16.2	3981
690	Soft Clay	40	0.90	1.30	0.0033	16.3	4878
691	Soft Clay	40	0.90	1.40	0.0028	16.3	5742
692	Soft Clay	40	0.90	1.50	0.0025	16.3	6611
693	Soft Clay	40	0.90	1.60	0.0022	16.3	7499
694	Soft Clay	40	1.20	0.60	0.0537	8.0	150
695	Soft Clay	40	1.20	0.70	0.0451	10.7	237
696	Soft Clay	40	1.20	0.80	0.0343	13.3	389
697	Soft Clay	40	1.20	0.90	0.0223	15.8	708
698	Soft Clay	40	1.20	1.00	0.0091	16.2	1780
699	Soft Clay	40	1.20	1.10	0.0056	16.2	2907
700	Soft Clay	40	1.20	1.20	0.0039	16.2	4200
701	Soft Clay	40	1.20	1.30	0.0032	16.3	5023
702	Soft Clay	40	1.20	1.40	0.0028	16.3	5845
703	Soft Clay	40	1.20	1.50	0.0024	16.3	6685
704	Soft Clay	40	1.20	1.60	0.0022	16.3	7550
705	Medium Clay	25	0.30	0.60	0.0297	11.0	370
706	Medium Clay	25	0.30	0.70	0.0237	13.4	564
707	Medium Clay	25	0.30	0.80	0.0185	15.8	854
708	Medium Clay	25	0.30	0.90	0.0040	17.0	4225
709	Medium Clay	25	0.30	1.00	0.0020	17.1	8569

710	Medium Clay	25	0.30	1.10	0.0016	17.1	10762
711	Medium Clay	25	0.30	1.20	0.0013	17.1	12858
712	Medium Clay	25	0.30	1.30	0.0012	17.1	14688
713	Medium Clay	25	0.30	1.40	0.0010	17.1	16318
714	Medium Clay	25	0.30	1.50	0.0009	17.1	18201
715	Medium Clay	25	0.30	1.60	0.0008	17.1	20144
716	Medium Clay	25	0.60	0.60	0.0274	12.1	441
717	Medium Clay	25	0.60	0.70	0.0211	14.6	692
718	Medium Clay	25	0.60	0.80	0.0094	16.9	1804
719	Medium Clay	25	0.60	0.90	0.0024	17.1	7086
720	Medium Clay	25	0.60	1.00	0.0018	17.1	9337
721	Medium Clay	25	0.60	1.10	0.0015	17.1	11175
722	Medium Clay	25	0.60	1.20	0.0013	17.1	12915
723	Medium Clay	25	0.60	1.30	0.0012	17.1	14652
724	Medium Clay	25	0.60	1.40	0.0010	17.1	16455
725	Medium Clay	25	0.60	1.50	0.0009	17.1	18324
726	Medium Clay	25	0.60	1.60	0.0008	17.1	20257
727	Medium Clay	25	0.90	0.60	0.0259	12.7	490
728	Medium Clay	25	0.90	0.70	0.0191	15.5	811
729	Medium Clay	25	0.90	0.80	0.0040	17.0	4237
730	Medium Clay	25	0.90	0.90	0.0022	17.1	7881
731	Medium Clay	25	0.90	1.00	0.0018	17.1	9732
732	Medium Clay	25	0.90	1.10	0.0015	17.1	11395
733	Medium Clay	25	0.90	1.20	0.0013	17.1	13053
734	Medium Clay	25	0.90	1.30	0.0012	17.1	14771
735	Medium Clay	25	0.90	1.40	0.0010	17.1	16560
736	Medium Clay	25	0.90	1.50	0.0009	17.1	18418
737	Medium Clay	25	0.90	1.60	0.0008	17.1	20342
738	Medium Clay	25	1.20	0.60	0.0237	13.4	564
739	Medium Clay	25	1.20	0.70	0.0167	16.4	983
740	Medium Clay	25	1.20	0.80	0.0029	17.0	5784
741	Medium Clay	25	1.20	0.90	0.0021	17.1	7998
742	Medium Clay	25	1.20	1.00	0.0018	17.1	9723
743	Medium Clay	25	1.20	1.10	0.0015	17.1	11370
744	Medium Clay	25	1.20	1.20	0.0013	17.1	13169
745	Medium Clay	25	1.20	1.30	0.0011	17.1	14873
746	Medium Clay	25	1.20	1.40	0.0010	17.1	16651
747	Medium Clay	25	1.20	1.50	0.0009	17.1	18500
748	Medium Clay	25	1.20	1.60	0.0008	17.1	20417
749	Medium Clay	30	0.30	0.60	0.0349	11.0	316
750	Medium Clay	30	0.30	0.70	0.0276	13.5	488
751	Medium Clay	30	0.30	0.80	0.0198	15.9	803

752	Medium Clay	30	0.30	0.90	0.0033	16.7	5124
753	Medium Clay	30	0.30	1.00	0.0019	16.8	8752
754	Medium Clay	30	0.30	1.10	0.0015	16.8	10842
755	Medium Clay	30	0.30	1.20	0.0013	16.8	12885
756	Medium Clay	30	0.30	1.30	0.0011	16.8	14710
757	Medium Clay	30	0.30	1.40	0.0010	16.8	16324
758	Medium Clay	30	0.30	1.50	0.0009	16.8	18207
759	Medium Clay	30	0.30	1.60	0.0008	16.8	20150
760	Medium Clay	30	0.60	0.60	0.0308	12.2	394
761	Medium Clay	30	0.60	0.70	0.0239	14.7	616
762	Medium Clay	30	0.60	0.80	0.0066	16.7	2520
763	Medium Clay	30	0.60	0.90	0.0023	16.7	7310
764	Medium Clay	30	0.60	1.00	0.0018	16.8	9419
765	Medium Clay	30	0.60	1.10	0.0015	16.8	11198
766	Medium Clay	30	0.60	1.20	0.0013	16.8	12923
767	Medium Clay	30	0.60	1.30	0.0011	16.8	14658
768	Medium Clay	30	0.60	1.40	0.0010	16.8	16461
769	Medium Clay	30	0.60	1.50	0.0009	16.8	18330
770	Medium Clay	30	0.60	1.60	0.0008	16.8	20263
771	Medium Clay	30	0.90	0.60	0.0296	12.8	431
772	Medium Clay	30	0.90	0.70	0.0210	15.6	741
773	Medium Clay	30	0.90	0.80	0.0034	16.7	4930
774	Medium Clay	30	0.90	0.90	0.0021	16.8	7985
775	Medium Clay	30	0.90	1.00	0.0017	16.8	9766
776	Medium Clay	30	0.90	1.10	0.0015	16.8	11415
777	Medium Clay	30	0.90	1.20	0.0013	16.8	13060
778	Medium Clay	30	0.90	1.30	0.0011	16.8	14778
779	Medium Clay	30	0.90	1.40	0.0010	16.8	16567
780	Medium Clay	30	0.90	1.50	0.0009	16.8	18425
781	Medium Clay	30	0.90	1.60	0.0008	16.8	20349
782	Medium Clay	30	1.20	0.60	0.0276	13.5	487
783	Medium Clay	30	1.20	0.70	0.0149	16.4	1100
784	Medium Clay	30	1.20	0.80	0.0028	16.7	5977
785	Medium Clay	30	1.20	0.90	0.0021	16.8	8060
786	Medium Clay	30	1.20	1.00	0.0017	16.7	9746
787	Medium Clay	30	1.20	1.10	0.0015	16.8	11378
788	Medium Clay	30	1.20	1.20	0.0013	16.8	13176
789	Medium Clay	30	1.20	1.30	0.0011	16.8	14880
790	Medium Clay	30	1.20	1.40	0.0010	16.8	16658
791	Medium Clay	30	1.20	1.50	0.0009	16.8	18508
792	Medium Clay	30	1.20	1.60	0.0008	16.8	20425
793	Medium Clay	35	0.30	0.60	0.0392	11.0	282

794	Medium Clay	35	0.30	0.70	0.0307	13.5	438
795	Medium Clay	35	0.30	0.80	0.0224	15.9	709
796	Medium Clay	35	0.30	0.90	0.0030	16.5	5585
797	Medium Clay	35	0.30	1.00	0.0019	16.5	8854
798	Medium Clay	35	0.30	1.10	0.0015	16.5	10897
799	Medium Clay	35	0.30	1.20	0.0013	16.5	12913
800	Medium Clay	35	0.30	1.30	0.0011	16.5	14729
801	Medium Clay	35	0.30	1.40	0.0010	16.5	16342
802	Medium Clay	35	0.30	1.50	0.0009	16.5	18224
803	Medium Clay	35	0.30	1.60	0.0008	16.5	20167
804	Medium Clay	35	0.60	0.60	0.0358	12.2	340
805	Medium Clay	35	0.60	0.70	0.0262	14.7	563
806	Medium Clay	35	0.60	0.80	0.0055	16.4	2981
807	Medium Clay	35	0.60	0.90	0.0022	16.5	7428
808	Medium Clay	35	0.60	1.00	0.0017	16.5	9475
809	Medium Clay	35	0.60	1.10	0.0015	16.5	11226
810	Medium Clay	35	0.60	1.20	0.0013	16.5	12942
811	Medium Clay	35	0.60	1.30	0.0011	16.5	14676
812	Medium Clay	35	0.60	1.40	0.0010	16.5	16479
813	Medium Clay	35	0.60	1.50	0.0009	16.5	18347
814	Medium Clay	35	0.60	1.60	0.0008	16.5	20281
815	Medium Clay	35	0.90	0.60	0.0337	12.8	379
816	Medium Clay	35	0.90	0.70	0.0233	15.6	668
817	Medium Clay	35	0.90	0.80	0.0031	16.5	5314
818	Medium Clay	35	0.90	0.90	0.0020	16.5	8052
819	Medium Clay	35	0.90	1.00	0.0017	16.5	9796
820	Medium Clay	35	0.90	1.10	0.0014	16.5	11433
821	Medium Clay	35	0.90	1.20	0.0013	16.5	13078
822	Medium Clay	35	0.90	1.30	0.0011	16.5	14795
823	Medium Clay	35	0.90	1.40	0.0010	16.5	16584
824	Medium Clay	35	0.90	1.50	0.0009	16.5	18442
825	Medium Clay	35	0.90	1.60	0.0008	16.5	20367
826	Medium Clay	35	1.20	0.60	0.0307	13.5	438
827	Medium Clay	35	1.20	0.70	0.0129	16.3	1269
828	Medium Clay	35	1.20	0.80	0.0027	16.5	6090
829	Medium Clay	35	1.20	0.90	0.0020	16.5	8110
830	Medium Clay	35	1.20	1.00	0.0017	16.5	9775
831	Medium Clay	35	1.20	1.10	0.0014	16.5	11397
832	Medium Clay	35	1.20	1.20	0.0013	16.5	13193
833	Medium Clay	35	1.20	1.30	0.0011	16.5	14897
834	Medium Clay	35	1.20	1.40	0.0010	16.5	16675
835	Medium Clay	35	1.20	1.50	0.0009	16.5	18525

836	Medium Clay	35	1.20	1.60	0.0008	16.5	20443
837	Medium Clay	40	0.30	0.60	0.0430	10.9	252
838	Medium Clay	40	0.30	0.70	0.0340	13.2	389
839	Medium Clay	40	0.30	0.80	0.0241	15.6	648
840	Medium Clay	40	0.30	0.90	0.0030	16.3	5334
841	Medium Clay	40	0.30	1.00	0.0018	16.3	8864
842	Medium Clay	40	0.30	1.10	0.0015	16.3	10932
843	Medium Clay	40	0.30	1.20	0.0013	16.3	12957
844	Medium Clay	40	0.30	1.30	0.0011	16.3	14775
845	Medium Clay	40	0.30	1.40	0.0010	16.3	16388
846	Medium Clay	40	0.30	1.50	0.0009	16.3	18267
847	Medium Clay	40	0.30	1.60	0.0008	16.3	20208
848	Medium Clay	40	0.60	0.60	0.0389	12.0	308
849	Medium Clay	40	0.60	0.70	0.0292	14.5	497
850	Medium Clay	40	0.60	0.80	0.0059	16.2	2747
851	Medium Clay	40	0.60	0.90	0.0022	16.3	7437
852	Medium Clay	40	0.60	1.00	0.0017	16.3	9513
853	Medium Clay	40	0.60	1.10	0.0014	16.3	11272
854	Medium Clay	40	0.60	1.20	0.0013	16.3	12988
855	Medium Clay	40	0.60	1.30	0.0011	15.5	14750
856	Medium Clay	40	0.60	1.40	0.0010	16.3	16521
857	Medium Clay	40	0.60	1.50	0.0009	16.3	18389
858	Medium Clay	40	0.60	1.60	0.0008	16.3	20321
859	Medium Clay	40	0.90	0.60	0.0360	12.6	349
860	Medium Clay	40	0.90	0.70	0.0251	15.4	612
861	Medium Clay	40	0.90	0.80	0.0031	16.3	5221
862	Medium Clay	40	0.90	0.90	0.0020	16.3	8085
863	Medium Clay	40	0.90	1.00	0.0017	16.3	9840
864	Medium Clay	40	0.90	1.10	0.0014	16.3	11478
865	Medium Clay	40	0.90	1.20	0.0012	16.3	13120
866	Medium Clay	40	0.90	1.30	0.0011	16.3	14836
867	Medium Clay	40	0.90	1.40	0.0010	16.3	16624
868	Medium Clay	40	0.90	1.50	0.0009	16.3	18482
869	Medium Clay	40	0.90	1.60	0.0008	16.3	20407
870	Medium Clay	40	1.20	0.60	0.0339	13.3	392
871	Medium Clay	40	1.20	0.70	0.0133	16.1	1204
872	Medium Clay	40	1.20	0.80	0.0027	16.3	6129
873	Medium Clay	40	1.20	0.90	0.0020	16.3	8158
874	Medium Clay	40	1.20	1.00	0.0017	16.3	9823
875	Medium Clay	40	1.20	1.10	0.0014	16.3	11443
876	Medium Clay	40	1.20	1.20	0.0012	16.3	13232
877	Medium Clay	40	1.20	1.30	0.0010	15.5	14964

878	Medium Clay	40	1.20	1.40	0.0010	16.3	16714
879	Medium Clay	40	1.20	1.50	0.0009	16.3	18564
880	Medium Clay	40	1.20	1.60	0.0008	16.3	20481
881	Stiff Clay	25	0.30	0.60	0.0250	12.8	513
882	Stiff Clay	25	0.30	0.70	0.0200	15.3	766
883	Stiff Clay	25	0.30	0.80	0.0062	17.0	2718
884	Stiff Clay	25	0.30	0.90	0.0012	17.1	14539
885	Stiff Clay	25	0.30	1.00	0.0007	17.1	23218
886	Stiff Clay	25	0.30	1.10	0.0006	17.1	28048
887	Stiff Clay	25	0.30	1.20	0.0005	17.1	32895
888	Stiff Clay	25	0.30	1.30	0.0005	17.1	37246
889	Stiff Clay	25	0.30	1.40	0.0004	17.1	41098
890	Stiff Clay	25	0.30	1.50	0.0004	17.1	45370
891	Stiff Clay	25	0.30	1.60	0.0003	17.1	49481
892	Stiff Clay	25	0.60	0.60	0.0229	13.9	609
893	Stiff Clay	25	0.60	0.70	0.0164	16.6	1014
894	Stiff Clay	25	0.60	0.80	0.0020	17.1	8341
895	Stiff Clay	25	0.60	0.90	0.0009	17.1	19910
896	Stiff Clay	25	0.60	1.00	0.0007	17.1	24682
897	Stiff Clay	25	0.60	1.10	0.0006	17.1	28767
898	Stiff Clay	25	0.60	1.20	0.0005	17.1	32797
899	Stiff Clay	25	0.60	1.30	0.0005	17.1	37048
900	Stiff Clay	25	0.60	1.40	0.0004	17.1	41421
901	Stiff Clay	25	0.60	1.50	0.0004	17.1	45693
902	Stiff Clay	25	0.60	1.60	0.0003	17.1	49815
903	Stiff Clay	25	0.90	0.60	0.0210	14.7	702
904	Stiff Clay	25	0.90	0.70	0.0068	17.0	2498
905	Stiff Clay	25	0.90	0.80	0.0011	17.1	15511
906	Stiff Clay	25	0.90	0.90	0.0008	17.1	21263
907	Stiff Clay	25	0.90	1.00	0.0007	17.1	25329
908	Stiff Clay	25	0.90	1.10	0.0006	17.1	29129
909	Stiff Clay	25	0.90	1.20	0.0005	17.1	33095
910	Stiff Clay	25	0.90	1.30	0.0005	17.1	37326
911	Stiff Clay	25	0.90	1.40	0.0004	17.1	41672
912	Stiff Clay	25	0.90	1.50	0.0004	17.1	45941
913	Stiff Clay	25	0.90	1.60	0.0003	17.1	50075
914	Stiff Clay	25	1.20	0.60	0.0189	15.6	824
915	Stiff Clay	25	1.20	0.70	0.0030	17.0	5734
916	Stiff Clay	25	1.20	0.80	0.0010	17.1	17175
917	Stiff Clay	25	1.20	0.90	0.0008	17.1	21512
918	Stiff Clay	25	1.20	1.00	0.0007	17.1	25221
919	Stiff Clay	25	1.20	1.10	0.0006	17.1	28993

920	Stiff Clay	25	1.20	1.20	0.0005	17.1	33362
921	Stiff Clay	25	1.20	1.30	0.0005	17.1	37572
922	Stiff Clay	25	1.20	1.40	0.0004	17.1	41892
923	Stiff Clay	25	1.20	1.50	0.0004	17.1	46156
924	Stiff Clay	25	1.20	1.60	0.0003	17.1	50301
925	Stiff Clay	30	0.30	0.60	0.0293	12.9	442
926	Stiff Clay	30	0.30	0.70	0.0214	15.4	719
927	Stiff Clay	30	0.30	0.80	0.0047	16.7	3518
928	Stiff Clay	30	0.30	0.90	0.0010	16.8	17041
929	Stiff Clay	30	0.30	1.00	0.0007	16.8	23582
930	Stiff Clay	30	0.30	1.10	0.0006	16.8	28203
931	Stiff Clay	30	0.30	1.20	0.0005	16.8	32958
932	Stiff Clay	30	0.30	1.30	0.0004	16.8	37273
933	Stiff Clay	30	0.30	1.40	0.0004	16.8	41126
934	Stiff Clay	30	0.30	1.50	0.0004	16.8	45382
935	Stiff Clay	30	0.30	1.60	0.0003	16.8	49493
936	Stiff Clay	30	0.60	0.60	0.0259	14.0	542
937	Stiff Clay	30	0.60	0.70	0.0126	16.5	1310
938	Stiff Clay	30	0.60	0.80	0.0016	16.7	10788
939	Stiff Clay	30	0.60	0.90	0.0008	16.8	20298
940	Stiff Clay	30	0.60	1.00	0.0007	16.8	24813
941	Stiff Clay	30	0.60	1.10	0.0006	16.8	28885
942	Stiff Clay	30	0.60	1.20	0.0005	16.8	32818
943	Stiff Clay	30	0.60	1.30	0.0005	16.8	37077
944	Stiff Clay	30	0.60	1.40	0.0004	16.8	41450
945	Stiff Clay	30	0.60	1.50	0.0004	16.8	45707
946	Stiff Clay	30	0.60	1.60	0.0003	16.8	49829
947	Stiff Clay	30	0.90	0.60	0.0231	14.8	643
948	Stiff Clay	30	0.90	0.70	0.0052	16.7	3188
949	Stiff Clay	30	0.90	0.80	0.0010	16.8	16248
950	Stiff Clay	30	0.90	0.90	0.0008	16.8	21439
951	Stiff Clay	30	0.90	1.00	0.0007	16.8	25348
952	Stiff Clay	30	0.90	1.10	0.0006	16.8	29218
953	Stiff Clay	30	0.90	1.20	0.0005	16.8	33118
954	Stiff Clay	30	0.90	1.30	0.0004	16.8	37357
955	Stiff Clay	30	0.90	1.40	0.0004	16.8	41703
956	Stiff Clay	30	0.90	1.50	0.0004	16.8	45958
957	Stiff Clay	30	0.90	1.60	0.0003	16.8	50091
958	Stiff Clay	30	1.20	0.60	0.0202	15.7	777
959	Stiff Clay	30	1.20	0.70	0.0014	16.0	11317
960	Stiff Clay	30	1.20	0.80	0.0010	16.8	17462
961	Stiff Clay	30	1.20	0.90	0.0008	16.8	21583

962	Stiff Clay	30	1.20	1.00	0.0007	16.8	25230
963	Stiff Clay	30	1.20	1.10	0.0006	16.8	28972
964	Stiff Clay	30	1.20	1.20	0.0005	16.8	33388
965	Stiff Clay	30	1.20	1.30	0.0004	16.8	37605
966	Stiff Clay	30	1.20	1.40	0.0004	16.8	41924
967	Stiff Clay	30	1.20	1.50	0.0004	16.8	46174
968	Stiff Clay	30	1.20	1.60	0.0003	16.8	50318
969	Stiff Clay	35	0.30	0.60	0.0326	12.9	396
970	Stiff Clay	35	0.30	0.70	0.0238	15.4	647
971	Stiff Clay	35	0.30	0.80	0.0040	16.5	4077
972	Stiff Clay	35	0.30	0.90	0.0009	16.5	17921
973	Stiff Clay	35	0.30	1.00	0.0007	16.5	23754
974	Stiff Clay	35	0.30	1.10	0.0006	16.5	28276
975	Stiff Clay	35	0.30	1.20	0.0005	16.5	33016
976	Stiff Clay	35	0.30	1.30	0.0004	16.5	37324
977	Stiff Clay	35	0.30	1.40	0.0004	16.5	41168
978	Stiff Clay	35	0.30	1.50	0.0004	16.5	45389
979	Stiff Clay	35	0.30	1.60	0.0003	16.5	49501
980	Stiff Clay	35	0.60	0.60	0.0286	14.0	490
981	Stiff Clay	35	0.60	0.70	0.0108	16.4	1508
982	Stiff Clay	35	0.60	0.80	0.0014	16.5	11982
983	Stiff Clay	35	0.60	0.90	0.0008	16.5	20482
984	Stiff Clay	35	0.60	1.00	0.0007	16.5	24897
985	Stiff Clay	35	0.60	1.10	0.0006	16.5	28885
986	Stiff Clay	35	0.60	1.20	0.0005	16.5	32865
987	Stiff Clay	35	0.60	1.30	0.0004	16.5	37131
988	Stiff Clay	35	0.60	1.40	0.0004	16.5	41493
989	Stiff Clay	35	0.60	1.50	0.0004	16.5	45716
990	Stiff Clay	35	0.60	1.60	0.0003	16.5	49838
991	Stiff Clay	35	0.90	0.60	0.0259	14.8	573
992	Stiff Clay	35	0.90	0.70	0.0042	16.5	3893
993	Stiff Clay	35	0.90	0.80	0.0010	16.5	16535
994	Stiff Clay	35	0.90	0.90	0.0008	16.5	21536
995	Stiff Clay	35	0.90	1.00	0.0007	16.5	25207
996	Stiff Clay	35	0.90	1.10	0.0006	16.5	29242
997	Stiff Clay	35	0.90	1.20	0.0005	16.5	33167
998	Stiff Clay	35	0.90	1.30	0.0004	16.5	37412
999	Stiff Clay	35	0.90	1.40	0.0004	16.5	41747
1000	Stiff Clay	35	0.90	1.50	0.0004	16.5	45968
1001	Stiff Clay	35	0.90	1.60	0.0003	16.5	50101
1002	Stiff Clay	35	1.20	0.60	0.0230	15.7	683
1003	Stiff Clay	35	1.20	0.70	0.0019	16.5	8697

1004	Stiff Clay	35	1.20	0.80	0.0009	16.5	17609
1005	Stiff Clay	35	1.20	0.90	0.0008	16.5	21632
1006	Stiff Clay	35	1.20	1.00	0.0007	16.5	25260
1007	Stiff Clay	35	1.20	1.10	0.0006	16.5	29014
1008	Stiff Clay	35	1.20	1.20	0.0005	16.5	33439
1009	Stiff Clay	35	1.20	1.30	0.0004	16.5	37660
1010	Stiff Clay	35	1.20	1.40	0.0004	16.5	41968
1011	Stiff Clay	35	1.20	1.50	0.0004	16.5	46186
1012	Stiff Clay	35	1.20	1.60	0.0003	16.5	50330
1013	Stiff Clay	40	0.30	0.60	0.0357	12.7	354
1014	Stiff Clay	40	0.30	0.70	0.0266	15.1	568
1015	Stiff Clay	40	0.30	0.80	0.0045	16.2	3611
1016	Stiff Clay	40	0.30	0.90	0.0009	16.3	17286
1017	Stiff Clay	40	0.30	1.00	0.0007	16.3	23738
1018	Stiff Clay	40	0.30	1.10	0.0006	16.3	28394
1019	Stiff Clay	40	0.30	1.20	0.0005	16.3	33137
1020	Stiff Clay	40	0.30	1.30	0.0004	16.3	37436
1021	Stiff Clay	40	0.30	1.40	0.0004	16.3	41245
1022	Stiff Clay	40	0.30	1.50	0.0004	16.3	45391
1023	Stiff Clay	40	0.30	1.60	0.0003	16.3	49502
1024	Stiff Clay	40	0.60	0.60	0.0320	13.8	430
1025	Stiff Clay	40	0.60	0.70	0.0068	15.6	2297
1026	Stiff Clay	40	0.60	0.80	0.0015	16.3	11195
1027	Stiff Clay	40	0.60	0.90	0.0008	16.3	20461
1028	Stiff Clay	40	0.60	1.00	0.0007	16.3	24945
1029	Stiff Clay	40	0.60	1.10	0.0006	16.3	28990
1030	Stiff Clay	40	0.60	1.20	0.0005	16.3	32985
1031	Stiff Clay	40	0.60	1.30	0.0004	16.3	37253
1032	Stiff Clay	40	0.60	1.40	0.0004	16.3	41569
1033	Stiff Clay	40	0.60	1.50	0.0004	16.3	45719
1034	Stiff Clay	40	0.60	1.60	0.0003	16.3	49841
1035	Stiff Clay	40	0.90	0.60	0.0290	14.6	504
1036	Stiff Clay	40	0.90	0.70	0.0047	16.2	3418
1037	Stiff Clay	40	0.90	0.80	0.0010	16.3	16463
1038	Stiff Clay	40	0.90	0.90	0.0008	16.3	21592
1039	Stiff Clay	40	0.90	1.00	0.0006	16.3	25474
1040	Stiff Clay	40	0.90	1.10	0.0006	16.3	29288
1041	Stiff Clay	40	0.90	1.20	0.0005	16.3	33289
1042	Stiff Clay	40	0.90	1.30	0.0004	16.3	37530
1043	Stiff Clay	40	0.90	1.40	0.0004	16.3	41822
1044	Stiff Clay	40	0.90	1.50	0.0004	16.3	45972
1045	Stiff Clay	40	0.90	1.60	0.0003	16.3	50106

1046	Stiff Clay	40	1.20	0.60	0.0248	15.5	624
1047	Stiff Clay	40	1.20	0.70	0.0020	16.3	8239
1048	Stiff Clay	40	1.20	0.80	0.0009	16.3	17628
1049	Stiff Clay	40	1.20	0.90	0.0008	16.3	21700
1050	Stiff Clay	40	1.20	1.00	0.0006	16.3	25343
1051	Stiff Clay	40	1.20	1.10	0.0006	16.3	29103
1052	Stiff Clay	40	1.20	1.20	0.0005	16.3	33562
1053	Stiff Clay	40	1.20	1.30	0.0004	16.3	37774
1054	Stiff Clay	40	1.20	1.40	0.0004	16.3	42041
1055	Stiff Clay	40	1.20	1.50	0.0004	16.3	46192
1056	Stiff Clay	40	1.20	1.60	0.0003	16.3	50336

Appendix E – Effective height factors (k) based on minimum values of RBS

D_f (m)	B_f (m)	RBS (kNm/rad)	h/t = 25 P_e (kN)	25 P_{cr} (kN)	25 k	30 P_e (kN)	30 P_{cr} (kN)	30 k	35 P_e (kN)	35 P_{cr} (kN)	35 k	40 P_e (kN)	40 P_{cr} (kN)	40 k
Loose Sand														
0.3	0.6	80	146	182	0.9	100	128	0.9	73	99	0.9	58	78	0.9
0.3	0.8	210	146	213	0.8	100	151	0.8	73	118	0.8	58	92	0.8
0.3	1.0	720	146	263	0.7	100	185	0.7	73	142	0.7	58	111	0.7
0.3	1.2	4,600	146	303	0.7	100	209	0.7	73	159	0.7	58	122	0.7
0.6	0.6	170	146	205	0.8	100	145	0.8	73	113	0.8	58	89	0.8
0.6	0.8	490	146	248	0.8	100	175	0.8	73	135	0.7	58	106	0.7
0.6	1.0	3,000	146	299	0.7	100	206	0.7	73	157	0.7	58	121	0.7
0.6	1.2	7,250	146	307	0.7	100	211	0.7	73	160	0.7	58	123	0.7
0.9	0.6	250	146	220	0.8	100	156	0.8	73	121	0.8	58	95	0.8
0.9	0.8	950	146	273	0.7	100	191	0.7	73	146	0.7	58	114	0.7
0.9	1.0	5,200	146	305	0.7	100	210	0.7	73	159	0.7	58	123	0.7
0.9	1.2	8,700	146	308	0.7	100	212	0.7	73	161	0.7	58	124	0.7
1.2	0.6	360	146	235	0.8	100	167	0.8	73	129	0.8	58	101	0.8
1.2	0.8	2,100	146	293	0.7	100	203	0.7	73	154	0.7	58	120	0.7
1.2	1.0	6,250	146	306	0.7	100	210	0.7	73	160	0.7	58	123	0.7
1.2	1.2	11,700	146	309	0.7	100	212	0.7	73	161	0.7	58	124	0.7
Medium Sand														
0.3	0.6	200	146	211	0.8	100	150	0.8	73	116	0.8	58	92	0.8
0.3	0.8	530	146	251	0.8	100	177	0.8	73	137	0.7	58	107	0.7
0.3	1.0	4,800	146	304	0.7	100	209	0.7	73	159	0.7	58	122	0.7
0.3	1.2	14,000	146	310	0.7	100	213	0.7	73	161	0.7	58	124	0.7
0.6	0.6	300	146	227	0.8	100	161	0.8	73	125	0.8	58	98	0.8
0.6	0.8	1,300	146	282	0.7	100	196	0.7	73	150	0.7	58	117	0.7
0.6	1.0	9,800	146	309	0.7	100	212	0.7	73	161	0.7	58	124	0.7
0.6	1.2	24,800	146	312	0.7	100	214	0.7	73	162	0.7	58	124	0.7
0.9	0.6	350	146	234	0.8	100	166	0.8	73	129	0.8	58	101	0.8
0.9	0.8	3,800	146	301	0.7	100	208	0.7	73	158	0.7	58	122	0.7
0.9	1.0	17,800	146	311	0.7	100	213	0.7	73	162	0.7	58	124	0.7
0.9	1.2	28,350	146	312	0.7	100	214	0.7	73	162	0.7	58	125	0.7
1.2	0.6	490	146	248	0.8	100	175	0.8	73	135	0.7	58	106	0.7
1.2	0.8	8,500	146	308	0.7	100	211	0.7	73	160	0.7	58	124	0.7
1.2	1.0	22,100	146	311	0.7	100	213	0.7	73	162	0.7	58	124	0.7
1.2	1.2	28,800	146	312	0.7	100	214	0.7	73	162	0.7	58	125	0.7
Dense Sand														

0.3	0.6	320	146	230	0.8	100	163	0.8	73	127	0.8	58	100	0.8
0.3	0.8	1,500	146	286	0.7	100	198	0.7	73	152	0.7	58	118	0.7
0.3	1.0	40,600	146	312	0.7	100	214	0.7	73	162	0.7	58	125	0.7
0.3	1.2	56,200	146	313	0.7	100	214	0.7	73	162	0.7	58	125	0.7
0.6	0.6	420	146	242	0.8	100	171	0.8	73	132	0.7	58	104	0.7
0.6	0.8	10,400	146	309	0.7	100	212	0.7	73	161	0.7	58	124	0.7
0.6	1.0	43,600	146	312	0.7	100	214	0.7	73	162	0.7	58	125	0.7
0.6	1.2	56,800	146	313	0.7	100	214	0.7	73	162	0.7	58	125	0.7
0.9	0.6	510	146	250	0.8	100	176	0.8	73	136	0.7	58	107	0.7
0.9	0.8	28,800	146	312	0.7	100	214	0.7	73	162	0.7	58	125	0.7
0.9	1.0	45,250	146	312	0.7	100	214	0.7	73	162	0.7	58	125	0.7
0.9	1.2	57,200	146	313	0.7	100	214	0.7	73	162	0.7	58	125	0.7
1.2	0.6	700	146	262	0.7	100	184	0.7	73	142	0.7	58	111	0.7
1.2	0.8	32,300	146	312	0.7	100	214	0.7	73	162	0.7	58	125	0.7
1.2	1.0	45,800	146	312	0.7	100	214	0.7	73	162	0.7	58	125	0.7
1.2	1.2	57,500	146	313	0.7	100	214	0.7	73	162	0.7	58	125	0.7
Soft Clay														
0.3	0.6	110	146	190	0.9	100	134	0.9	73	105	0.8	58	82	0.8
0.3	0.8	240	146	218	0.8	100	155	0.8	73	120	0.8	58	95	0.8
0.3	1.0	580	146	255	0.8	100	180	0.7	73	138	0.7	58	108	0.7
0.3	1.2	3,120	146	299	0.7	100	206	0.7	73	157	0.7	58	121	0.7
0.6	0.6	140	146	198	0.9	100	140	0.8	73	109	0.8	58	86	0.8
0.6	0.8	300	146	227	0.8	100	161	0.8	73	125	0.8	58	98	0.8
0.6	1.0	950	146	273	0.7	100	191	0.7	73	146	0.7	58	114	0.7
0.6	1.2	3,450	146	300	0.7	100	207	0.7	73	157	0.7	58	122	0.7
0.9	0.6	140	146	198	0.9	100	140	0.8	73	109	0.8	58	86	0.8
0.9	0.8	340	146	233	0.8	100	165	0.8	73	128	0.8	58	100	0.8
0.9	1.0	1,650	146	288	0.7	100	200	0.7	73	152	0.7	58	118	0.7
0.9	1.2	3,800	146	301	0.7	100	208	0.7	73	158	0.7	58	122	0.7
1.2	0.6	150	146	200	0.9	100	142	0.8	73	111	0.8	58	87	0.8
1.2	0.8	400	146	240	0.8	100	170	0.8	73	131	0.7	58	103	0.8
1.2	1.0	1,500	146	286	0.7	100	198	0.7	73	152	0.7	58	118	0.7
1.2	1.2	4,050	146	302	0.7	100	208	0.7	73	158	0.7	58	122	0.7
Medium Clay														
0.3	0.6	250	146	220	0.8	100	156	0.8	73	121	0.8	58	95	0.8
0.3	0.8	640	146	259	0.8	100	182	0.7	73	140	0.7	58	110	0.7
0.3	1.0	8,500	146	308	0.7	100	211	0.7	73	160	0.7	58	124	0.7
0.3	1.2	12,850	146	310	0.7	100	213	0.7	73	161	0.7	58	124	0.7
0.6	0.6	300	146	227	0.8	100	161	0.8	73	125	0.8	58	98	0.8
0.6	0.8	1,800	146	290	0.7	100	201	0.7	73	153	0.7	58	119	0.7
0.6	1.0	9,300	146	308	0.7	100	212	0.7	73	161	0.7	58	124	0.7
0.6	1.2	12,900	146	310	0.7	100	213	0.7	73	161	0.7	58	124	0.7

0.9	0.6	350	146	234	0.8	100	166	0.8	73	129	0.8	58	101	0.8
0.9	0.8	4,200	146	303	0.7	100	208	0.7	73	158	0.7	58	122	0.7
0.9	1.0	9,700	146	309	0.7	100	212	0.7	73	161	0.7	58	124	0.7
0.9	1.2	13,000	146	310	0.7	100	213	0.7	73	161	0.7	58	124	0.7
1.2	0.6	390	146	239	0.8	100	169	0.8	73	131	0.7	58	103	0.8
1.2	0.8	5,750	146	305	0.7	100	210	0.7	73	159	0.7	58	123	0.7
1.2	1.0	9,700	146	309	0.7	100	212	0.7	73	161	0.7	58	124	0.7
1.2	1.2	13,150	146	310	0.7	100	213	0.7	73	161	0.7	58	124	0.7
Stiff Clay														
0.3	0.6	350	146	234	0.8	100	166	0.8	73	129	0.8	58	101	0.8
0.3	0.8	2,700	146	297	0.7	100	205	0.7	73	156	0.7	58	121	0.7
0.3	1.0	23,200	146	311	0.7	100	213	0.7	73	162	0.7	58	124	0.7
0.3	1.2	32,900	146	312	0.7	100	214	0.7	73	162	0.7	58	125	0.7
0.6	0.6	430	146	243	0.8	100	172	0.8	73	133	0.7	58	104	0.7
0.6	0.8	8,300	146	308	0.7	100	211	0.7	73	160	0.7	58	124	0.7
0.6	1.0	24,650	146	312	0.7	100	214	0.7	73	162	0.7	58	124	0.7
0.6	1.2	32,750	146	312	0.7	100	214	0.7	73	162	0.7	58	125	0.7
0.9	0.6	500	146	249	0.8	100	176	0.8	73	136	0.7	58	106	0.7
0.9	0.8	15,500	146	310	0.7	100	213	0.7	73	161	0.7	58	124	0.7
0.9	1.0	25,200	146	312	0.7	100	214	0.7	73	162	0.7	58	124	0.7
0.9	1.2	33,050	146	312	0.7	100	214	0.7	73	162	0.7	58	125	0.7
1.2	0.6	650	146	259	0.8	100	182	0.7	73	140	0.7	58	110	0.7
1.2	0.8	17,150	146	311	0.7	100	213	0.7	73	162	0.7	58	124	0.7
1.2	1.0	25,200	146	312	0.7	100	214	0.7	73	162	0.7	58	124	0.7
1.2	1.2	33,350	146	312	0.7	100	214	0.7	73	162	0.7	58	125	0.7